

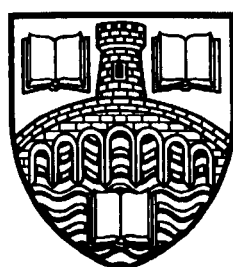
**The Role of the Skin of Early Post-hatch Turbot
(*Scophthalmus maximus* L.) in Osmoregulation**

Thesis submitted for the degree of
Doctor of Philosophy

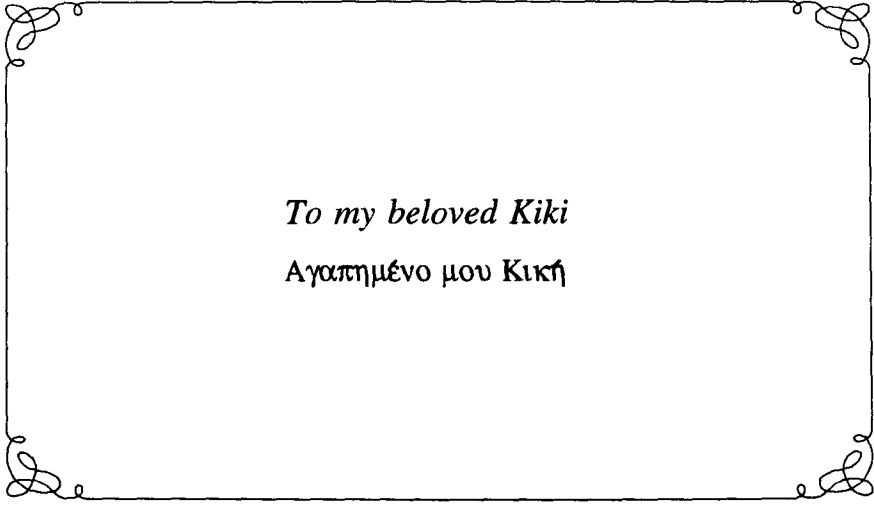
By

Kevin Peter Robinson B.Sc. (Hons)

Department of Biological and Molecular Sciences
University of Stirling



September 1996



To my beloved Kiki

Αγαπημένο μου Κική

Declaration

I hereby declare that this thesis has been compiled by myself and is the result of my own investigation. It has neither been accepted or is being submitted for any other degree. All sources of information and citations have been duly acknowledged.

Kevin Peter Robinson

K.P.Robinson

Acknowledgements

My gratitude and sincerest appreciation go to Drs Bill Wales and Peter Tytler who introduced me to the fascinating field of marine fish larval physiology. They provided sound advice, guidance, moral support and expert knowledge (and exercised a new threshold for patience). Thanks also to the Department of Biological and Molecular Sciences and Professor John Sargent, Head of the School of Natural Sciences, for the provision of excellent laboratory facilities during the course of my research training.

An indispensable condition for my studies has been the excellent technical assistance received throughout. I especially want to thank Mrs Jacqueline Ireland for all her support, advice and interest throughout the project; Mr Linton Brown (my EM Guru) for accomplished tuition in microscopical techniques and expertise with the ultramicrotome; Mr Lewis Taylor for developing the numerous slides and photomicrographs so exceptionally well and with such efficiency; Mr Willie Thompson for unmatched advice with electrical equipment and circuitry, for troubleshooting and for hasty repairs of often archaic apparatus; and finally Mr Derek Fish and Mr John Dyer (the workshop posse) for the construction of numerous "urgently required" gadgets, the frequent loan of the hammer drill and the customary cups of black tea.

Warmest thanks go to my numerous colleagues, past and present, for their support, interest and comradery over the years, especially Ian Morgan, Scot Mathieson, Keith Todd, Rosli and Sari Hashim, Jonathan Read, Cara McConnell, George Cheyong, Marcello Bucci and Rudhi Prihabi; to my dearest friends, Jon and Emma Sandoe, Simon Hornsby, Petros and Miranda Dimitriou (and family), Yiannis Vrotsis, Fofi Calochristos, Konstantinos Margaris (thankyou Kostas for all your help in the final stages of thesis assembling and for illustration 2.1), Nikos Streftaris, Andrew Lake (and family), Zena Boyiatzi, George Papathakos, Mariola Rebisz, George Papadopoulos, Samuel Ait (thankyou for the loan of your house whilst in Lebanon), Alex Karafillides and Nada Jarmooz; to my spiritual guide Veronica Newton; and to my new extensive family in Halandri, Athens.

Finally, but most importantly, immeasurable thanks to the 3 most important people in my life: to my beautiful Kiki for all the love, encouragement, tireless support and wonderful experiences shared; to my remarkable mother for her continual faith and unconditional love (I love you Mum) and to my wonderful Grandmother (at last - here it is!!!).

The project was gratefully funded by a studentship provided by the National Environment Research Council (Project No. GT4/90/ALS/58). The Southdown Trust also provided a small, but gratefully received, monetary contribution during a period of financial hardship.

Abstract

To date, the structural significance of the skin of fish larvae in osmoregulation has received little attention and the evidence for salt secretion by cutaneous chloride cells is based largely on morphological observations. Thus, in the present study, a combination of microscopical and electrophysiological techniques were utilised to determine the role of the skin of early post-hatch turbot larvae in osmoregulation.

A number of specialised structural features were revealed in the skin of the turbot larva with electron microscopy which would appear to provide some protection against the high osmotic and ionic gradients tending to dehydrate and salt load the body tissue and fluids. In the heterogenous epidermis, consisting of both transporting and non-transferring cells, only the shallow junctions between chloride cells and accessory cells were believed to permit ion influx and/or water loss via the paracellular pathway; the extensive junctions between adjacent pavement cells and pavement cells and neighbouring chloride cells effectively occluding the passage of ions and water through the extracellular space. Chloride cells were revealed in the skin and prebranchial epithelium of the turbot larva from hatching, but accessory cells, and thus "leaky" junctions, were only observed in association with the closely juxtaposed chloride cells in the prebranchial epithelium which, although densely packed, represented just a small area of the otherwise "tight" skin. Water and ion permeation through the external plasma membrane of the superficial pavement cells might further be impeded by the extracellular glycocalyx coat observed in TEM. In addition, the large numbers of mucous cells, which were a characteristic feature of the skin of the turbot larva, may produce a protective mucus coating of low permeability.

The apparent "tightness" of the skin was reflected by the measurements of diffusional water permeability (P_{diff}) from early stage larvae which suggested that the larvae of turbot were relatively impermeable to water compared with the gills of adults. Nevertheless, the rates of water turnover were still sufficiently high that a net osmotic loss of water must be replaced by water uptake through drinking. The observation that the P_{diff} of early stage turbot larvae increased with development substantiates earlier supposition that the drinking rates of larvae are a direct function of the permeability of the larva to water.

A study of the chronology of chloride cell development utilising specific fluorochromes and electron microscopy revealed that the prebranchial chloride cells, which closely resembled the chloride cells described in the branchial epithelium of juveniles, were both numerous and well equipped to participate in active salt extrusion in turbot larvae even

at hatching. In view of the early hypertrophy and proliferation of the prebranchial cells, their rapid increase in Na^+,K^+ -ATPase binding sites, and the subsequent degeneration of the cutaneous chloride cells observed with larval development, it was concluded that the prebranchial chloride cells are the primary site for active ion excretion shortly after yolksac absorption. The potential importance of the cutaneous chloride cells in salt extrusion was also considered, but in view of the apparent lack of accessory cell associations and the small number of apical pits observed in SEM and TEM sections, questions were raised as to the significance of these cells in ion excretion.

Measurements of the transepithelial electrical potential (TEP) from early stage turbot using intracellular microelectrode techniques confirmed that the larvae of turbot maintain ionic gradients by the active extrusion of ions that enter into the body cavity down electrical or chemical gradients. The TEP was found to be largely the result of a Na^+ diffusion potential with an additive electrogenic potential due to Cl^- transport, which was somehow functionally connected to Na^+,K^+ -ATPase. Furthermore, the concentration of Na^+ in the external bathing medium was found to have a direct regulatory influence on the rate of Cl^- secretion, suggesting that the active secretion of Cl^- across the skin must be coupled to Na^+ . These conclusions are consistent with the current theories proposed for salt extrusion by the chloride cells in the adult teleost.

Table of Contents

Acknowledgements	i
Abstract	ii
Contents	iv
List of Tables	vii
List of Figures	ix

<u>Chapter 1. Introduction</u>	1
---	---

<u>Chapter 2. Materials & Methods</u>	11
2.1. Rearing and handling of larvae	12
2.1.1. Culture methods	12
2.1.2. Specimen selection	13
2.2. Histological procedures	15
2.2.1. Transmission electron microscopy (TEM)	15
A. Fixation and embedding	15
B. Section cutting and staining	15
2.2.2. Scanning electron microscopy (SEM)	16
2.3. Vital staining with fluorescent probes	18
2.3.1. DASPMI staining	18
2.3.2. Anthroylouabain staining	19
2.3.3. Imaging microscopy	21
2.4. Water turnover rates, surface area estimates and diffusional water permeabilities	23
2.5. Microelectrode studies of the skin	26
2.5.1. Preparation of microelectrodes	26
2.5.2. Animals	26

2.5.3. Experimental set-up	27
2.5.4. Potential measurement	31
2.5.5. The effect of temperature on TEP measurement	32
2.5.6. Ouabain inhibition	32
2.5.7. The effect of salinity on the TEP measurement	33
2.5.8. Ion substitution experiments	33
2.5.9. Theoretical considerations in TEP prediction	34
2.6. Solutions and chemicals	37
2.7. Data analysis	37
Chapter 3. Results	38
3.1. The ultrastructure and development of the larval skin	39
3.1.1. General morphology of the larval skin	39
3.1.2. Skin thickness and chloride cell development	65
3.2. Vital staining with fluorescent probes	73
3.2.1. The distribution of DASPMI-stained chloride cells	73
3.2.2. Chloride cell morphology	78
3.2.3. Localisation and activity of Na^+,K^+ -ATPase	78
3.3. The water turnover rates and diffusional water permeabilities of early post-hatch turbot larvae	89
3.4. Microelectrode studies	95
3.4.1. Measurement of the TEP	95
3.4.2. Nernst and Goldman kinetics	99
3.4.3. The effect of incubation temperature on the TEP	100
3.4.4. The influence of ouabain	100
3.4.5. The effect of environmental salinity on the TEP	104
3.4.6. The effects of alterations of $[\text{Na}^+]$ and $[\text{Cl}^-]$ on the TEP	109

Chapter 4. Discussion	114
4.1. The skin as a limiting membrane to the movement of water and ions	115
4.2. The chloride cell as the site of active transport in the larval integument	120
4.3. Water balance in the early post-hatch stages of marine fish larvae	125
4.4. The nature of the transepithelial potential and its ionic contributions	130
4.5. Concluding remarks	142
References	145-160
Appendices	161-172

List of Tables

Table	Page
1.1. The osmolarity and ionic composition of the major ions in the plasma and surrounding media of representative marine and freshwater teleost fishes	3
2.1. A description of the stages of larval <i>S. maximus</i> used in the present study, based mainly upon their morphological characteristics	14
3.1. The mean thickness (\pm S.E) of the epidermis measured from turbot larvae during development	66
3.2. Measurements of the dorsal, ventral and lateral epidermal thicknesses from three sites in the integument of developmental stage 2 turbot larvae, at 7 days post-hatching	67
3.3. Measurements of the cross sectional area (\pm S.E., $n=20$) of DASPMI-stained chloride cells from the developmental stages of turbot larvae	80
3.4. Measurements of the cross sectional area and mean cell fluorescence (\pm S.E., $n=50$) of anthroylouabain-positive chloride cells in turbot larvae aged between 2 and 7 days post-hatching	86
3.5. Parameters (\pm S.E.) of first order rate equations used for regression analysis of time courses of water uptake and for calculating the permeability of larvae	91
3.6. Measurements of the mean wet and dry weights of turbot larvae, from hatching to approximately 8-10 days post-hatching, used in the estimation of the water content of individuals	93
3.7. TEP measurements (\pm S.E.) recorded from different stages of turbot larvae bathed in ASW at 15°C	98
3.8. TEP measurements (\pm S.E.) recorded from stage 1c-d larvae incubated at 10 and 20°C	102
3.9. Nernst potentials for sodium and chloride, goldman predictions and observed TEP measurements for stage 1c-d larvae incubated at 10, 15 and 20°C	103

3.10. The effect of serosally injected ouabain action on the TEP measured from stage 1c-d larvae	105
3.11. TEP measurements (\pm S.E.) recorded from stage 1c-d larvae acclimatised in 24 and 44% seawater respectively at 15°C	106
3.12. Nernst potentials for sodium and chloride, goldman predictions and observed TEP measurements for stage 1c-d larvae incubated in 24, 34 and 44% seawater	108
3.13. TEP measurements made upon alteration of the Cl^- and Na^+ ion concentrations in the external bathing solution	110
3.14. Nernst potentials for sodium and chloride, goldman predictions and observed TEP measurements for stage 1c-d larvae in Na^+ and Cl^- substituted ASW bathing media	112
4.1. Rate constants (K_i) for influx of tritiated water in adult, larval and embryonic teleosts	126
4.2. The ${}^3\text{H}_2\text{O}$ permeability coefficients of diffusion for eggs, larvae and adults of teleost fish	127
4.3. Measured transepithelial potentials from adult teleost species	131
4.4. The ionic composition of the body fluids of some adult and larval teleost fish species	140

List of Figures

Figure	Page
1.1. Illustrations showing salt and water exchange in adult teleost fish	5
1.2. Drawing showing the ultrastructural features of a typical chloride cell in the opercular epithelium of <i>Fundulus heteroclitus</i>	7
2.1. Schematic illustrations detailing the microinjection setup used in the present study	20
2.2. Diagram showing the positioning of a fish larva and electrodes for recording	28
2.3. Diagrammatic representation of the recording dish and electrical apparatus used in the measurement of transepithelial electrical potentials from larval turbot	30
3.1. Scanning electron micrograph of the epidermal cell surface from the mid lateral yolksac region of a newly hatched turbot larva ($\times 860$)	41
3.2. Scanning electron micrograph of the skin surface of a stage 1c-d larva ($\times 1,300$)	41
3.3. Scanning electron micrograph from a stage 1a larva showing the numerous raised microridges covering the external cell surfaces of the superficial pavement cells ($\times 3,000$)	43
3.4. Electron micrograph of the dorsal skin of a stage 2 larva ($\times 6,600$)	43
3.5. Low magnification electron micrograph from the trunk region of a day 3 turbot larva ($\times 5,000$).	44
3.6. Electron micrographs showing the junctional contact points between epidermal cells in the larval skin	46
3.7. Electron micrograph of a mature mucous cell in the superficial epidermis ($\times 5,000$)	49

3.8.	Electron micrograph showing two dehisced superficial mucous cells open at the surface of the epidermis ($\times 3,300$)	49
3.9.	Scanning electron micrograph of a newly hatched turbot larva showing the abundance and distribution of superficial mucous cells covering the entire surface of the skin ($\times 100$)	51
3.10.	Scanning electron micrograph of an early stage 2 larva, approximately 6 days after hatching ($\times 55$)	51
3.11.	High magnification scanning electron micrograph of the surface epithelium showing numerous mature mucous cells bulging out of the superficial cell layer ($\times 1,700$)	53
3.12.	Scanning electron micrograph of an apical chloride cell pit located near the gill opening of a stage 1 larva ($\times 4,300$)	53
3.13.	Electron micrograph ($\times 5,000$) of a chloride cell from the prebranchial region of a stage 1d larva	55
3.14.	Electron micrograph of a "cutaneous" chloride cell from the ventral trunk region of an early stage 2 larva ($\times 0000$)	55
3.15.	Electron micrograph of a cutaneous chloride cell from the yolksac epithelium of a stage 1 larva ($\times 9,800$)	57
3.16.	Electron micrograph showing a group of closely juxtaposed prebranchial chloride and accessory cells from a newly hatched turbot ($\times 3,300$)	57
3.17.	High power electron micrograph of a prebranchial chloride cell showing details of mitochondria ($\times 20,000$)	59
3.18.	High power electron micrograph showing the microtubular system in the sub-apical region of a cutaneous chloride cell from a stage 1c larva ($\times 33,000$)	59
3.19.	Electron micrograph showing the continuity of the microtubular system of a chloride cell (left) with the lateral plasma membrane ($\times 20,000$)	61
3.20.	Electron micrograph of a multicellular prebranchial pit showing the contribution of the accessory cell to the wall of the apical cavity ($\times 18,000$)	61

3.21. Electron micrograph of the prebranchial chloride cell pit showing junctional contact between adjacent cell types ($\times 20,000$)	64
3.22. Electron micrograph of the prebranchial chloride cell pit showing junctional contact between adjacent cell types ($\times 16,000$)	64
3.23. Electron micrograph from a stage 3a turbot larva of a cutaneous chloride cell showing clear signs of degeneration/autolysis ($\times 3,300$)	69
3.24. Electron micrograph from a stage 3a turbot larva of a cutaneous chloride cell showing the apparent breakdown of the membrane systems and cristae of mitochondria and deterioration of the microtubular system ($\times 20,000$)	69
3.25. High power electron micrograph of the microtubular system from the prebranchial chloride cell of a stage 1a turbot larva ($\times 33,000$)	72
3.26. High power electron micrograph of the microtubular system from the prebranchial chloride cell of a stage 3a turbot larva ($\times 33,000$)	72
3.27. Drawings showing the changes in the distribution of DASPMI-stained chloride cells in the skin of turbot larvae between 1 and 13 days post-hatching	74
3.28. Chloride cell distribution in the skin of the stage 1a yolk-sac turbot larva as revealed by DASPMI-staining	75
3.29. The distribution of mitochondria-rich, DASPMI-stained chloride cells in the skin of the stage 1c-d turbot larva, 4-6 days post-hatching	77
3.30. Photomicrographs illustrating the morphological differences between cutaneous and prebranchially located chloride cells	79
3.31. Photomicrograph showing the distribution of Na^+,K^+ -ATPase-rich cells in the skin of a yolk-sac turbot larva as revealed by anthroylouabain staining	81
3.32. Photomicrograph of anthroylouabain-stained chloride cells in the prebranchial region of a stage 1a turbot larva	83
3.33. Photomicrographs of anthroylouabain-stained cutaneous chloride cells showing changes in the localisation of Na^+,K^+ -ATPase with larval development	84

3.34. Computer enhanced epifluorescence images of the skin of larval turbot showing anthroylouabain fluorescence in cutaneous and prebranchial chloride cells respectively	87
3.35. Graph to show the mean total fluorescence (\pm S.E.) in anthroylouabain-stained prebranchial and cutaneous chloride cells of turbot aged from 2 to 7 days post-hatching	88
3.36. Graph to show the time courses of water influx in the early developmental stages of the turbot larva	90
3.37. Exponential transformations of the water influx data, based on equation 2-1	92
3.38. Recordings of TEP's showing (a) the typical abrupt positive shift in voltage as the tip of a microelectrode is manually advanced into the fluid filled haemocoel of a turbot larva; and (b) the utilisation of negative capacitance to facilitate microelectrode impalement	96
3.39. Graph to show the effect of incubation temperature on the TEP recorded from stage 1c-d turbot larvae	101
3.40. Graph to show the effect of the external salinity on the TEP recorded from stage 1c-d turbot larvae	107
3.41. Graphs to show the effects of external Cl^- and Na^+ concentrations on the TEP recorded from stage 1c-d turbot larvae	111
4.1. Hypothetical model for NaCl transport through the chloride cell	135

Ionic regulation of osmotic fluids is an essential characteristic of all aquatic organisms, but the regulation of osmolality of extracellular fluids is not universal. Most marine invertebrates are osmoconformers that maintain the osmotic concentration of their extracellular fluids approximately equal to that of the surrounding water. However, other metazoans such as teleost fish are osmoregulators, maintaining the concentration of their extracellular fluids either above (hypertonic) or (freshwater teleosts) or below

The tubot *Acanthocinus australis* maintains a constant internal milieu of 3.0% NaCl in its body fluids which is 1.102 times greater than seawater (see Fig. 1). Compared to the external seawater which is 1.024 times greater (see Fig. 1) (cf. 1955). Therefore, since the body fluids are markedly hyperosmotic to the surrounding seawater, there is a high osmotic pressure gradient across the body membranes.

particularly from the large peneside and rectal, the seawater fish must ingest the external medium which, together with water absorbed by the anterior intestine. However, because water uptake is coupled with salt intake the osmotic problem overcomes by drinking the seawater is replaced by one which is solved

In his work with seawater-adapted rats, Anconia (1926; 1930), Huxley Smith (1930) was first to recognise that oral irrigation produced a "urine" in the bladder. He showed that the marine teleost kidney is not capable of reabsorption since that is hyperosmotic to the blood and proposed that elimination of the excess salt absorbed must take place through some excretorial pathway, presumably the rectum. This was unequivocal in

Ionic regulation of osmotic fluids is an essential characteristic of all aquatic organisms, but the regulation of osmolality of extracellular fluids is not universal. Most marine invertebrates are osmoconformers that maintain the osmotic concentration of their extracellular fluids approximately equal to that of the surrounding water. However, other metazoans such as teleost fish are osmoregulators, maintaining the concentration of their extracellular fluids either above (hyporegulators - freshwater teleosts) or below (hyporegulators - marine teleosts) that of the external medium (Table 1.1).

The turbot, *Scophthalmus maximus* L., is a stenohaline teleost species which maintains a constant internal milieu of 384 mOsm.kg^{-1} (Andrew Cossins, *pers. com.*) compared to the external seawater which is $1109 \text{ mOsm.kg}^{-1}$ (in Sverdrup *et al.*, 1955). Therefore, since its body fluids are markedly hypotonic to the surrounding seawater, there is a high tendency for osmotic water loss and/or salt loading. To compensate for the loss of water, particularly from the large permeable gill surfaces, the seawater fish must ingest the external medium which, together with salts, is absorbed by the anterior intestine. However, because water uptake is coupled with salt intake the osmotic problem overcome by drinking the seawater is replaced by an ionic problem.

In his work with seawater-adapted eels, *Anguilla rostrata* (Lesueur), Homer Smith (1930) was first to recognise that oral ingestion presented a "salt load" to the animal. He showed that the marine teleost kidney is not capable of producing a urine that is hyperosmotic to the blood and proposed that elimination of the excess salt ingested must take place through some extrarenal pathway, presumably across the gills. The first unequivocal *in*

Table 1.1. The osmolarity and ionic composition of the major ions in the plasma and surrounding media of representative marine and freshwater teleost fishes.

Ionic composition (mM.l^{-1})	Seawater		Freshwater	
	Plasma ^a	Medium ^b	Plasma ^c	Medium ^d
Na^+	180	458.8	141	0.25
Cl^-	158	535.3	117	0.23
K^+	4.9	10.18	3.8	0.01
Ca^{2+}	5.0	9.93	2.7	0.07
Mg^{2+}	3.8	52.41	1.7	0.04
Osmolarity (mOsm.l^{-1})	371	1109	340	1.0

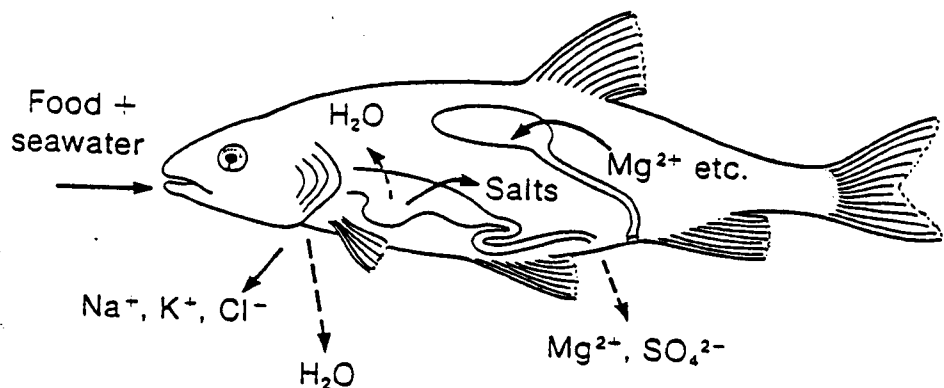
^a Smith (1929), ^b Sverdrup (1955), ^c Robertson (1954), ^d Potts & Parry (1964).

vitro evidence for extrarenal salt extrusion by the teleost gill was subsequently provided by Ancel Keys with his description of chloride transport in a doubly perfused heart-gill preparation (Keys, 1931*a,b*). Keys & Willmer (1932) then carried out a histological examination of the gill epithelium and discovered the cellular basis for this transport activity - the "chloride cell" - a large, granular, eosinophilic cell exhibiting the cytological and cytochemical properties of a secretory cell. This early work, providing the structural framework for all subsequent investigations (see extensive reviews by Maetz, 1971 and 1974; Maetz & Bornancin, 1975; Kirschner, 1979; Evans, 1980*a,b* and 1982; Evans *et al.*, 1982; and Péqueux *et al.*, 1988), formed the basis of the Smith-Krogh model for teleostean osmoregulation (Smith, 1930; Krogh, 1939) (Fig. 1.1).

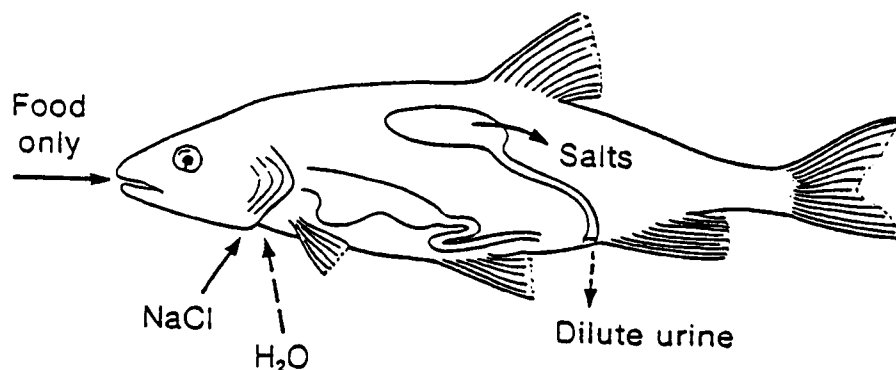
Regulation of the osmotic concentration of body fluids is also known to occur in the embryonic and larval stages of many marine teleosts (Holliday & Blaxter, 1960; Guggino, 1980*a*; Hølleland & Fyhn, 1986; Riis-Vestergaard, 1982), including the turbot (Brown & Tytler, 1993), but the processes of osmotic and ionic regulation are less fully understood than in the adult. The larvae of many species hatch at a very early stage of organogenesis and many of the effector organs associated with osmoregulation in adults are either absent, as in the case of functional gills, or at an early stage of development, as with the gut and kidney (Alderice, 1988). However, like adults, both eggs and larvae are capable of maintaining body fluids between 11 and 14‰ (350-440 mOsm) and thus effective regulatory mechanisms for the replacement or reduction of osmotic water loss and for the excretion of excess salts must be present.

In place of the adult organs, primordial cells and organs are believed to perform the necessary functions required for water and salt balance. For example, the gut of embryos

A. Marine Teleost



B. Freshwater Teleost



Solid arrows indicate active processes; broken arrows, passive processes.

Fig. 1.1. Salt and water exchange in adult teleost fish. (A) The hydromineral problems of a hyporegulating teleost in seawater are two-fold: net diffusional gain of ions (predominantly Na⁺ and Cl⁻) and net osmotic loss of water. To offset these potential ionic and osmotic non-equilibria, the marine teleost ingests the seawater (which adds to the ionic load), excretes very small quantities of isosmotic urine, extrudes excess divalent ions rectally as well as renally, and extrudes excess monovalent ions across the gills. (B) Teleosts in freshwater face the opposite problem: net ionic loss and net osmotic influx. The freshwater teleost does not drink the medium, but excretes copious volumes of dilute urine, and actively extracts needed ions from the freshwater medium across the gills.

and larvae has been described by Tanaka (1973) and Rombout *et al.* (1978) as closed and non-functional. However, several studies have recently shown that the gut of newly hatched larvae, in spite of its extremely primordial nature, is both patent and actively involved in osmoregulation (Mangor-Jensen & Adoff, 1987; Tytler & Blaxter, 1988*a,b*). Drinking behaviour is evident even in dechorionated embryos (Guggino, 1980*a*) and post-hatched larvae are able to regulate their drinking rate to compensate for changes in environmental temperature and salinity (Tytler & Blaxter, 1988*b*; Tytler & Ireland, 1994). The pronephric kidney may also be active soon after hatching (Todd, 1996) although little is currently known about its role in urine production and divalent ion excretion at this stage.

In the absence of gills, the larval skin has been proposed as the main site of ion excretion. Primordial chloride cells first appear in embryos soon after epiboly (Alderice, 1988) and persist in the skin until the gills appear (Katsura & Hamada, 1986), after which branchial chloride cells proliferate as the gills elaborate. Shelbourne (1957), investigating the site of chloride regulation in plaice larvae (*Pleuronectes platessa* L.) by a modification of Leschke's chloride test, was the first to show that the integument, and particularly the yolksac, was the probable site of iono- and osmoregulation in newly hatched larvae. This hypothesis was later supported by several further studies (Holliday, 1962; Holliday & Jones, 1965 and 1967; Weisbart, 1968), but Lasker & Threadgold (1968) were the first to actually describe mitochondria-rich chloride cells in the skin of the larva. Subsequently, integumental chloride cells, structurally resembling the cells observed in the gills and opercular epithelium of adult fish (Fig. 1.2), have been located in the skin of numerous embryonic and larval forms, including: the puffer, *Fugu niphobles* (Jordan & Snyder), Iwai (1969); plaice, *Pleuronectes platessa*, Roberts *et al.* (1973); red seabream,

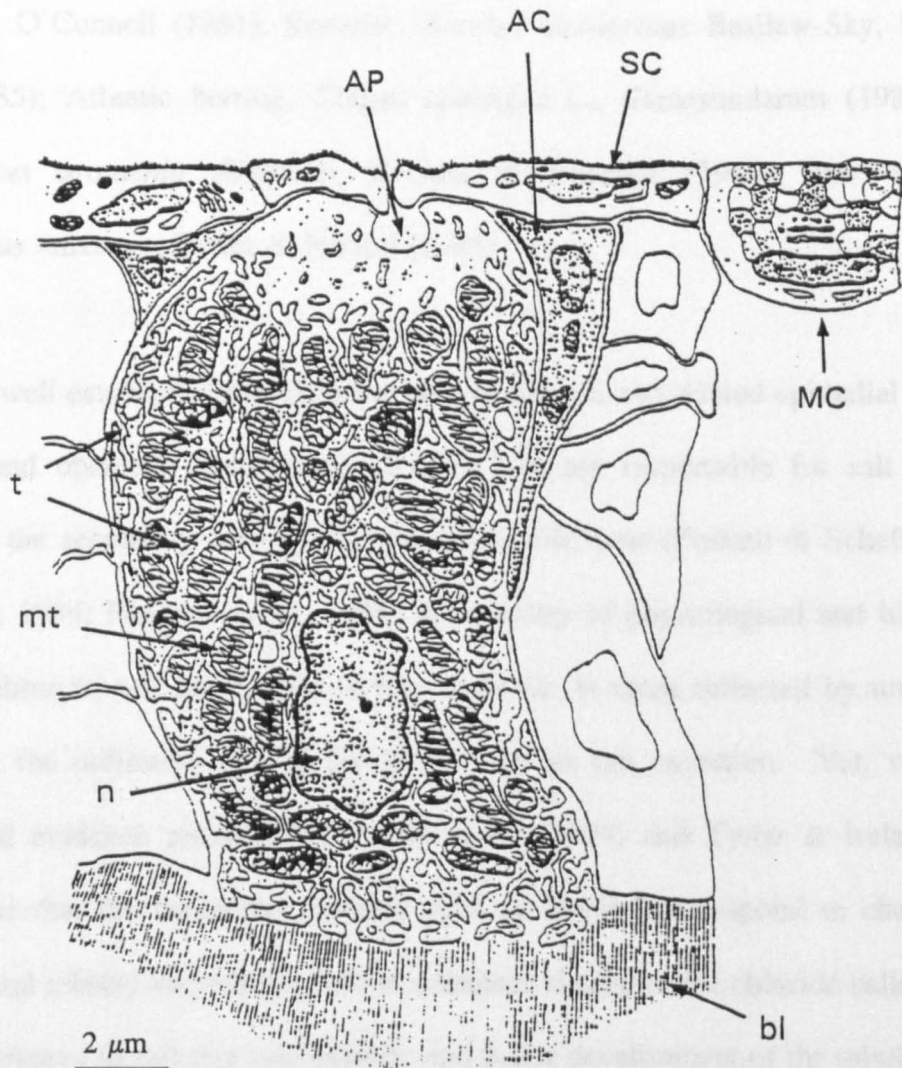


Fig. 1.2. Drawing showing the ultrastructural features of a typical chloride cell in the opercular epithelium of *Fundulus heteroclitus*. The cell is characterised by large numbers of well developed mitochondria and an extensive microtubular system forming an extension of the basolateral plasma membrane. The ion pump, a Na^+,K^+ -activated ATPase, is located on the cytoplasmic side of the tubular system (Karnaky *et al.*, 1976; Hootman & Philpott, 1979), and ATP required to drive the pump is produced by the abundant mitochondria. AC: accessory cell; AP: apical pit of chloride cell; bl: basal lamina; MC: mucous producing cell; mt: mitochondria; n: nucleus; SC: superficial pavement or respiratory cell; t: microtubular system. Redrawn from Degnan *et al.* (1977).

Pagrus major (Temminck & Schlegel), Yamashita (1978); northern anchovy, *Engraulis modax* (L.), O'Connell (1981); flounder, *Kareius bicoloratus* Basilew-Sky, Hwang & Hirano (1985); Atlantic herring, *Clupea harengus* L., Somasundaram (1985); goby, *Chaenogobius urotaenia* (Bleeker), Katsura & Hamada (1986); and the turbot, *Scophthalmus maximus*, Tytler & Ireland (1995).

Whilst it is well established that chloride cells in the gill and related epithelial structures (jaw skin and opercular epithelium) of adult fish are responsible for salt secretion, specifically the secondary active transport of chloride ions (Foskett & Scheffey, 1982; Zadunaisky, 1984; Péqueux *et al.*, 1988), the paucity of physiological and biochemical studies of chloride cell function in larvae, however, is often reflected by uncertainties surrounding the definitive role of the larval cells in salt excretion. Yet, very recent experimental evidence provided by Ayson *et al.* (1994) and Tytler & Ireland (1995) demonstrates that the cutaneous chloride cells of larval fish respond to challenges in environmental salinity and temperature in a manner similar to the chloride cells in adults; showing increases in cell size and number, and better development of the tubular systems and mitochondria. Since high temperatures and salinity have also been shown to increase drinking rates and water permeability in fish larvae (Tytler *et al.*, 1993; Tytler & Ireland, 1994), which will inevitably require an increase in salt pumping, the former observations by Ayson *et al.* and Tytler & Ireland strongly suggest the importance of the cutaneous chloride cells for the excretion of excess ions across the skin.

In view of the literature, it is apparent that embryos and newly hatched larvae may possess much of the regulatory apparatus of the adult fish. In contrast with adults, however, larvae possess an adverse surface area to mass ratio for osmoregulation (DeSilva, 1973)

which would be expected to result in a very rapid exchange of ions. Furthermore, the larval skin (the exchange surface) is very thin - in newly hatched plaice (*Pleuronectes platessa*) the diffusional distance is just 5 µm (Roberts *et al.*, 1973) whereas Jones *et al.* (1966) found the epidermis of larval herring (*Clupea harengus*) to be much thinner, varying in thickness from 2.0 to 3.2 µm - also indicating the potential for rapid exchange. Yet, estimations of the diffusional permeability coefficients for salts and water suggest that the larvae of marine fish are less permeable than adults (Tytler & Bell, 1989).

It is reasoned that the low permeability of larvae must lie in the physical properties of the skin, but to date the structural significance of the skin in osmoregulation has received little attention. Early ultrastructural investigations by Jones *et al.* (1966), Wellings & Brown (1969) and Roberts *et al.* (1973) have provided broad descriptions of the cytology and histochemistry of the larval skin, but the majority of subsequent light and electron microscope studies have focused primarily on the identification and fine structure of the early chloride cells (Lasker & Threadgold, 1968; Hwang & Hirano, 1985; Katsura & Hamada, 1986; Hwang, 1989 and 1990). The latter studies propose that salt excretion is a function of the cutaneous chloride cells in newly hatched larvae but, even with more recent developments by Ayson *et al.* (1994) and Tytler & Ireland (1995), the evidence for this hypothesis is still largely circumstantial and physiological studies are clearly required to determine whether or not the primordial chloride cells are actively involved in ion pumping in the larval fish.

In the present study, a combination of microscopical and electrophysiological techniques were utilised to examine the role of the skin of early post-hatch turbot larvae in salt and water balance. The following questions were posed:

- 1) How does the skin of early post-hatch larvae participate in the regulation of water loss and salt loading?
- 2) Is it permeable? Does it pump ions?
- 3) If so, which ions are pumped and where are the sites for ion pumping?
- 4) How do these regulatory mechanisms change with the rapid development of larvae?

Thus, a transmission and scanning electron microscopical investigation was conducted to examine the general structure and development of the larval skin. In addition, specific vital fluorochromes were used to reveal and quantify the key enzymes (anthroylouabain), organelles (DASPMI) and receptor sites in primordial chloride cells, to show the distribution and activity of these cells with larval development. Radioisotopes were used to measure the rates of water turnover from which estimations of the diffusional water permeability of the larva could be made. In the electrophysiological approach, conventional microelectrodes were utilised to measure transepithelial potentials from which interpretations of the movements of ions across the skin could be made.

With the application of these wide ranging techniques it was hoped to establish a necessary insight into the role of the skin of marine fish larvae in osmoregulation. Accordingly, the success of the techniques would provide a foundation for further development in future studies.

2.1. Materials & Methods

2.1.1. Culture methods

Eggs of the turbot *Scophthalmus maximus* L. were obtained from Golden Sea Produce, Hunterston, Scotland. Each batch and tank emerged from a single female, induced to spawn using a controlled protocol and fertilized by the sperm of a single male. Following transportation to the University laboratory in insulated containers, the eggs were

allowed to stand for approximately 10 minutes at room temperature and many of which had eggs become opercular. After removal of the opercular surface, unfertilized eggs were discarded. The remaining eggs, number of approximately 954, placed

CHAPTER TWO

Materials & Methods

into 3 Ete glass bottles (Pyrex) maintained under constant temperature of 10°C. Culture medium was supplied to circulate the eggs and was sterilized by autoclaving at approximately one

Following hatching and until the larvae were released from the bottom of the incubation tanks, the larvae were held in bottles having a 7 mm internal diameter. Thereafter, one larva at a time was removed from the bottom of each bottle (twice daily) and held in a sterilized vial. Midway through the yolk-sac stage, approximately 10 days post-hatch, larvae were fed with the marine roach *Brevoortia hoyi* (Diel et al., 1980) at 10% body weight. The roach were cultured in plastic containers (200 ml) containing a mixture of yeast extract and the unicellular green algae *Chlorella vulgaris*. The growth rate of the sterilized roach was measured as follows:

2.1. Rearing and Handling of Larvae**2.1.1. Culture methods**

Eggs of the turbot *Scophthalmus maximus* L. were obtained from Golden Sea Produce, Hunterston, Scotland. Each batch had been stripped from a single female, induced to spawn using a controlled photoperiod, and fertilised by the sperm of a single male. Following transportation to the University aquarium in insulated containers, the eggs were allowed to stand for approximately 30 min. Live eggs are transparent and buoyant, while dead eggs become opaque and sink (Jones, 1972), thus sunken and opaque eggs were discarded. The remaining eggs were subdivided into batches of approximately 500, placed into 5 litre glass beakers containing filtered seawater of 34‰ salinity, and incubated under continuous subdued lighting conditions at a temperature of 15°C. Gentle aeration was supplied to circulate the eggs and provide sufficient dissolved oxygen. Approximately one quarter of the water was replaced daily with fresh, filtered seawater.

Following hatching, egg cases and unhatched eggs were removed from the bottom of the incubation beakers by siphoning with a flexible tube of 2 mm internal diameter. Thereafter, one third of the water volume was siphoned off from the bottom of each beaker twice daily and replaced with fresh filtered seawater. Midway through the yolk-sac stage, approximately 3 days post-hatching, larvae were fed with the marine rotifer *Brachionus plicatilis* Müller at a density of 5 rotifers per ml. The rotifers were cultured in plastic containers (20-30 litres in volume) with bakers yeast, vitamin premix and the unicellular alga *Nannochloropsis* sp. The density of rotifers within the incubation beakers was measured by taking five random 1 ml samples from each, using a one millilitre

graduated pipette, and counting the rotifer number whilst in the pipette. The daily addition of new rotifers could then be adjusted accordingly to replenish the existing rotifer stock (5 per ml). *Nannochloropsis* was also added daily to the incubation beakers as a “conditioner”, both to control the water quality and provide a supplementary feed to maintain the rotifer population.

From 10 days post-hatching, larvae were fed with freshly hatched brine shrimp nauplii, *Artemia salina* (L.). The *Artemia* eggs (EG grade, Artemia Systems, N.V. Can: 061553; 2 g.l⁻¹) were hatched at 25°C in strongly aerated, filtered sea water (34‰). After hatching, the nauplii were separated from the shells and unhatched cysts, rinsed thoroughly, and added to the incubation beakers at a density of 4 nauplii per ml.

2.1.2. Specimen selection

In the following investigation, turbot larvae were sampled at four distinctive stages during their early development (Table 2.1). Post-yolksac specimens were always sampled from within the water column where they swam freely and were typically active, exhibiting the normal hunting behaviour. Only larvae with a straight notochord were selected (Hahnenkamp *et al.*, 1993) and darkly pigmented larvae were typically rejected; the dark colour serving as an indication of the poor health/decline of a larva (Cousin & Baudin Laurencin, 1987).

Table 2.1. A description of the stages of larval *S. maximus* used in the present study, based mainly upon their morphological characteristics (adapted from Al-Maghazachi and Gibson, 1984).

Stage	Sub stage	Age post [†] hatching	Length [*] (mm)	Morphological Characteristics
1				Larvae symmetrical, yolksac present:
	1a	Day 1	2.2 ±0.15	Head bent downwards and attached to yolksac; large quantities of yolk and one oil globule present; gut almost a straight tube.
<hr/>				
	1c-1d	Day 4-6	2.9 ±0.13	Yolksac being absorbed; mouth and anus opening; development and ventral bending of intestine; primordial dorsal fin extending above eyes; onset of feeding.
2				Larvae symmetrical, development of spines and air bladder:
	2b-2c	Day 8-10	3.6 ±0.15	Gut with loop; intestine reaching abdominal wall; swimbladder visible in depression of gastro-intestinal space; numerous spines on operculum; bony ridge above eyes; primordial dorsal fin extending above auditory sac.
3				Appearance of fin rays, notochord straight:
	3a-3b	Day 11-13	4.8 ±0.20	Swim bladder fully inflated; hypural fin rudiment very small; up to seven fin rays present; extension of fin margin.

[†] At an incubation temperature of 15°C
^{*} Mean ±S.D.(n=10), from present study

2.2.

Histological Procedures

2.2.1. Transmission electron microscopy (TEM)

A. Fixation and embedding

Selected larvae were fixed by immersion in a modified Karnovsky's mixture, consisting of 2% paraformaldehyde plus 2.5% gluteraldehyde buffered with 0.2 M sodium cacodylate (pH 7.2) (Appendix A), for 3-4 h at room temperature (Karnovsky, 1965). The larvae were then washed in several changes of the cacodylate buffer over a 2 h period and post-fixed in 1% osmium tetroxide in 0.2% sodium cacodylate for 4 h in a fume cupboard. This method is considered to preserve all cell components well, especially microtubules. The formaldehyde penetrates faster than the gluteraldehyde and temporarily stabilises structures that are subsequently stabilised by gluteraldehyde (Karnovsky, 1971; Cioni *et al.*, 1991).

Following fixation, the specimens were dehydrated through a graded series of ethanolic solutions (Appendix B) and left overnight in a 1:1 mixture of ethanol and LR White medium grade acrylic resin (London Resin Company). The next day, they were transferred into 100% LR White for 24 h. Finally, the larvae were embedded with fresh resin in polypropylene bean capsules by incubation in an oven at 60°C for 22 h.

B. Section cutting and staining

For light microscopy, semi-thin (0.5 µm) sections of larvae were cut using a Reichert OM-U3 Ultramicrotome (C. Reichert, Austria) equipped with a glass knife. The sections were placed on a water droplet on a microscope slide and dried with a hotplate at 60°C. They were then stained with methylene blue for approximately 40 seconds and mounted beneath

a coverslip using Pertex mounting medium. Observations were made using a Zeiss standard RA microscope and camera lucida drawings were made of the epithelial perimeter of selected transverse sections.

Subsequently, ultrathin sections (70-90 nm) with gold interface colours were cut for electron microscopy with the Reichert OM-U3 Ultramicrotome using a diatome diamond knife. The sections were collected on formvar-carbon coated, 200 mesh copper grids and double stained, first with 8% uranyl acetate (Pease, 1964) for 20 minutes in the dark, and next with lead citrate (Reynolds, 1963) for an additional 5 minutes. Finally, the grids were washed with 0.02 M NaOH, rinsed with distilled water and air dried.

Observations were made using a JEM-100C transmission electron microscope (JOEL Ltd., Japan) operated at 80 kV, and electron micrographs were taken on Kodak 4489 EM film. The thickness of the skin was measured from electron micrographs at either $\times 3,500$ or $\times 5,000$ magnification at three points along the cell membrane of each randomly selected cell from four larvae.

2.2.2. Scanning electron microscopy (SEM)

For SEM, whole larvae were immersed in modified Karnovsky's fixative for 1-2 weeks; this long fixation period ensuring removal of the exterior mucous coat covering the surface epithelium (Mattey *et al.*, 1980). On removal from the fixative, the larvae were washed in several changes of sodium cacodylate buffer (pH 7.2) over a 2 h period and then dehydrated through a graded series of either ethanol or acetone concentrations (Appendix B). This was followed by drying for 2 h with liquid CO₂ in a critical point dryer (E-3000, Polaron Equipment Ltd.) using acetone as a transitional fluid. The larvae

2. Materials & Methods

were then mounted on aluminium stubs, using sticky pads and silver paint, and coated with 90-120 nm of gold/palladium using an Edwards B150S Sputter Coater (British Oxygen Co. Ltd.). Observations were made using an ISI-60A scanning electron microscope (International Scientific Instruments, U.K.) operated at 15 kV. Micrographs were recorded on Ilford FP4 roll film.

2.3.

Vital Staining with Fluorescent Probes

2.3.1. DASPMI (2-(4-Dimethylaminostyryl)-1-methylpyridinium iodide) staining

DASPMI (Sigma), a vital stain binding specifically with mitochondrial protein (Bereiter-Hahn, 1976), was used to identify mitochondrion-rich chloride cells in the skin of turbot larvae to assess the density and distribution of these cells during early larval development. When placed in a bathing solution containing DASPMI, larvae were shown to rapidly absorb this highly permeant probe; the procedure requiring only that sufficient time was allowed for diffusion into the cells and adequate aeration was provided to maintain metabolism. Thus, larvae were incubated in 0.095 g.l⁻¹ DASPMI in aerated, 34‰ sea water for 3 h at 15°C.

Following exposure, larvae were removed from the DASPMI solution using a wide mouth, fire-polished pipette, and trapped by filtering them through an electron microscope capsule (modified with enlarged pores to allow this process). The larvae were then thoroughly rinsed by sequentially passing them through four specimen jars each containing 3 ml of fresh filtered sea water at the corresponding salinity and temperature. To facilitate microscopical examination, particularly for the purpose of photography, the larvae were finally transferred into an anaesthetic bath containing 20 mg.l⁻¹ benzocaine in seawater. Individual larvae were then placed, in several drops of this solution, onto glass cavity microscope slides and were covered with glass cover slips. A Zeiss standard RA microscope modified for epifluorescence with a 100 W mercury lamp, a 450-490 nm band-pass excitation filter, 510 nm chromatic beam splitter and a 515-565 nm longwave pass (FITC) filter were used to examine the larvae for DASPMI staining. Photographs were taken on 400 ASA Fujichrome colour slide film.

2.3.2. Anthroylouabain staining

Other larvae were treated with anthroylouabain (Sigma), a fluorescent stain with a high specificity for Na^+,K^+ -ATPase (Fortes, 1977; McCormick 1990). Following anaesthesia in 20 mg.l^{-1} benzocaine in seawater, an isosmotic solution of 0.1 mM.l^{-1} anthroylouabain in physiological saline (formula after Johnston in Lockwood, 1963) was delivered into the blood circulatory system of selected larvae by injection through a micropipette.

The injection system consisted of the two parts illustrated in figure 2.1: a syringe and micrometer drive (top) and a micropipette holder (bottom) which was fastened to a micromanipulator. Micropipettes were prepared from borosilicate glass capillaries (GC150TF-10, Clark Electromedical Instruments, UK) which were pulled to produce tip sizes of $0.3\text{-}0.6 \mu\text{m}$ using a Narishige Type-PE2 vertical two-stage micropipette puller (Narishige Instrument Laboratories, Japan). The pipettes were backfilled to the shoulder with anthroylouabain solution using a Microfil 34 gauge syringe needle (67 mm in length) equipped with a $0.2 \mu\text{m}$ pore Anatop filter (World Precision Instruments, USA). About 3 mm of paraffin oil was then placed into the pipette and the remainder of the barrel was backfilled with distilled water; the paraffin oil serving as an immiscible membrane between the two solutions. After the pipette holder, catheter tubing and precision syringe (illustrated in Fig. 2.1) had also been filled with distilled water, and once all air bubbles had been eliminated from the system, the micropipette was then carefully inserted into the holder and sealed by compression of an O-ring. Finally, the injection system was tested before use by ejecting controlled volumes of the fluorochrome into a water saturated paraffin oil bath.

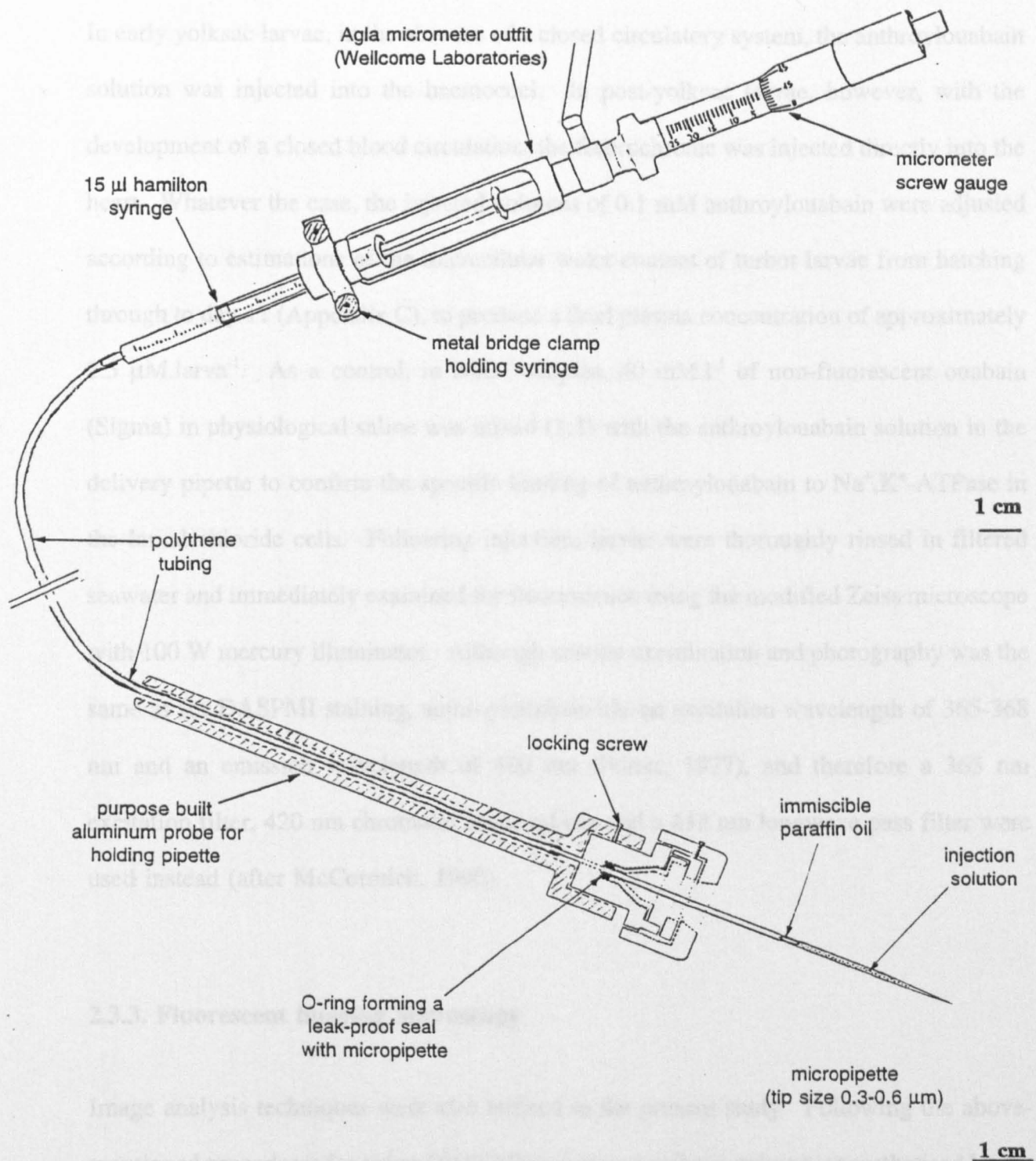


Fig. 2.1. Schematic illustrations detailing the microinjection set-up used in the present study. The system pressure was generated by a micrometer outfit which was used to drive the plunger of a precision microlitre syringe (top). Solution could thus be ejected through the tip of a micropipette in a controlled manner. The purpose built micropipette holder (bottom) was fastened to a micromanipulator allowing positional control of the delivery pipette tip.

In early yolk sac larvae, in the absence of a closed circulatory system, the anthroylouabain solution was injected into the haemocoel. In post-yolk sac larvae, however, with the development of a closed blood circulation, the fluorochrome was injected directly into the heart. Whatever the case, the injected volumes of 0.1 mM anthroylouabain were adjusted according to estimations of the intercellular water content of turbot larvae from hatching through to day 11 (Appendix C), to produce a final plasma concentration of approximately 2.5 $\mu\text{M.larva}^{-1}$. As a control, in some samples, 40 mM.I⁻¹ of non-fluorescent ouabain (Sigma) in physiological saline was mixed (1:1) with the anthroylouabain solution in the delivery pipette to confirm the specific binding of anthroylouabain to Na⁺,K⁺-ATPase in the larval chloride cells. Following injection, larvae were thoroughly rinsed in filtered seawater and immediately examined for fluorescence using the modified Zeiss microscope with 100 W mercury illuminator. Although routine examination and photography was the same as for DASPMI staining, anthroylouabain has an excitation wavelength of 365-368 nm and an emission wavelength of 480 nm (Fortes, 1977), and therefore a 365 nm excitation filter, 420 nm chromatic beam splitter and a 418 nm longwave pass filter were used instead (after McCormick, 1990).

2.3.3. Fluorescent imaging microscopy

Image analysis techniques were also utilised in the present study. Following the above-mentioned procedures for either DASPMI or anthroylouabain staining, anaesthetised larvae were examined using an Olympus (BHS) microscope incorporating a reflected light fluorescence attachment (BH2-RFC) with a 100 W u.v. mercury lamp and the appropriate excitation filters (as above). Fluorescent images of DASPMI or anthroylouabain-stained chloride cells were detected and captured by a Hamamatsu C2400 video camera

2. Materials & Methods

(Hamamatsu Photonics, Japan). The captured images, based on the integration of 180 scans over 5 seconds, were subsequently analysed using an image-processing software package (Image 1.38) run on an Apple Macintosh Quadra 900 computer.

Images of DASPMI-stained chloride cells were simply analysed for area, but in anthroylouabain-stained cells further measurements of the mean and total fluorescence (area \times mean fluorescence) were also determined. For the latter analysis, larvae were initially examined under low power magnification and reduced transmitted light illumination to prevent photobleaching of the fluorochrome-stained cells. Having selected a suitable field of view, the light source was shuttered whilst the high power $\times 40$ objective was set in place. The larval skin was then fully exposed to the mercury light source and images of the anthroylouabain-positive chloride cells were captured accordingly. Photographs of the video images were taken on Polaroid colour slide film.

2.4. Water Turnover Rates, Surface Area Estimates and Diffusional Water Permeabilities

Measurements of the influx of water were made from stage 1a 1c-d and 2b-c turbot larvae respectively. For each stage, two hundred larvae were transferred into a 100 ml glass beaker containing 80 ml of seawater filtered through a 0.22 µm micropore. The beaker was sealed and placed into a water bath maintained at 15°C, the incubation temperature of the larvae. A 40 µl volume of tritiated water (185 MBq.ml^{-1}) (Amersham International plc, England) was added to the beaker volume and mixed thoroughly to produce a working solution containing approximately $1.5 - 3.0 \times 10^7 \text{ cpm.ml}^{-1}$.

Four samples each containing five larvae were removed from the radiolabelled solution at regular intervals over a 7 h period, and then finally at 24 h to obtain an equilibrium level. The larvae were caught with a wide-mouthing, fire polished pipette and trapped by filtering them through a tea strainer held over the exposure beaker. They were washed by sequentially passing the tea strainer through three wash baths, each containing 100 ml of fresh filtered seawater, over a 4-5 minute period. Fine forceps were used to remove the larvae from the final wash bath, and after carefully dabbing dry with a folded Kleenex medical wipe, the four samples were each placed into separate Pico Prias scintillation vials (Packard) containing 0.5 ml of Soluene-350 (Packard). The vials were then left overnight, at room temperature, to dissolve.

The following day, 5 ml of scintillation fluid (Hionic Fluor, Packard) was added to each vial. The vials were then mixed thoroughly by vigorous shaking and placed in the dark for approximately 1 h to allow stabilisation. Subsequently the radioactivity was assayed

2. Materials & Methods

using a Tricarb 2000CA liquid scintillation analyzer (Packard Instrumentation Co. Inc., USA).

Rate constants of influx and equilibrium levels of the tritiated water were calculated from the time courses of uptake of radioactivity by each larval stage. These parameters were analysed using the first-order rate equation after Motais & Isaia (1972):

$$Q = Q_{\text{limit}} (1 - e^{-K_i \cdot t}) \quad (2-1)$$

which gave estimates of the equilibration radioactivity levels within larvae (Q_{limit}) and the rate constants of ${}^3[\text{H}_2\text{O}]$ uptake (K_i), where Q is the radioactivity of the larvae at time t after initial exposure to the ${}^3[\text{H}_2\text{O}]$.

The diffusional permeability coefficients (P_{diff}) were calculated from the equation after Motais & Isaia (1972) and Tytler & Bell (1989):

$$P_{\text{diff}} = \frac{F_{\text{trit}}}{A \cdot [\text{H}_2\text{O}]} \quad \text{cm} \cdot \text{s}^{-1} \quad (2-2)$$

where F_{trit} is the influx of tritiated water (mM.s^{-1}), A is the surface area of the larva (cm^2) and $[\text{H}_2\text{O}]$ is the internal water concentration (mM.cm^{-3}).

Measurements for the calculation of the surface area of larvae were made with an eyepiece micrometer. Due to the difficulty in measuring the surface area of an irregular surface, estimates of the surface areas of newly hatched, stage 1a larvae were calculated considering the yolksac to be a sphere ($4\pi r^2$) and the tail a cone (πrl). For post-yolksac stages, however, the surface area was calculated as being equal to a cylinder (πdl) where

2. Materials & Methods

d was the average depth of five measurements taken at the following positions along the body: (i) through the midpoint of the eye; (ii) halfway between the eye and the anus (through the mid-gut region); (iii) immediately posterior to the anus; (iv) between the anus and the base of the caudal fin; and (v) just anterior to the base of the caudal fin. In fact, the mean value of d was always close to the measurement made at position iv.

In addition, measurements of the individual wet and dry weights of larvae were also made to provide estimates of the water content and volume of larvae at each developmental stage. Excess water was dried from a sample of 10 to 20 larvae which were then weighed, using a sensitive electronic balance (Mettler HL52, Gallenkamp), to the nearest four decimal places. Dry weight measurements were made from oven-dried larvae showing no further weight change after reweighing at intervals. The individual body weights were determined simply by dividing the bulk weights of each sample by the number of individuals within each respective sample.

2.5.

Microelectrode Studies of the Skin

2.5.1. Preparation of microelectrodes

Conventional microelectrodes were prepared from thin-walled borosilicate glass capillaries (1.5 mm o.d. × 1.17 mm i.d.) (GC150TF-10, Clark Electromedical Instruments), cleaned in concentrated nitric acid. They were pulled immediately before use on a vertical two-stage micropipette puller (Narishige Type PE-2, Narishige Instru. Lab. Japan); the first stage of the pull provided by gravity and the final pull adjusted by current flowing through a solenoid. The micropipettes¹ were stored with their tips immersed in distilled water, accomplished by pressing the pipette stems into a ring of modelling clay that was adhered to the top/inside of a 100 ml beaker, where they were left until use. This prehydration of the tips, as observed by Thomas (1978), seemed to help stabilise the electrical properties of the microelectrode.

Pipette tips were filled by capillarity and the barrels were backfilled individually with 3 M KCl using a 34 gauge Microfil syringe needle (World Precision Instruments, USA). Trapped air bubbles remaining in the shoulder of the pipette were dislodged by either gently tapping the pipette barrel or by using the heat from a 40 W light bulb. Microelectrode resistance (R_{ME}) varied between 10 and 25 MΩ when measured in 3 M KCl.

2.5.2. Animals

Larvae were caught with a wide-mouth, fire-polished pipette and trapped by filtering the water through an electron microscope capsule with a mesh base which was then placed

¹ Following the usage of Thomas (1978), the fine tipped tapering glass capillary tube will be called a micropipette. When filled with electrolyte solution and used for measuring potentials it becomes a microelectrode. Strictly it is not an electrode at all; the real electrode is the junction between the metal, usually silver, and electrolyte in the stem of the micropipette.

into a 5 ml specimen jar containing benzocaine anaesthetic (20 mg.l^{-1}) made up in artificial seawater (ASW). Not only were the larvae suitably confined for examination and staging by this method, but they could also be transferred within the microscope capsule from one specimen jar to another for the administration of drugs and/or changes in seawater composition.

Following anaesthesia, larvae were then placed into $1.25 \times 10^{-6} \text{ M}$ α -bungarotoxin in benzocaine-ASW for approximately 10 minutes. The α -bungarotoxin was used to effectively immobilise the larvae by blocking the movement of acetylcholine at the neuromuscular endplates. In turbot aged beyond day 6-7 post-hatching the skin often had to be scored for the neuromuscular blocking action of this toxin to take effect. In this case, the larva was anaesthetised as before but then its fins were lightly "nicked" with a pin before placing it into the α -bungarotoxin.

2.5.3. Experimental set-up

A small glass bathing dish (radius 17 mm, height 16 mm) was constructed into which a 6 mm basal layer of Sylgard silicone plastic was dispensed and allowed to harden. A thin Sylgard platform (approximately $20 \times 20 \times 2 \text{ mm}$) was also made and this was placed into the glass dish and secured to the basal silicone layer by pins. Several troughs were cut into the translucent platform, appropriately shaped and of a size suitable for holding or confining larvae, into which immobilised specimens were placed and shallowly immersed in benzocaine-ASW (Fig. 2.2). According to Thomas (1978), "the importance of anchoring a preparation is fundamental in facilitating and maintaining microelectrode

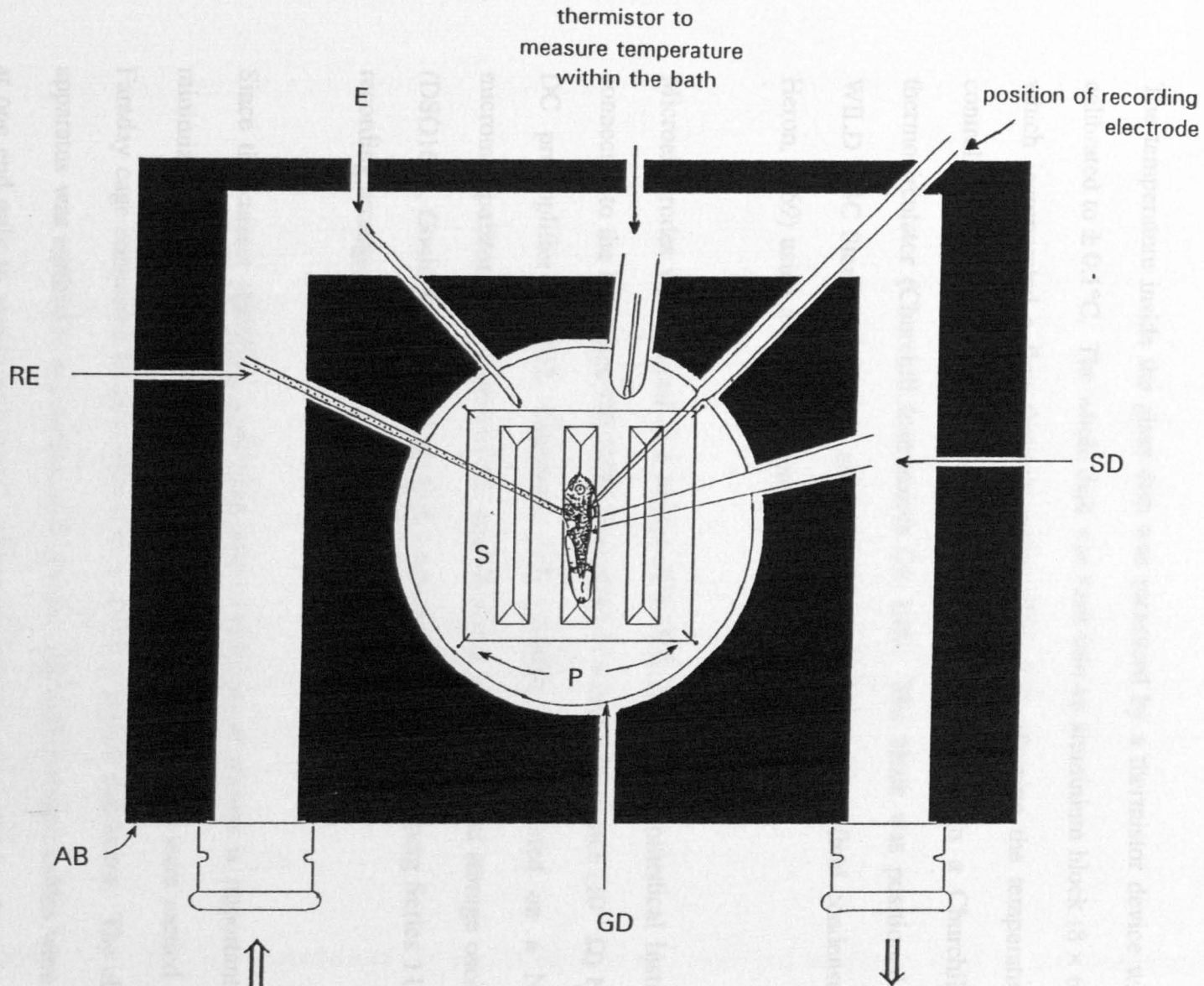


Figure 2.2. Diagram showing the positioning of a fish larva and electrodes for recording. AB - aluminium block incorporating flow through system; E - earth to bath; GD - glass dish containing seawater bathing medium; P - pins; RE - reference electrode; S - sylgard platform with troughs; SD - suction device.

impalements". To this end a suction device was constructed to hold the larva firmly, thus assisting electrode impalements.

The temperature inside the glass dish was measured by a thermistor device which was calibrated to $\pm 0.1^{\circ}\text{C}$. The whole dish was sunk into an aluminium block ($8 \times 6 \times 3$ cm) which incorporated a flow-through system (Fig. 2.2) allowing the temperature to be controlled either above or below ambient by a coolant from a Churchill chiller thermocirculator (Churchill Instruments Co. Ltd). The block was positioned under a WILD M3C Stereo-microscope and was illuminated by a 'dark field condenser' (after Heron, 1969) using a cold light source directed from below.

Microelectrodes were placed in a holder (EH-3MS, Clark Electromedical Instruments) connected to the headstage (NL102G Neurolog) of a high impedance ($10^{11} \Omega$) Neurolog DC preamplifier (NL102, Digitimer, U.K.) which was mounted on a Narishige micromanipulator. The output of the amplifier was fed to a digital storage oscilloscope (DSO1604, Gould Electronics Ltd. U.K.) and tape recorder (Tandberg Series 115). The recording arrangements are presented in figure 2.3.

Since the correct shielding, grounding and referencing of signals is important for the minimization of noise (Purves, 1981), all electrical measurements were carried out in a Faraday cage connected to an independent earth by a copper conductor. The electronic apparatus was earthed to a common point in the cage and screened cables were earthed at one end only to avoid earth loops. The bath solution was referenced to the ground isolated common of the preamplifier.

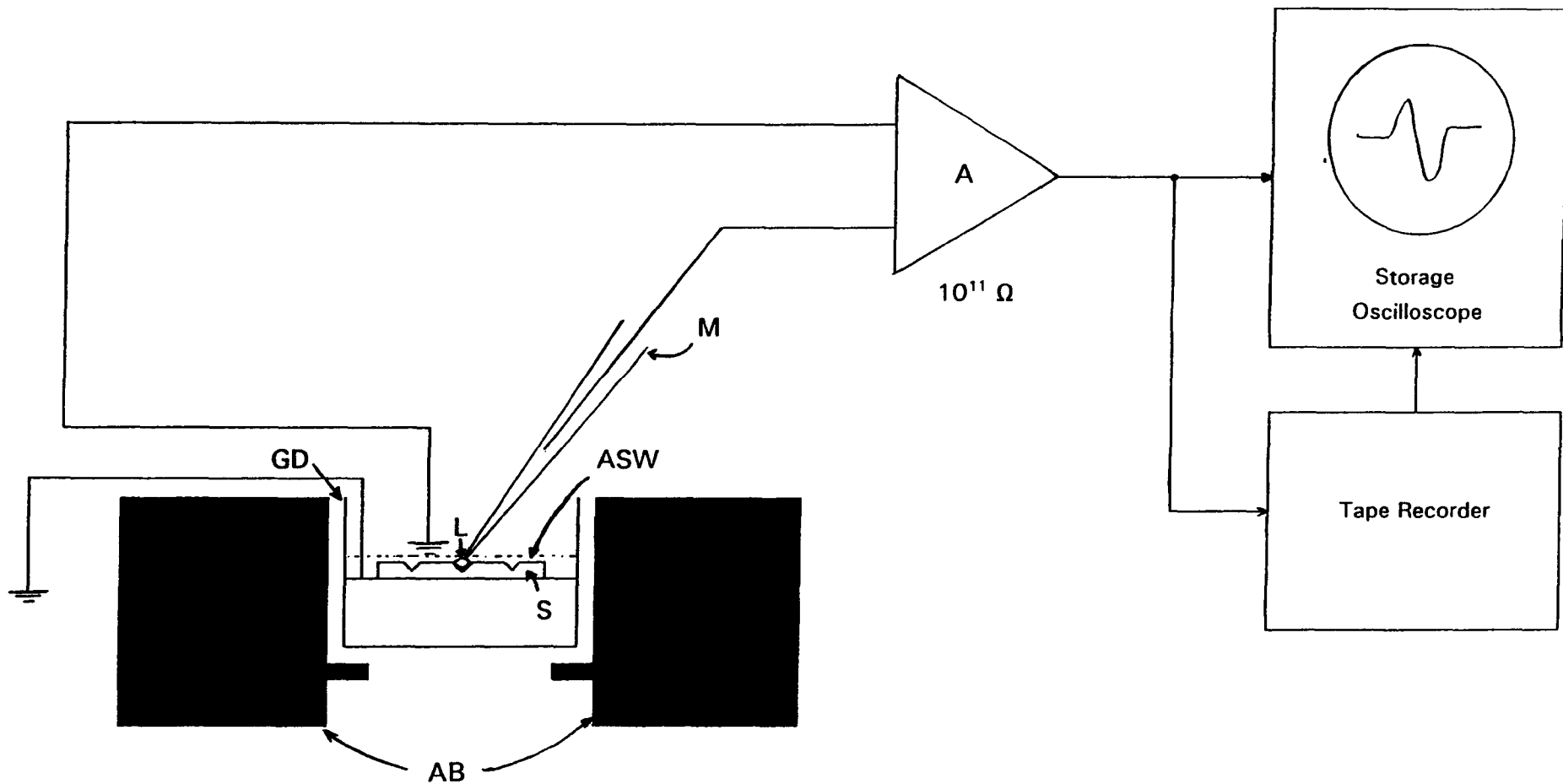


Figure 2.3. Diagrammatic representation of the recording dish and electrical apparatus used in the measurement of transepithelial electrical potentials in larval turbot. A - amplifier; AB - aluminium block with through-flow system; ASW - artificial seawater bathing medium; GD - glass dish with basal layer of silicone plastic; L - turbot larva; M - microelectrode; S - sylgard platform.

2.5.4. Potential measurement

The transepithelial potential (TEP) was recorded from turbot larvae by measuring the internal electrical potential (voltage) within the fluid-filled body cavity, using a conventional glass microelectrode, with respect to an external silver/silver chloride reference electrode lying adjacent to the larva in the bathing medium.

Recording microelectrodes were manually advanced under stereomicroscopic observation in a direction perpendicular to the surface of the larval skin. Before a microelectrode penetrated the body cavity, the potential difference (p.d.) between it and the reference electrode was zero. As the tip of the recording electrode was advanced slowly, however, a change in potential was registered on the storage oscilloscope as a shift in the voltage trace, indicating penetration into the internal fluid-filled space. The p.d. between the body cavity and external medium represented the transepithelial potential.

Impalements were only accepted as successful when the following criteria were fulfilled: (i) the change in recorded potential was abrupt on penetration of the body cavity; (ii) the recording remained stable within 1-2 mV immediately after impalement; (iii) slight vertical movements of the microelectrode up and down did not affect the measured potential or the resistance of the microelectrode (R_{ME}); (iv) the microelectrode was not obstructed during penetration, thus $\Delta R_{ME} < 25\%$; and (v) near identical measured potentials (within 2 mV) were obtained in repeated impalements. Such criteria have been shown to reflect the quality of a careful impalement in various microelectrode studies on epithelia (Nagel, 1976; Zeuthen, 1978; Nagel & Essig, 1982; Schöen & Erljij, 1985).

2.5.5. The effect of temperature on TEP measurement

In order to determine whether or not the observed potentials were dependent upon an electrogenic component, the effect of temperature was investigated. Eggs were incubated at 10, 15 and 20°C respectively in batches of approximately 300 in 3 litre beakers containing freshly filtered, aerated seawater. Larvae were reared as described in section 2.1. However, for larvae incubated at 20°C it was necessary to change the incubation water more frequently to minimize bacterial growth. TEP measurements were recorded as described earlier and larvae were maintained at their respective incubation temperatures throughout the recording procedure.

2.5.6. Ouabain inhibition

The Na^+,K^+ -ATPase inhibitor ouabain was also employed to determine whether the electrical potentials were dependent upon Na^+,K^+ -ATPase activity. Ouabain was delivered into the blood circulatory system of selected turbot larvae by injection through a micropipette. The ouabain was initially dissolved in dimethylsulfoxide (DMSO) and then made up into a 20 mM.l⁻¹ stock solution with physiological saline. The procedure for measuring the TEP was carried out as before. However, after determination of the potential, the isosmotic ouabain solution was injected into the haemocoel or heart of each larva (using the microinjection procedure and assumptions detailed in section 2.3.2 and appendix C respectively) to produce an estimated final ouabain concentration of 0.5 mM.larva⁻¹. The injection pipette was then removed and the TEP was further recorded for up to 10 minutes.

The addition of methylene blue to the ouabain solution provided a visible marker to ensure delivery of the inhibitor into the blood circulatory system.

2.5.7. The effect of salinity on TEP measurement

Post hatched larvae were incubated in 5 litre beakers for 4 days at 15°C and at salinities of 24, 34 and 44‰ respectively. Upon hatching, the salinity of each incubation beaker was altered progressively, over 36 hours, by the addition of distilled water or NaCl solution as appropriate. The TEP was recorded as before and all salinity values were checked using a refractometer calibrated against NaCl solutions of known concentration.

2.5.8. Ion substitution experiments

Na⁺ and Cl⁻ ions in the bathing solution were substituted with equimolar amounts of choline and methylsulphate ions respectively. To ensure that any changes in the TEP were due only to changes in the ionic composition of the bathing solution and were not the result of ionic flow due to osmotic effects, the osmolarity of all solutions was measured using a Wescor 5100C vapour pressure osmometer (Chelab Scientific Products, England). The ionic constituents and measurements of osmolarity for each solution are given in appendix D.

2.5.9. Theoretical considerations in TEP prediction

Models for the prediction of transepithelial potentials have generally centred on expansion of the Nernst equation² to that of the Goldman or constant field model which predicts the potential (in volts) in relation to the internal and external ion concentrations (in mM) of the major ion species and their relative permeabilities (Goldman, 1943). Hence, in terms of Na⁺ and Cl⁻:

$$E = \frac{RT}{F} \ln \frac{P_{Na}[Na^+]_o + P_{Cl}[Cl^-]_i}{P_{Na}[Na^+]_i + P_{Cl}[Cl^-]_o} \quad (2-3)$$

where E is the potential between the external seawater medium (**o**) and the larval body fluids (**i**), R is the gas constant (8.314), T is the absolute temperature (in degrees Kelvin), F is the Faraday constant (96487 g.equiv charge), and P_{Na} and P_{Cl} are the permeability constants for Na and Cl respectively. Thus, when P_{Na} and P_{Cl} are constant, the Goldman equation can be simplified to:

$$E = \frac{RT}{F} \ln \frac{[Na^+]_o + \alpha [Cl^-]_i}{[Na^+]_i + \alpha [Cl^-]_o} \quad (2-4)$$

where α is the ratio of Cl⁻ to Na⁺ conductance, i.e. permeability (P_{Cl}/P_{Na}).

Whilst this model has been effectively used in predictions of the TEP (House, 1963; Smith, 1969a; Evans, 1980b; Potts, 1984; Taylor, 1985), it is only based on the passive and independent diffusion of ions and does not take into account the effect of the electrogenic ionic movements. However, a second model, after Fletcher (1978b),

² For derivation of the Nernst equation see Appendix E.

describes the observed potential as the linear sum of the electrogenic potential and the product of the transport numbers and Nernst potentials of each permeant ion:

$$E = \sum t_i E_i + E_A \quad (2-5)$$

where t_i is the transport number of the permeant ion whose Nernst potential is E_i , and E_A is the electrogenic component.

This thermodynamically-based description provides a basis for interpreting and predicting how the electrical potential changes with salinity and inhibition (Potts *et al.*, 1991). If the permeability to divalent ions is negligible, and providing E_A remains constant, then when the ambient seawater is diluted or concentrated x times:

$$\delta E = (1 - 2t_{Cl}) \frac{RT}{F} \ln x$$

and thus,

$$\delta E = (1 - 2t_{Cl}) \delta E_N \quad (2-6)$$

where δE_N is the change in the Nernst potential and t_{Cl} is the transport number for chloride (Fletcher, 1978b). The transport numbers for both Cl^- and Na^+ can be determined using data from ion substitution studies. For either ion:

$$t = \frac{\delta E}{\delta E_N} \quad (2-7)$$

where δE is the change in potential observed when the concentration of an ion in the external medium is changed, and δE_N is the calculated change in the Nernst potential of

2. Materials & Methods

the same ion (Croghan *et al.*, 1965). It therefore follows, with reference to equation 2-5, that the diffusion component (E_D) of the transepithelial potential E can be defined as:

$$E_D = t_{Na} E_{Na} + t_{Cl} E_{Cl} \quad (2-8)$$

where E_{Na} and E_{Cl} are the Nernst potentials for Na and Cl respectively. Unfortunately, this is only strictly true if E_A remains almost constant, but in calculations of E_D using this approach, δE were kept small so that E_A was unlikely to change substantially.

Both of the above theoretical methods were used in predictions of the transepithelial potentials in turbot larvae in the present study.

2.6.

Solutions and chemicals

All solutions were made-up as close as possible to the time of use and many were refrigerated to minimize bacterial action. Stock solutions of artificial media were prepared separately each week and mixed as required.

The basic ASW used was prepared from the formula by Lyman & Flemming (1940) (in Sverdrup *et al.*, 1955) and comprised (in mM.l⁻¹): NaCl, 402.0; KCl, 8.9; CaCl₂, 9.9; MgCl₂, 52.4; Na₂SO₄, 27.6; NaHCO₃, 2.3; SrCl₂, 0.15; H₃BO₃, 0.42; NaF, 0.07; KBr, 0.8; oxygenated with 95% O₂/5% CO₂ to give a pH of 8.1.

Ouabain and its fluorescent derivative anthrooylouabain were initially dissolved in dimethylsulfoxide (DMSO) instead of ethanol, due to the reduced toxicity of DMSO. They were then made-up in teleost physiological saline containing (in mM.l⁻¹): NaCl, 142.0; KCl, 2.6; NaH₂PO₄.2H₂O, 3.2; NaHCO₃, 18.5; MgCl₂.6H₂O, 1.0; CaCl₂.2H₂O, 2.7 (after Johnston in Lockwood, 1963).

2.7.

Data analysis

All tabulated mean results are given as the mean \pm one standard error (\pm S.E.) (n = number of replicates). The differences between groups were tested using the paired students t-test and statistical significance was taken at the level of $P<0.01$. Student t-tests, regression analysis and analysis of variance were all performed using MINITAB Release 9 for Windows (Clecom Ltd., England).

3.1. The Ultrastructure and Development of the Larval Skin

3.1.1. General morphology of the larval skin

Scanning electron micrographs of the skin of the larvae larva showed that its surface was covered by a mosaic of polygonal pavement cells, separated by numerous mucous gland cells and occasional epidermal pores (Figs. 3.1 and 3.2). The pavement cells were clearly defined by prominent ridge border where adjacent cells abutted, and were covered with a more-or-less uniform layer of pale surface mucus. A distinct, though not well-defined, transverse striation was visible in some of the cells.

CHAPTER THREE

Results

In contrast to the multilayered cuticle found in the very first nymphal instar, the very thin epithelium of the larval cuticle, measured at 0.1–0.2 μ m in thickness in newly hatched larvae, was characterised by just two or three layers of columnar epidermal cells (Figs. 3.1 and 3.2).

The external plasmalemma of the epidermal cells (Figs. 3.3 and 3.4) to form the microridges observed in SEM, and its surface was covered by a thin and irregular filamentous layer, 0.1–0.25 μ m in diameter, containing the amorphous glycocalyx covering (Fig. 3.5). Neighbouring epidermal cells in the superficial layer were conspicuously anchored to one another by peripherally located interdigitations or desmosomes (Figs. 3.4 and 3.6), whereas those situated in deeper layers, since the lateral membranes of opposing cells did not come close to the apical surface, however, the opposing membranes of these adjacent cells were apparently fused at the cell apices by tight junctions (Fig. 3.7), which formed a complex network which completely encircled each cell, thus effectively preventing any exchange of material between the adjacent cells.

3.1. The Ultrastructure and Development of the Larval Skin

3.1.1. General morphology of the larval skin

Scanning electron micrographs of the skin of the turbot larva showed that its surface was covered by a mosaic of polygonal pavement cells, interrupted by numerous mucous gland cells and occasional epidermal pores (Figs. 3.1 and 3.2). The pavement cells were clearly defined by prominent ridge border where adjacent cells abutted, and were covered with a maze-like pattern of raised surface microridges, 0.1-0.15 μm in width (Fig. 3.3), which showed considerable variability in their surface sculpture.

In contrast to the multilayered epithelium of most adult teleost fish, the very thin epithelium of the larval turbot, measuring only $2.52 \pm 0.38 \mu\text{m}$ in thickness in newly hatched larvae, was comprised of just two outer layers of cells of irregular height (Figs. 3.4 and 3.5): a superficial layer and a basal layer of squamous pavement cells. The external plasmalemma of the superficial pavement cells was folded (Fig. 3.4) to form the microridges observed in SEM, and its surface was covered by a thin and irregular filamentous layer, 0.1-0.25 μm in thickness, constituting the extracellular glycocalyx covering (Fig. 3.5). Neighbouring pavement cells in the superficial layer were conspicuously anchored to one another by prominent intercellular bridges or desmosomes (Figs. 3.4 and 3.5), commonly forming "zipper-like" complexes along the lateral membranes of opposing cells (Figs. 3.5 and 3.6). Close to the epidermal surface, however, the opposing membranes of adjacent pavement cells were intimately fused at the cell apices by tight junctions or *zonulae occludens* (Figs. 3.5 and 3.6) which completely encircled each cell, thus fully occluding the extracellular space between the adjacent cells.

Fig. 3.1. Scanning electron micrograph of the epidermal surface from the mid lateral yolksac region of a newly hatched turbot larva ($\times 860$). Individual superficial pavement cells are each defined by prominent ridge borders. cb: cell boundary. Scale bar is 10 μm .

Fig. 3.2. Scanning electron micrograph of the skin surface of a stage 1c-d larva ($\times 1,300$). Note the numerous superficial mucous cells (MC), seen also in the previous micrograph, located at the intersection between adjacent pavement cells, and also the epidermal pit at the bottom centre of the micrograph, shown by arrowheads. Scale bar is 5 μm .

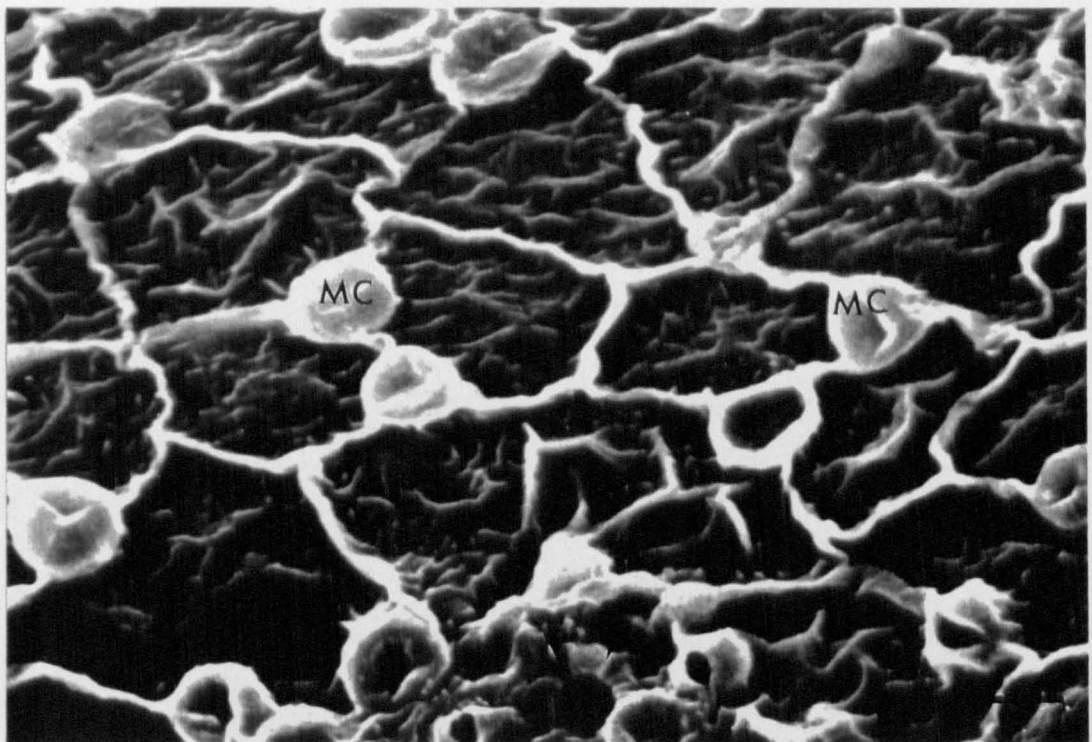
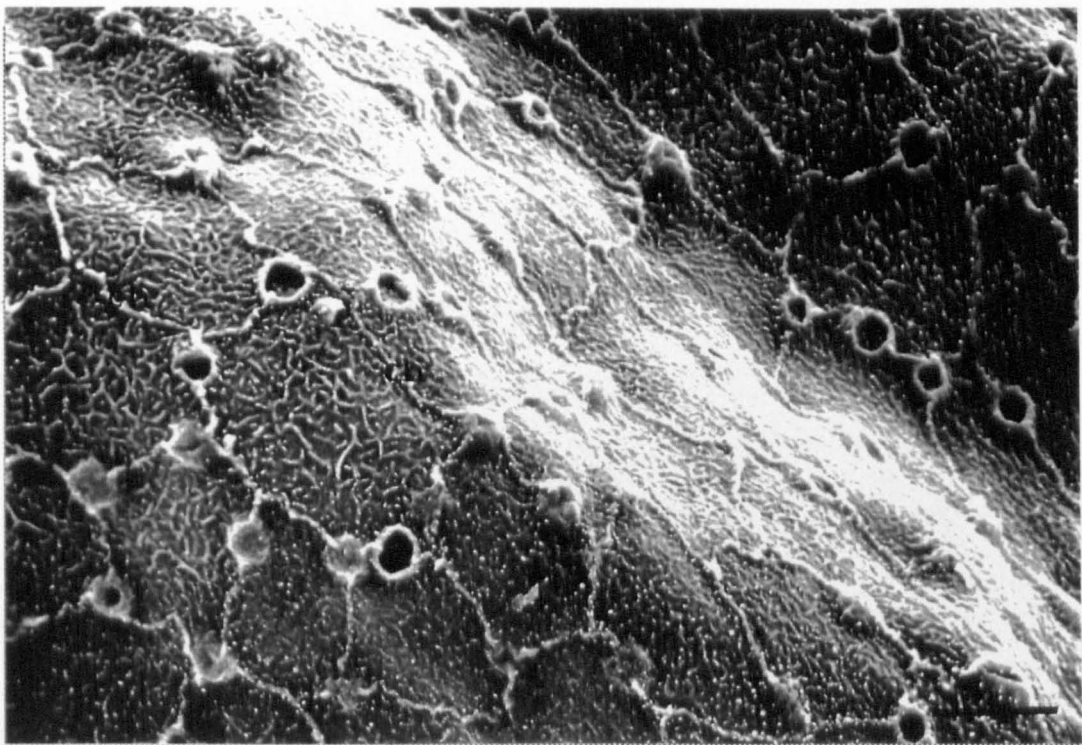
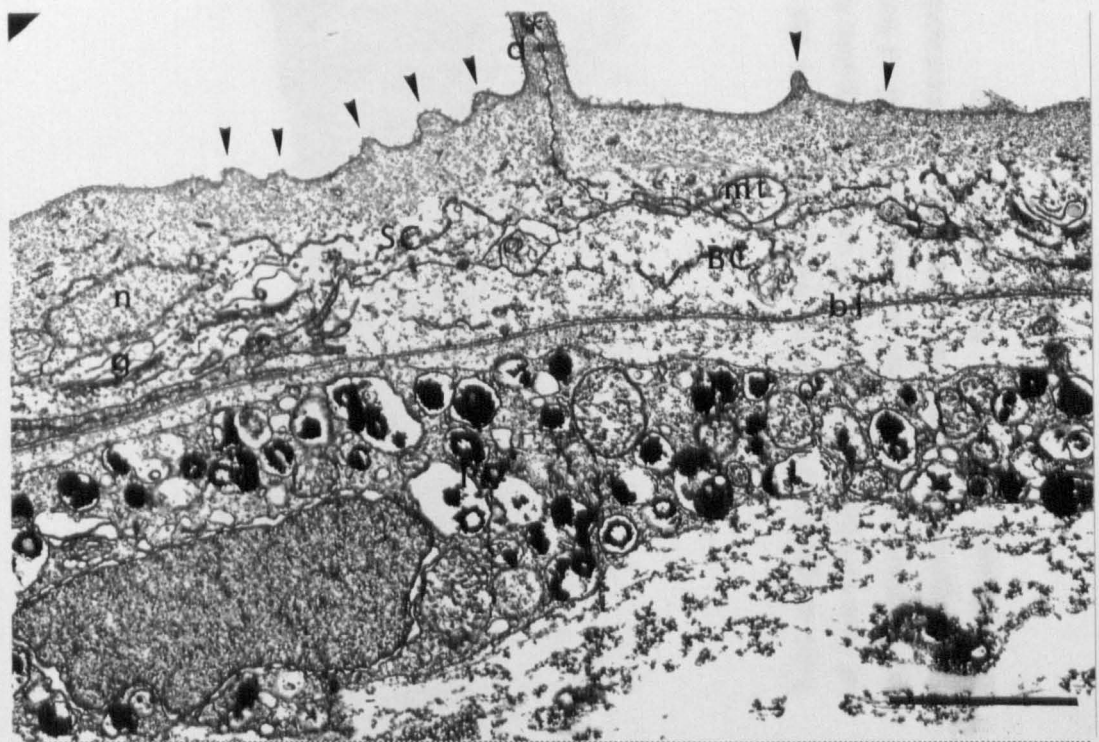
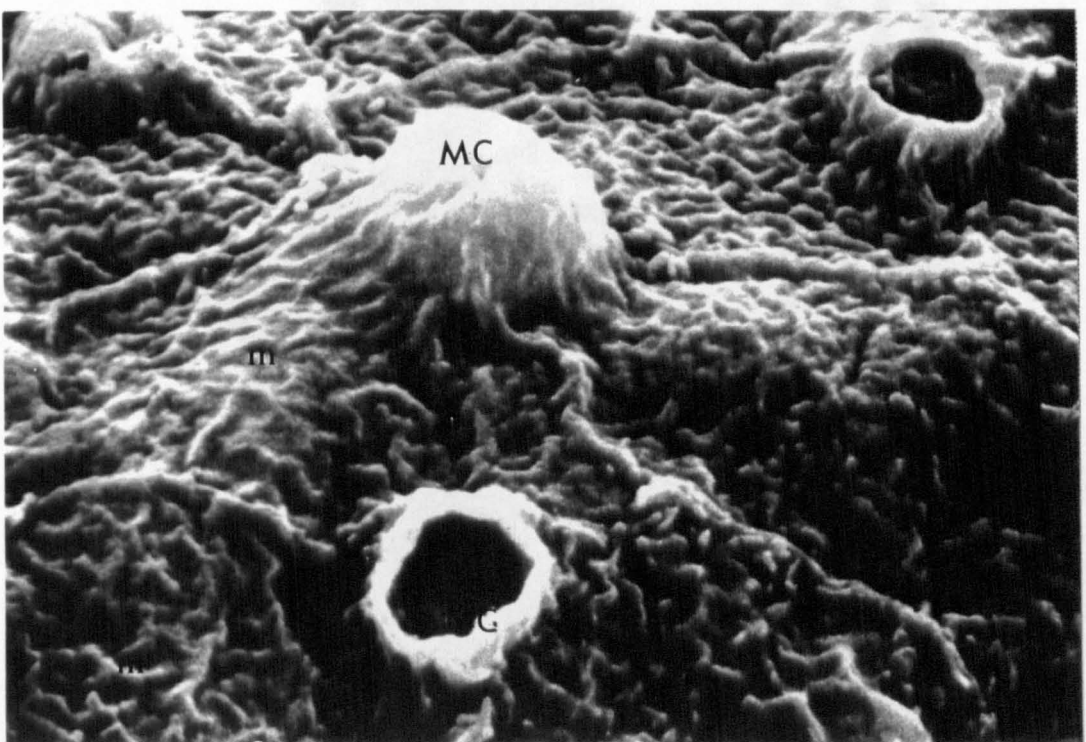


Fig. 3.3. Scanning electron micrograph from a stage 1a larva showing the numerous raised microridges (m) covering the external cell surfaces of the superficial pavement cells ($\times 3,000$). Note the irregular surface sculpture of the microridges. cb: pavement cell boundary; MC: mucous-producing cell. Scale bar is 3 μm .

Fig. 3.4. Electron micrograph of the dorsal skin of a stage 2 turbot larva ($\times 6,600$). Note the prominent ridge border (cell boundary) (indicated by asterisk) formed by abutting pavement cells in the superficial layer (SC). The microridges seen in SEM are indicated by arrowheads. BC: basal pavement cell layer; bl: basal lamina; d: desmosome; g: golgi apparatus; mt: mitochondria; n: nucleus; PC: immature pigment-containing cell. Scale bar is 2 μm .



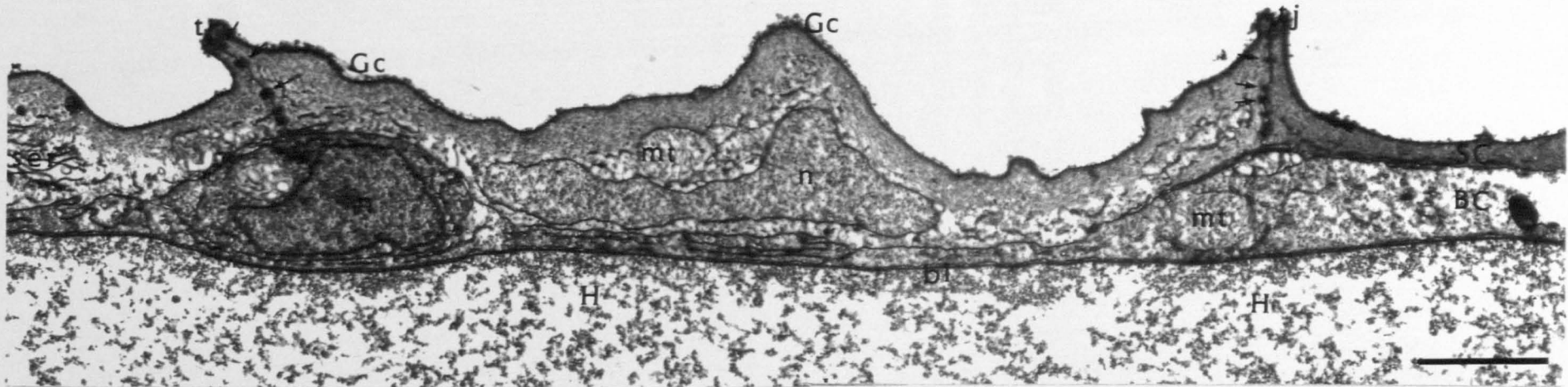
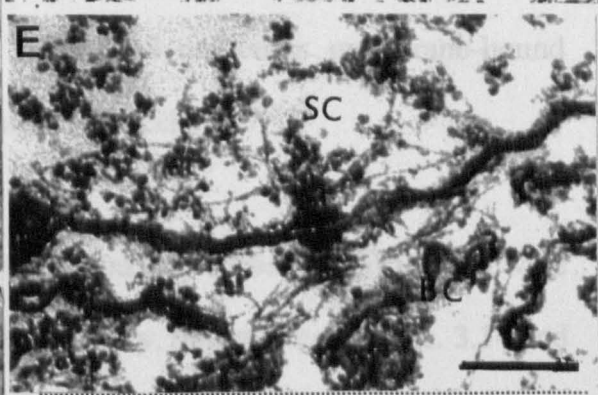
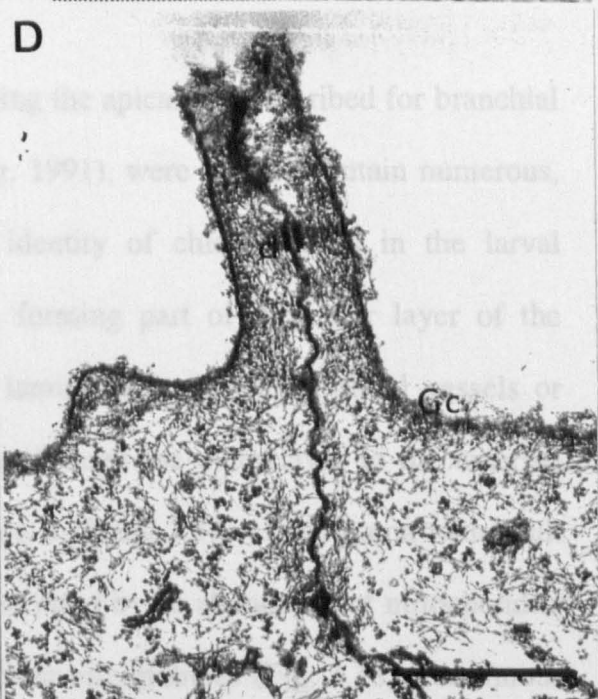
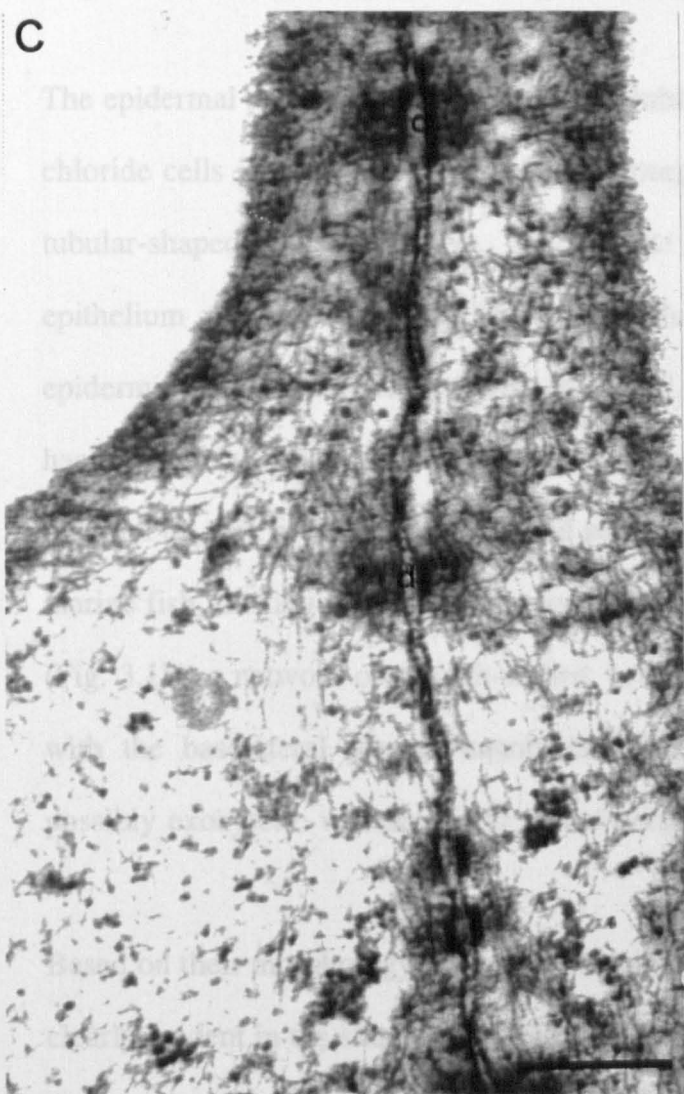
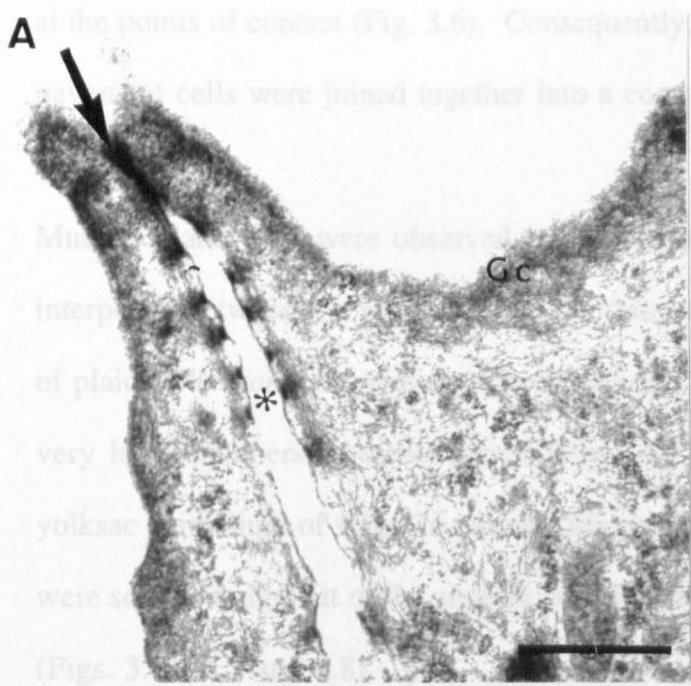


Fig. 3.5. Low magnification electron micrograph from the trunk region of a day 3 turbot larva ($\times 5,000$). The thin epidermis consists of just two layers of pavement cells of irregular height: a superficial layer of cells (SC), and a basal cell layer (BC) which is continuous with the basal lamina (bl). Contact between adjacent superficial cells is characterised by apical tight junctions (tj) and desmosomes (small arrowheads). Gc: extracellular glycocalyx layer; H: haemocoel; mt: mitochondria; n: cell nucleus; ser: endoplasmic reticulum. Scale bar is $2 \mu\text{m}$.

Fig. 3.6. Electron micrographs showing the junctional contact points between epidermal cells in the larval skin. A. and B. show the occluding apical tight junctions (arrows) between adjacent superficial pavement cells of stage 1a turbot ($\times 10,000$ and $\times 13,000$ respectively). Early desmosomes (d), without obvious tonofibrillar connections, can be seen along the lateral surfaces of opposing cells below the tight junctions. C. By developmental stage 1c, the desmosomal complexes are well formed between lateral cell membranes ($\times 33,000$). D and E. Micrographs showing desmosomes in the epidermis of a stage 2 larva, approximately 8 days after hatching. The example shown in E was found between the two layers of the epidermis, fastening the superficial cell later to the basal layer. *: Intercellular space, possibly an artefact; Gc: glycocalyx; tj: tight junction. Scale bars: micrographs A, B and D are 1 μm ; and C and E are 0.3 μm .



at the points of contact (Fig. 3.6). Consequently, the apical membranes of the superficial pavement cells were joined together into a continuous sheet.

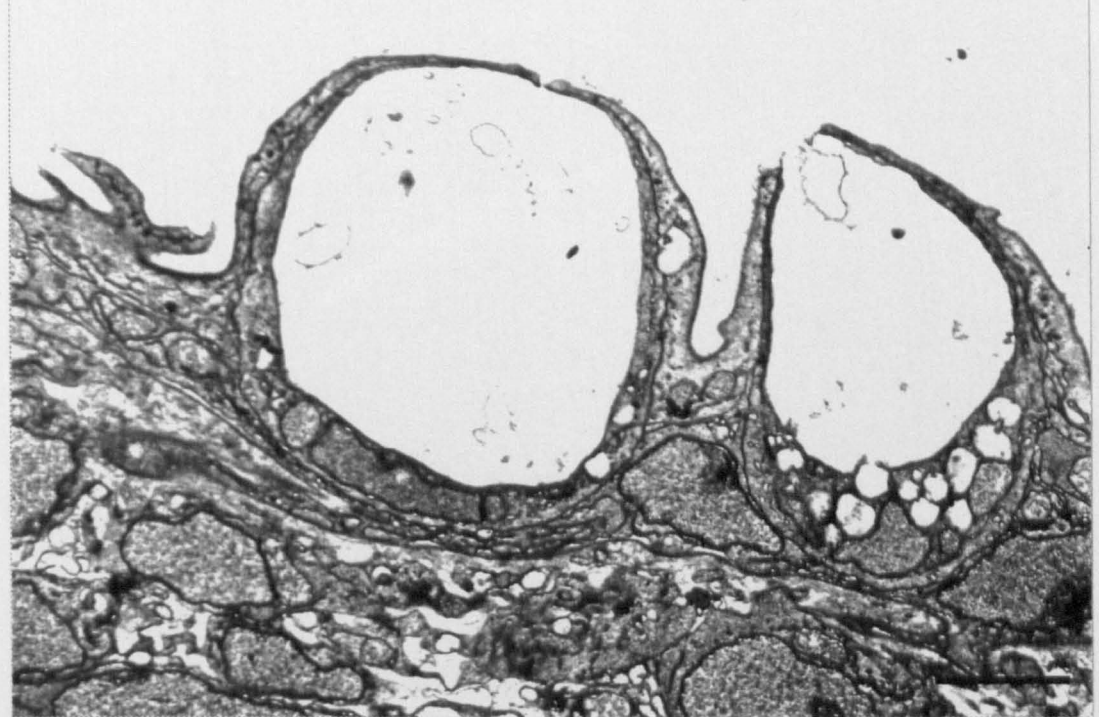
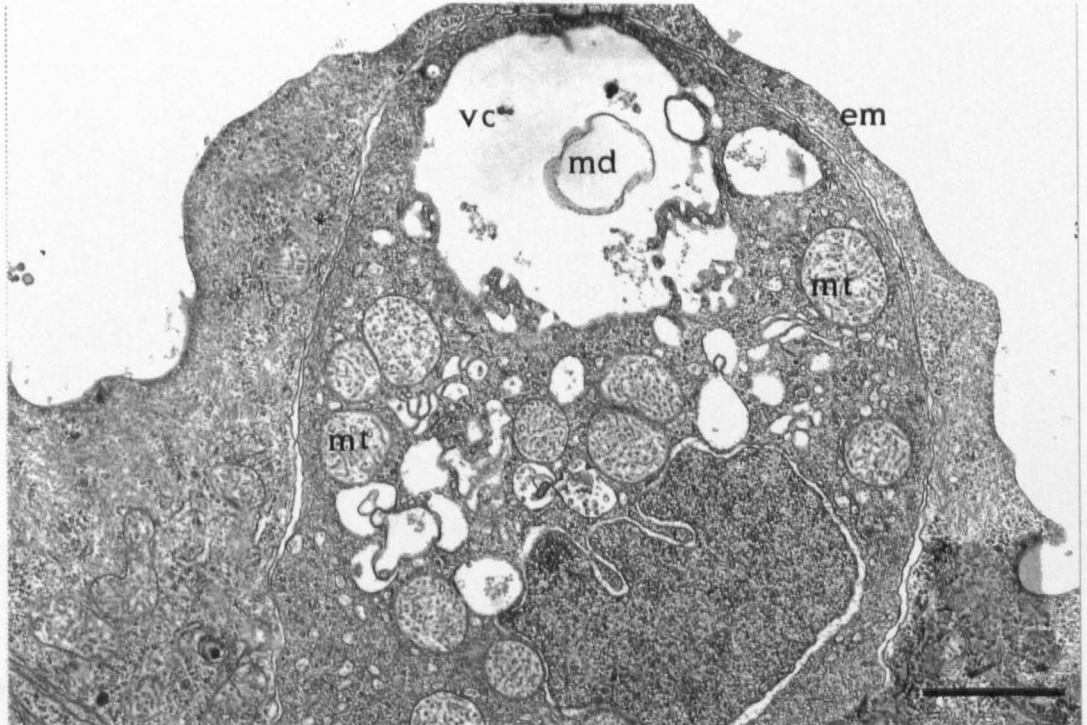
Mucous gland cells were observed, at various stages of maturation (Figs. 3.7 and 3.8), interposed between the pavement cells within both cell layers. In contrast to the larvae of plaice (*Pleuronectes platessa*) (Roberts *et al.*, 1973), the mucous cells were present in very large numbers in turbot larvae (Figs. 3.9 and 3.10) (990 ± 133 cells mm^{-2} in the yolksac epithelium of stage 1a turbot). Mature cells, containing large vesicles of mucous, were seen to bulge out of the superficial layer of the very thin epidermis before dehiscing (Figs. 3.11, 3.7 and 3.8).

The epidermal pores observed in SEM, resembling the apical pits described for branchial chloride cells in adult fish (Pisam & Rambourg, 1991), were seen to contain numerous, tubular-shaped projections (Fig. 3.12). The identity of chloride cells in the larval epithelium was confirmed by TEM, the cells forming part of the inner layer of the epidermis in close association with the basal lamina and underlying blood vessels or haemolymph (Figs. 3.13 to 3.16), but breaking through the outer layer to the external medium by way of such pores or apical pits (Figs. 3.13 and 3.14). In common with adult marine fish, the larval chloride cells were characterised by an abundance of mitochondria (Fig. 3.17), a network of smooth-walled, branching microtubules (Fig. 3.18), continuous with the basolateral plasma membrane (Fig. 3.19), and numerous membrane-bound possibly exocytotic vesicles in the apical portions of the cell.

Based on their morphology, distribution and arrangement, two types of chloride cell were clearly evident in the skin of turbot larvae. Firstly, solitary, flattened cells (Figs. 3.14 and 3.15), referred to here as cutaneous chloride cells (after Tytler & Ireland, 1995), were

Fig. 3.7. Electron micrograph of a mature mucous cell in the superficial epidermis ($\times 5,000$). The membrane-bound mucous droplets occurring within the central cell cytoplasm have been disrupted in this specimen. Note the abundant mitochondria (mt), a typical feature of the maturing mucous cell. em: external membrane of superficial epidermal cell; md: mucous droplet; vc: vacuole. Scale bar is 2 μm .

Fig. 3.8. Electron micrograph showing two dehisced superficial mucous cells open at the surface of the epidermis ($\times 3,300$). The nucleus and organelles have been displaced to the basal edges of the cells by the large quantities of mucous previously contained within their cytoplasma. Scale bar is 3 μm .



Figs. 3.9 and 3.10. Scanning electron micrographs of turbot larvae revealing the abundance and distribution of superficial mucous cells (indicated by arrows) covering the entire surface of the skin ($\times 100$ and $\times 55$ respectively). Fig. 3.9. Newly hatched day 1 turbot larva. Fig. 3.10. Early stage 2 larva, approximately 6 days after hatching. Scale bars are 100 μm .

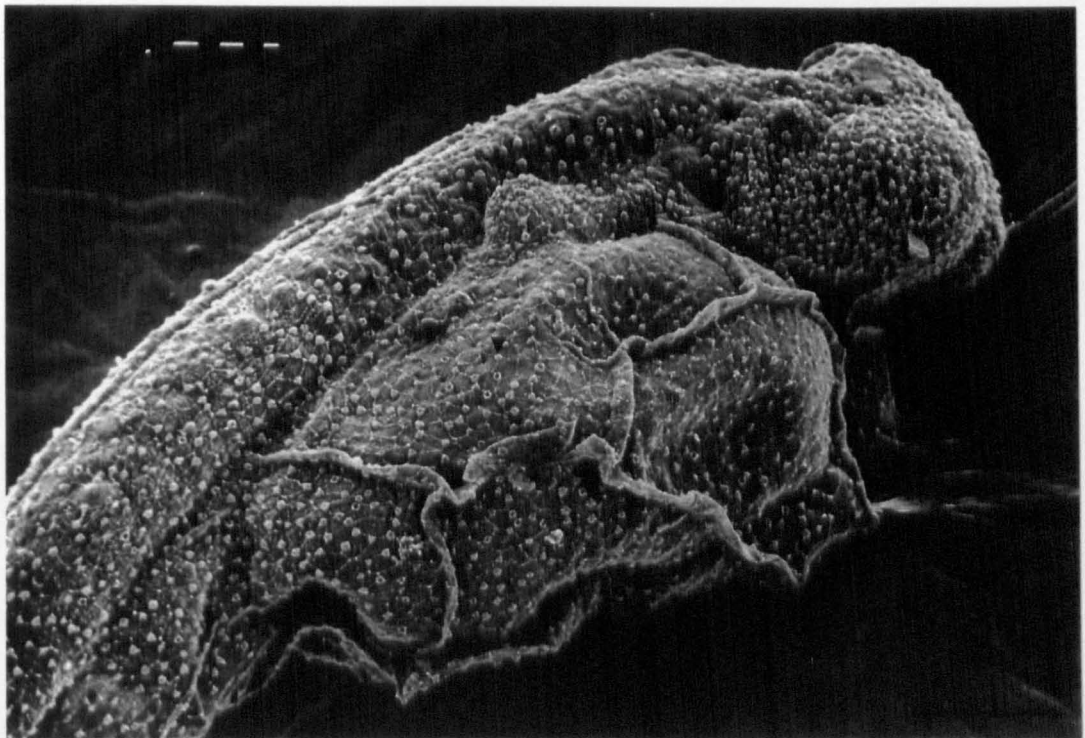


Fig. 3.11. High magnification scanning electron micrograph of the surface epithelium showing numerous mature mucous cells bulging out of the superficial cell layer ($\times 1,700$). Note the septum (arrows) apparent on the majority of the bulging mucous cells, the line along which the cells split and open to release their contents, visible in transverse section in the previous figure. After releasing their contents the compartmentalising membranes of these cells appear to breakdown (asterisks). Scale bar is 5 μm .

Fig. 3.12. Scanning electron micrograph of an apical chloride cell pit (AP) located near the gill opening of a stage 1 larva ($\times 4,300$). Note the uniform microvillus-like projections within the cell pit. cb: pavement cell boundary; m: microridges; MC: surface mucous cell. Scale bar is 2 μm .

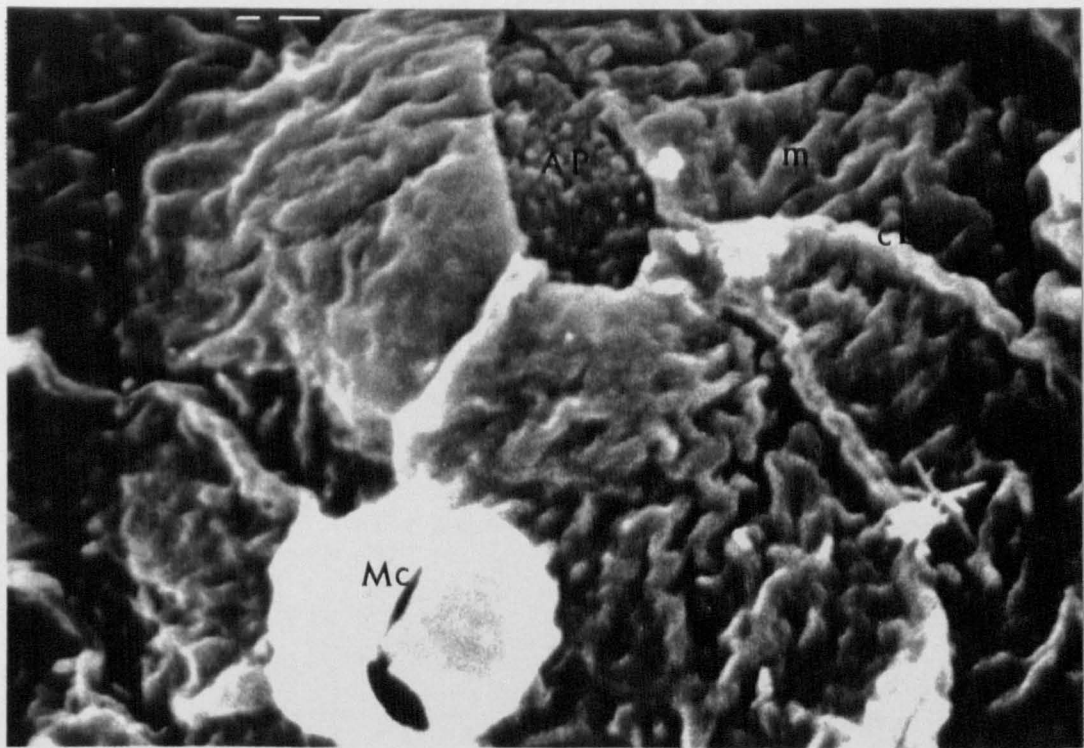
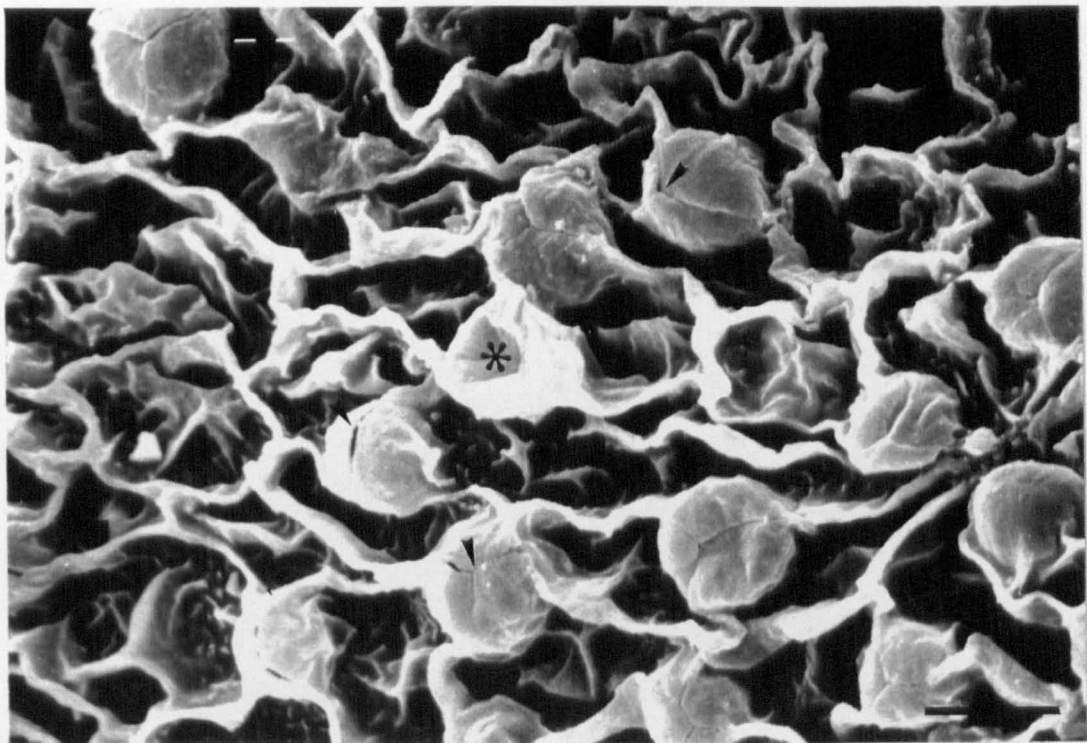


Fig. 3.13. Electron micrograph ($\times 5,000$) of a chloride cell from the prebranchial region of a stage 1d larva. The cell is in contact with the external environment via a prominent apical pit (AP), and the basement cell membrane is closely associated with the basal lamina (bl) overlying the fluid-filled haemocoelomic space (H) below. Note the dense population of mitochondria (mt) and the characteristic branching microtubular system (t). The tubular-shaped projections observed in the previous SEM figure are indicated by arrows. Note also the adjacent "accessory cell" (AC) lying in an indentation at the surface of the chloride cell. Scale bar is $2 \mu\text{m}$.

Fig. 3.14. Electron micrograph of a "cutaneous" chloride cell from the ventral trunk region of a stage 2 larva ($\times 2,500$). In contrast to the prebranchial chloride cell, the solitary cutaneous cell is typically flattened in shape and exhibits a larger surface area. The aperture to the apical pit of the cell (arrowhead) is very narrow, superficial pavement cells (SC) typically overlapping the pit except for a small passageway connecting the external aqueous environment with the simple, shallow crypt space below. bl: basal lamina; H: haemocoel; MC: mucous producing cell. Scale bar is $4 \mu\text{m}$.

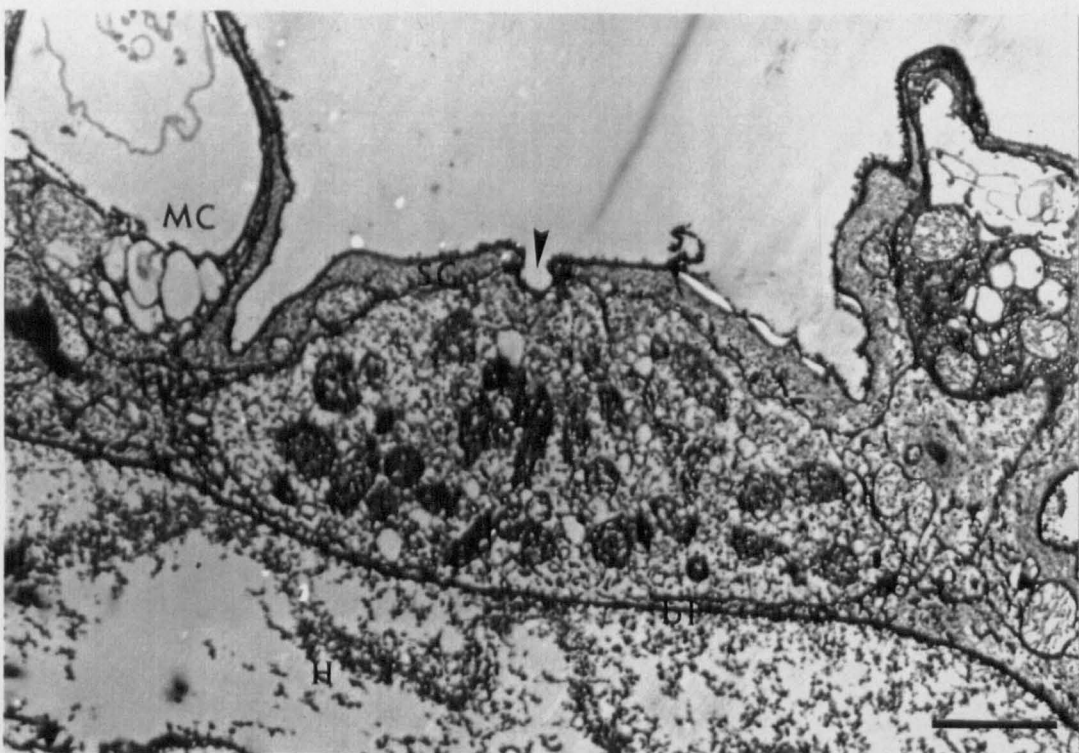
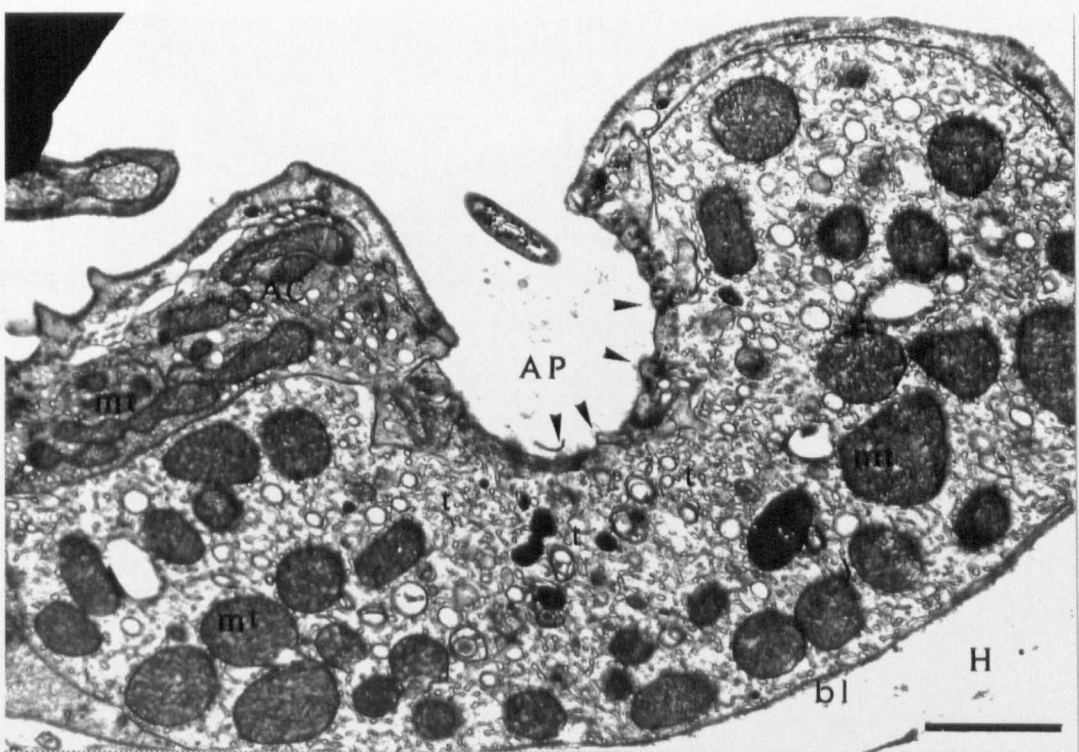


Fig. 3.15. Electron micrograph of a cutaneous chloride cell from the yolk sac epithelium of a stage 1 larva ($\times 9,800$). The basal membrane of the cell is clearly in close contact with the basal lamina (bl), but the fact that the apical membrane does not extend to the apical surface may be due to the section cutting through the edge of the cell rather than the middle. The microtubules (t) appear to be very expanded in this micrograph. H: haemocoel. Scale bar is $3 \mu\text{m}$.

Fig. 3.16. Electron micrograph showing a group of closely juxtaposed prebranchial chloride and accessory cells (AC) from a newly hatched turbot ($\times 3,300$). Note the epidermis has been expanded to several times its normal height to accommodate the large chloride cells. The accessory cells remain in the superficial regions of the epidermis, never reaching its basal lamina. Scale bar is $2 \mu\text{m}$.

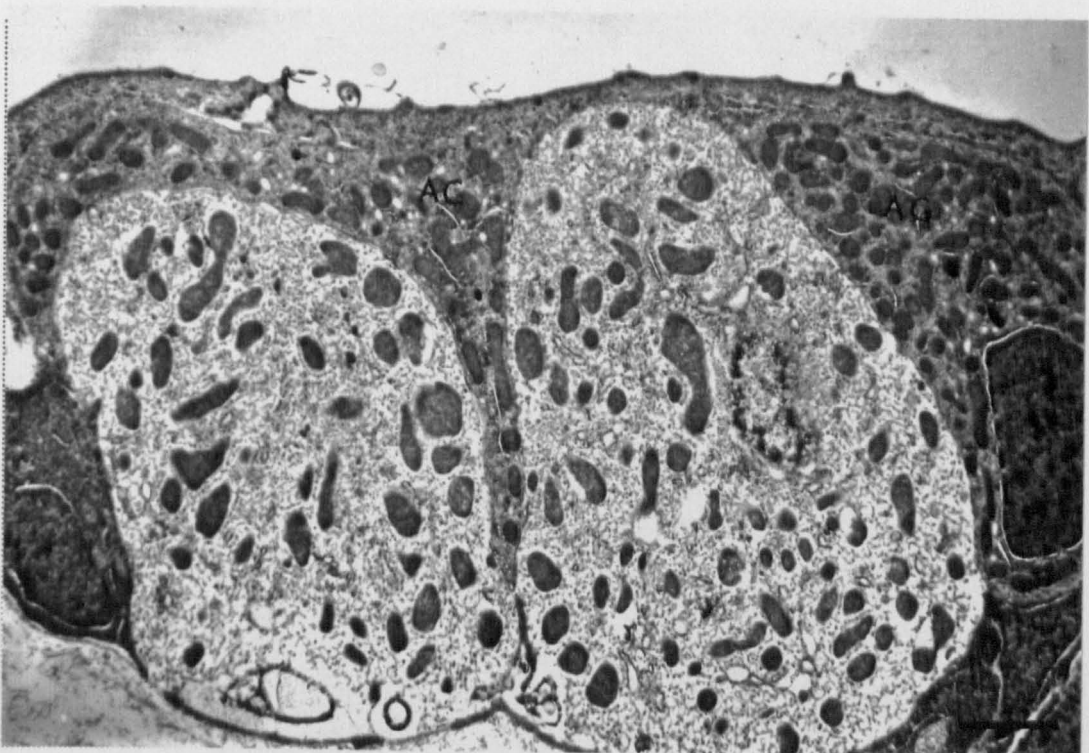
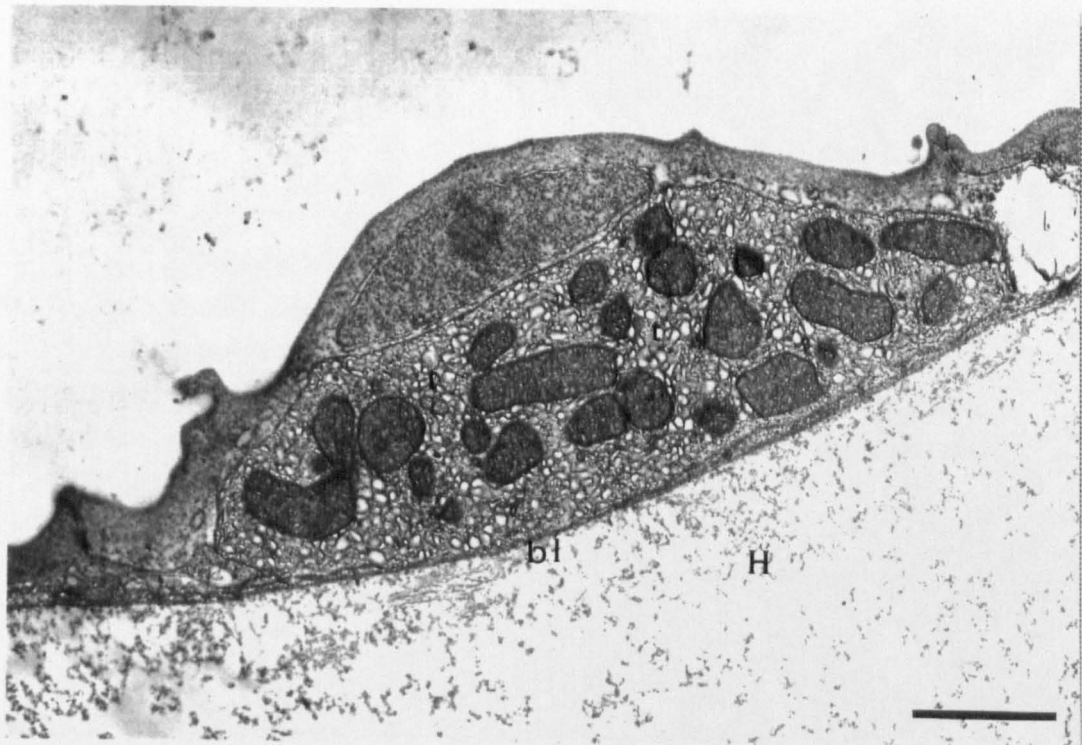


Fig. 3.17. High power electron micrograph of a prebranchial chloride cell showing details of mitochondria ($\times 20,000$). Note the lightly coloured matrices and numerous villous cristae of the mitochondria. r: small aggregates of ribosomes; t: microtubular system; vc: vacuoles. Scale bar is $0.5 \mu\text{m}$.

Fig. 3.18. High power electron micrograph showing the microtubular system in the sub-apical region of a cutaneous chloride cell from a stage 1c larva ($\times 33,000$). The densely stained membranous tubules form an extensive network, unevenly distributed throughout the cytoplasm. In this micrograph, the tubules are tightly anastomosed around small polygonal meshes (arrows). Scale bar is $0.3 \mu\text{m}$.

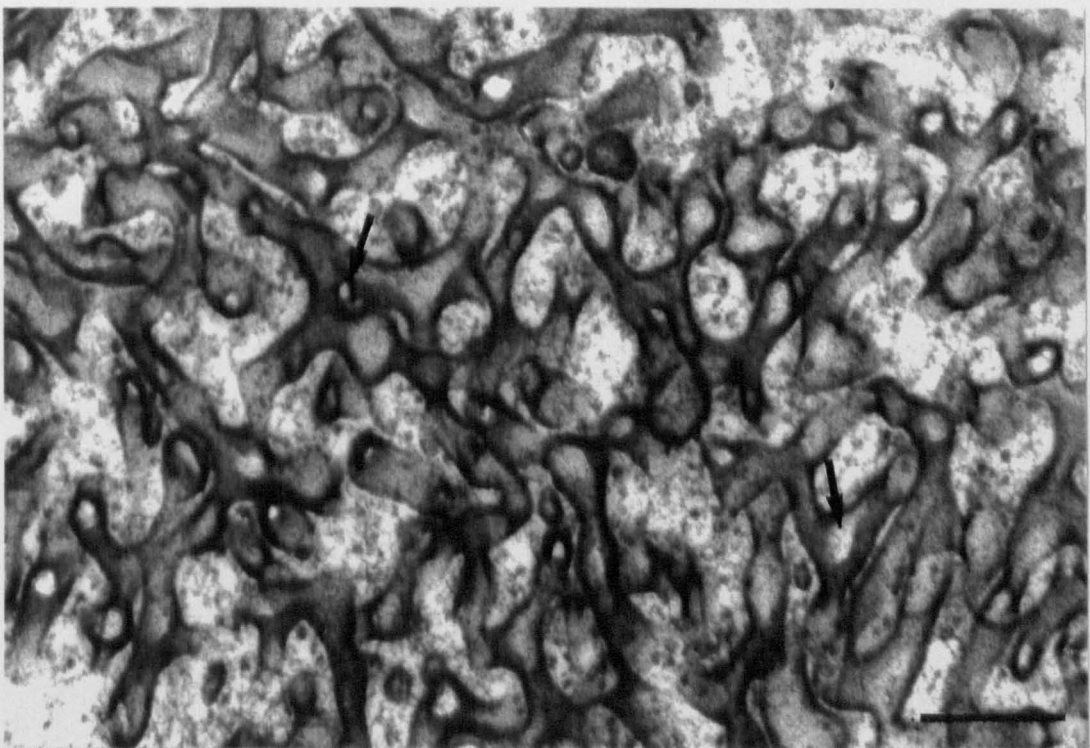
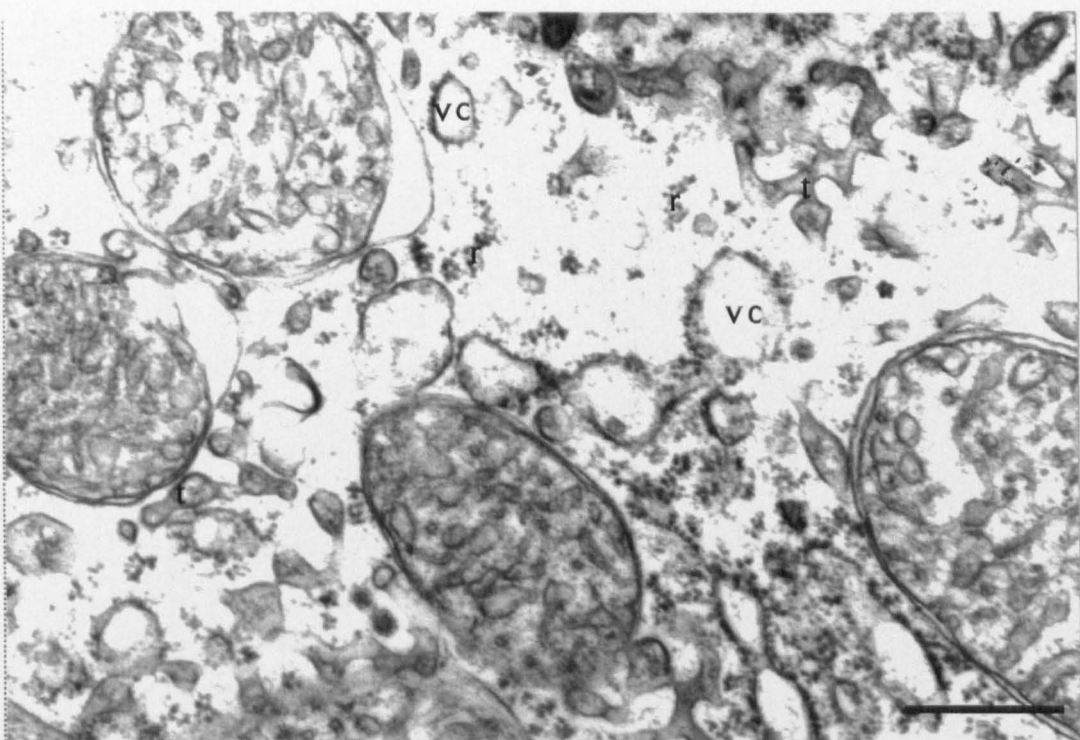
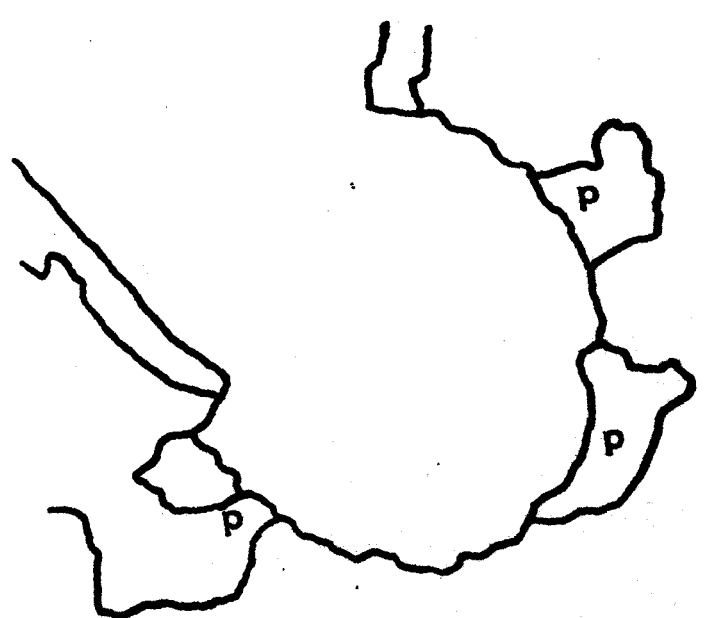
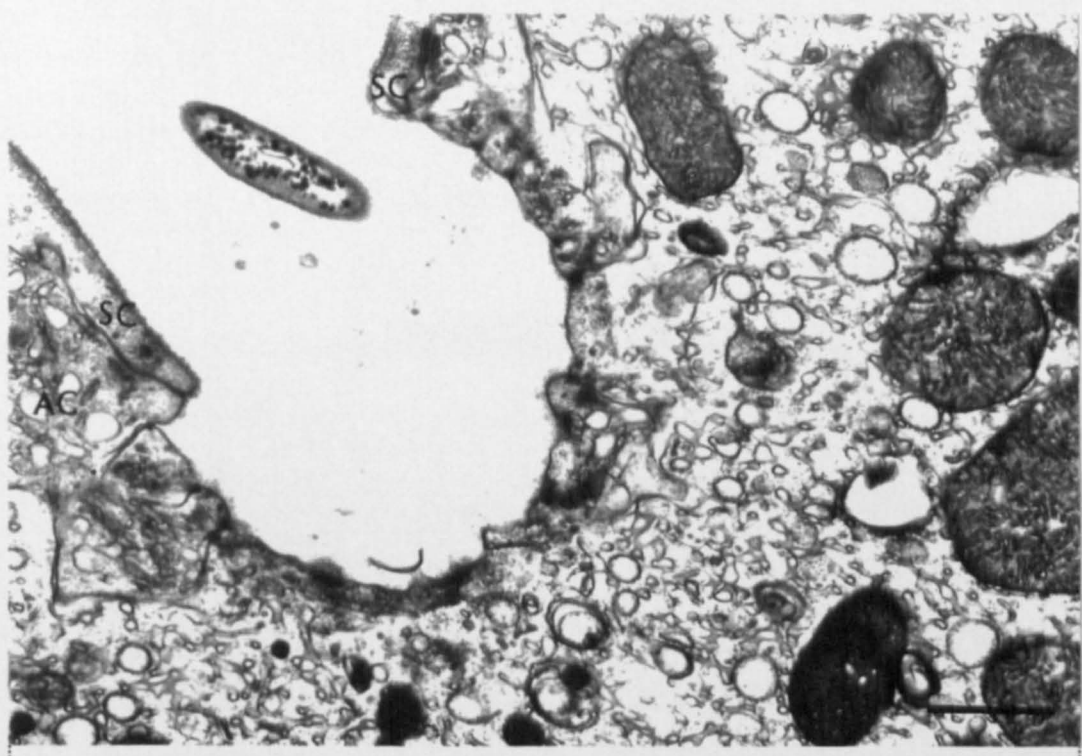
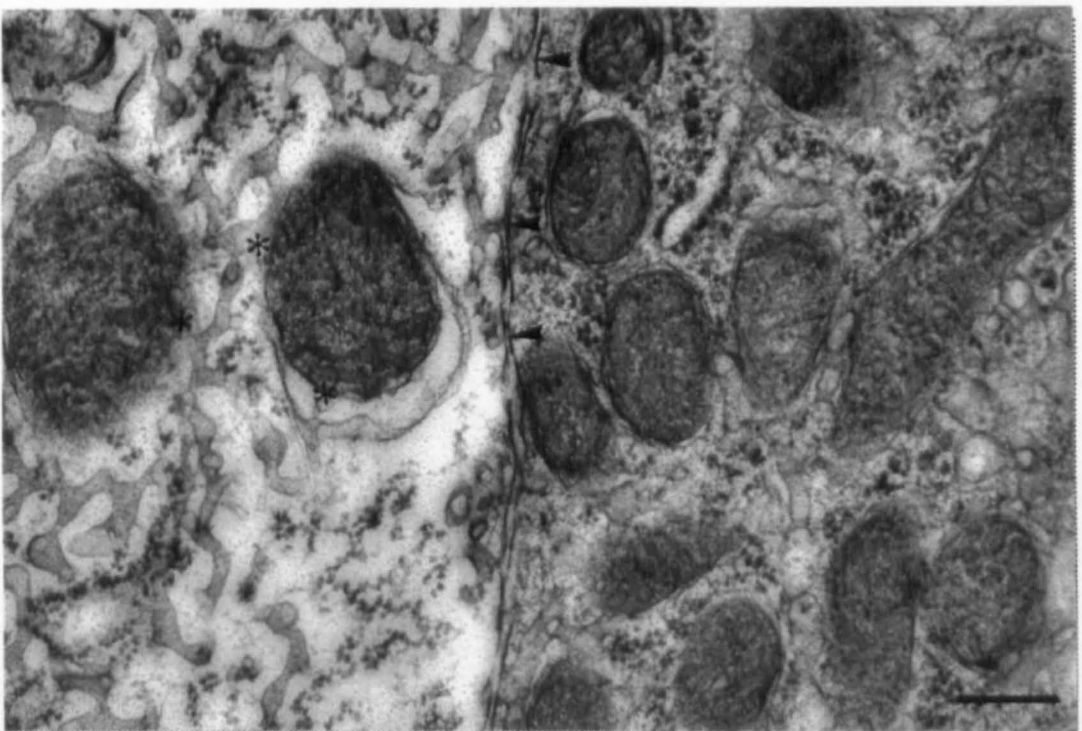
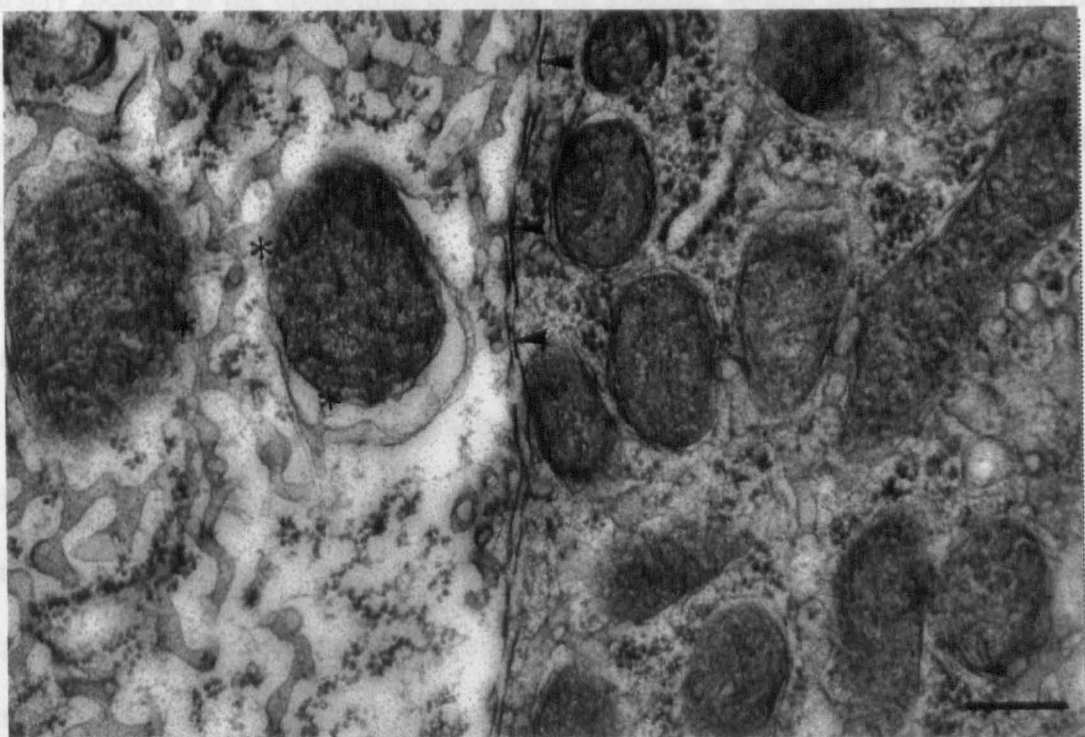


Fig. 3.19. Electron micrograph showing the continuity of the microtubular system of a chloride cell (left) with the lateral plasma membrane ($\times 20,000$). Invaginations of the plasma membrane into the tubular system are indicated by arrowheads. The darker cell on the right is an accessory cell. Although the tubular system and mitochondria can be distinguished in both cell types, the accessory cell is generally less well differentiated. In the chloride cell, note also the intimate association of the mitochondria with the tubules (shown by asterisks). Scale bar is $0.5 \mu\text{m}$.

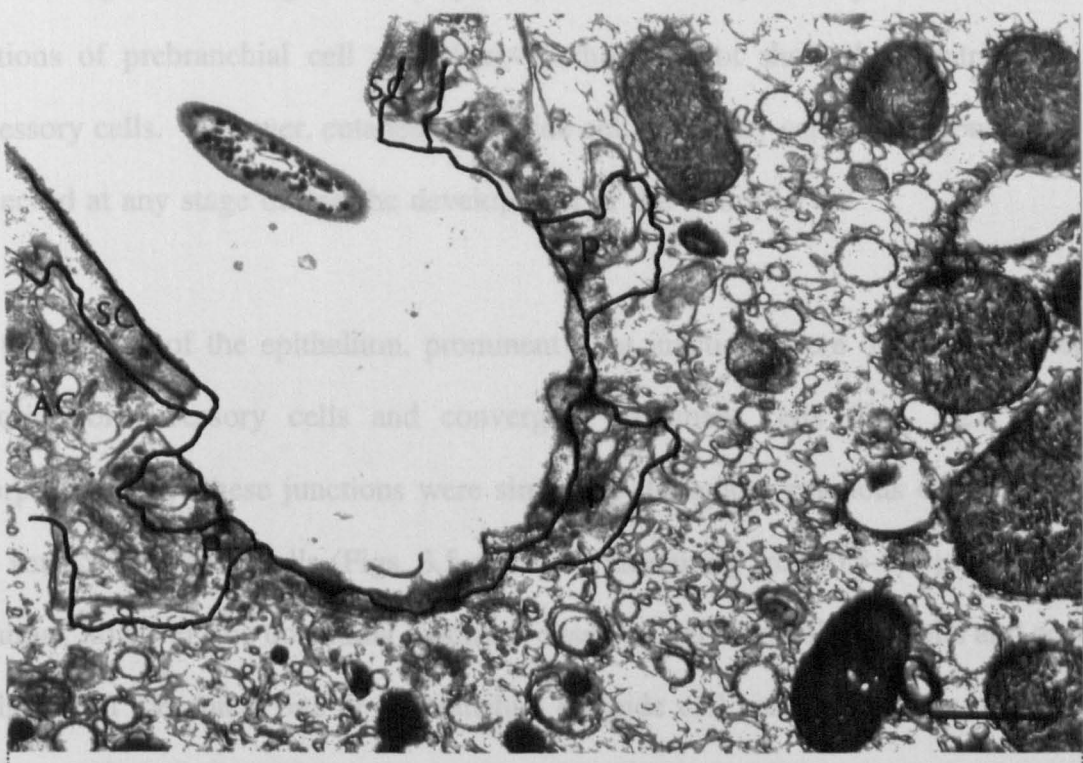
Fig. 3.20. Electron micrograph of a multicellular prebranchial pit showing the contribution of the accessory cell to the wall of the apical cavity ($\times 18,000$). Cytoplasmic processes (p) can be seen extending distally from the accessory cell body (AC), intermingled with the apical margins of the juxtaposed chloride cell. SC: overlapping superficial pavement cells. Scale bar is $1 \mu\text{m}$.







(Fig. 3.20). The surfaces of the numerous prebranchial cell pits were thereby formed by a mosaic of cell processes, varicosities, epithelial cells and interdigitating accessory cells contributing to the margin of the pit. Epithelial cells in very rare instances were sections of prebranchial cell pits, and the latter were never found at any stage.



sparingly located in the epithelium covering the yolk sac, ventral and lateral trunk regions and occasionally the head of larvae. However, a second type of "prebranchial" chloride cell was also observed in the region where the gills eventually form, occurring in closely juxtaposed groups of two or more cells (Figs. 3.13 and 3.16).

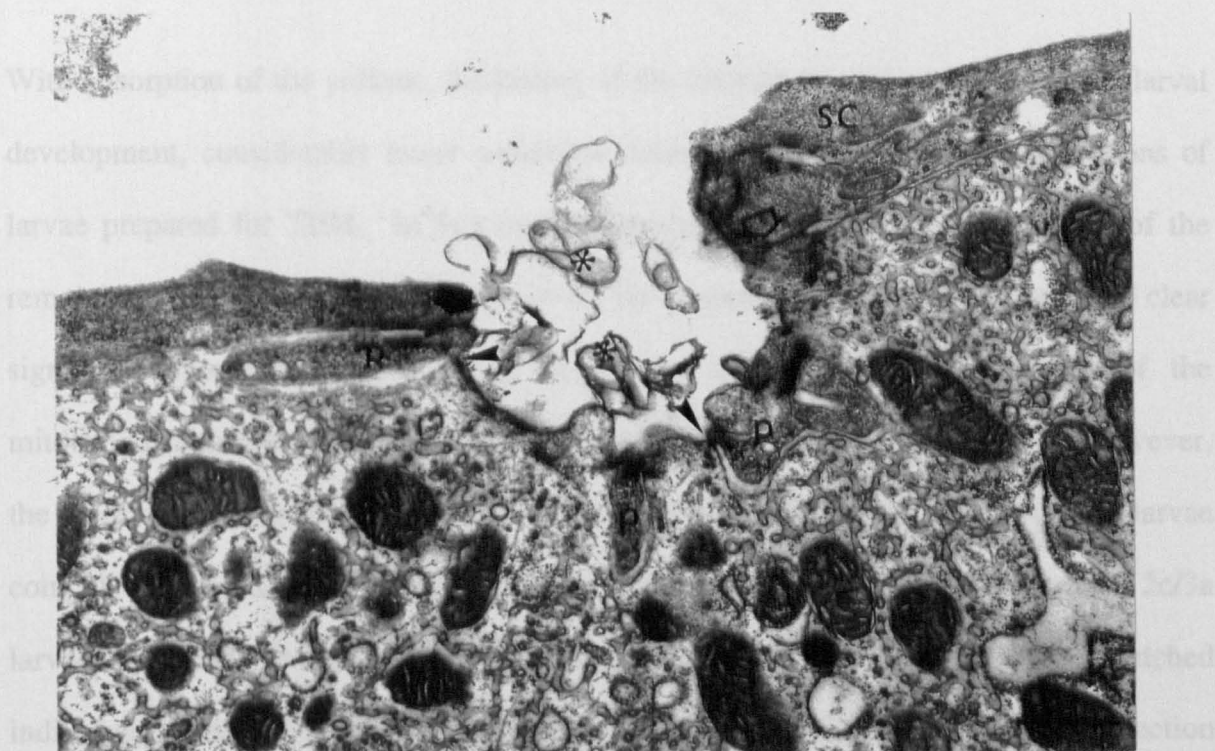
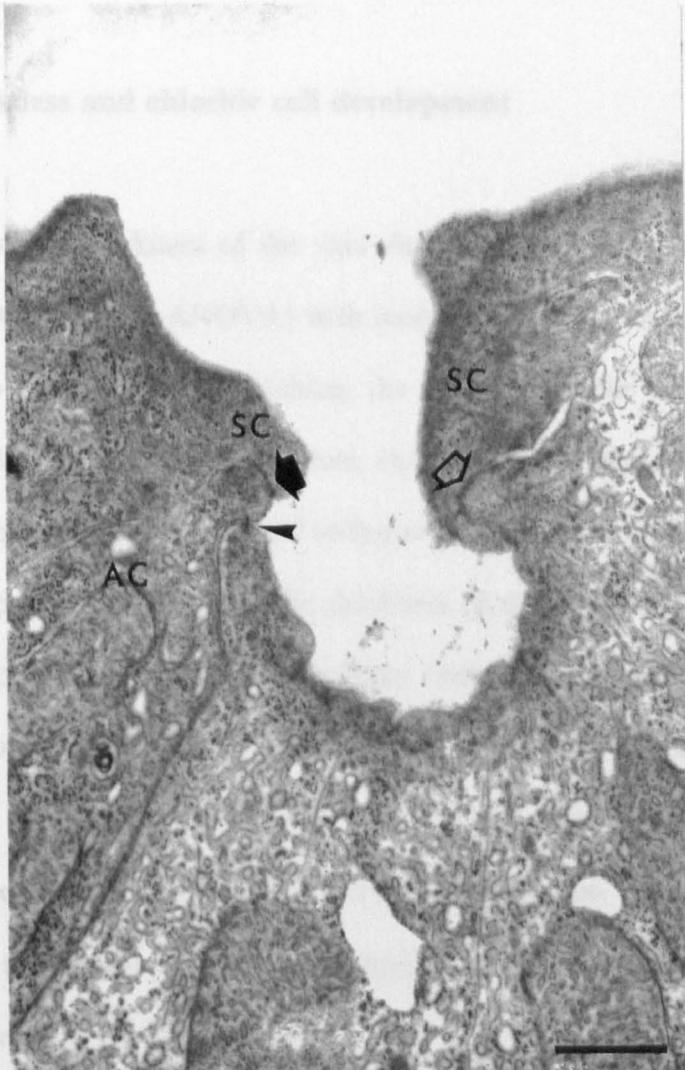
"Accessory cells", described by Sardet *et al.* (1979) and Pisam & Rambour (1991), were invariably seen in close association with the prebranchial chloride cells (Figs. 3.13, 3.16 and 3.19). The electron opaque accessory cells were usually positioned in an indentation of the surface of the adjacent chloride cell just beneath the superficial pavement cell layer (Fig. 3.13), and cytoplasmic processes, extending distally from the accessory cell body, were often seen intermingled with the apical membrane of the adjacent prebranchial cell (Fig. 3.20). The surfaces of the multicellular prebranchial cell pits were thereby formed by a mosaic of cell processes, with both chloride cells and interdigitating accessory cells contributing to the margin of the apical pit itself. Only in very rare instances were sections of prebranchial cell pits observed that did not show this contribution from accessory cells. However, cutaneous chloride cell-accessory cell associations were never observed at any stage during the development of the turbot larva.

At the surface of the epithelium, prominent tight junctions were observed between the chloride or accessory cells and converging pavement cells (Fig. 3.21 and 3.22). Morphologically, these junctions were similar to the apical junctions observed between the surface pavement cells (Figs. 3.5 and 3.6), measuring from 0.5-0.8 μm in depth. In contrast, however, the occluding junctions observed between chloride cells and accessory cells within the apical pits of prebranchial chloride cell complexes were comparatively shallow (Figs. 3.21 and 3.22), rarely exceeding 0.1 μm in depth.

Figs. 3.21 and 3.22. Electron micrographs of the prebranchial chloride cell pit showing junctional contact between adjacent cell types ($\times 20,000$ and $\times 16,000$ respectively). The apical junctions between chloride and accessory cells (AC) (shown by arrowheads) are very shallow compared with the deeper, tight junctions linking overlapping pavement cells (SC) and chloride cells (clear arrows) or accessory cells (black arrows). In figure 3.22, note the flocculent extracellular material (*) in the apical pit. p: accessory cell process. Scale bars are 2 and 3 μm respectively.

3.1.2. Skin thickness and epidermal cell development

Measurements of skin thickness in the larval stages revealed a significant increase in epidermal thickness ($P<0.001$) from stage 1 to 3, so that by stage 3 the epidermal thickness was approximately double that at stage 1 (Table 3.1). The increased epidermal thickness was due to an increase in the number of layers of epidermal cells (Table 3.1) such that by stage 3 the epidermal layer had developed a multi-layered structure. At stage 1, the lipid-rich, water-barrier was located in the basal layer of the epidermis (Fig. 3.1a). However, quantitative measurements of the epidermal thickness in the different regions of the body to the next stage (stage 2) revealed considerable regional differences in the thickness of the upper and lower epidermal layers (Table 3.2). A one-way analysis of variance (ANOVA) showed that the epidermal thickness was significantly thinner ($P<0.001$) in the head and tail regions respectively compared with the mid-body and trunk regions.



3.1.2. Skin thickness and chloride cell development

Measurements of the thickness of the skin showed a significant increase in epidermal thickness ($P<0.001$, oneway ANOVA) with increase in the age of larvae (Table 3.1) such that by stage 3a-b, 10 days post-hatching, the thickness of the blood-water barrier was approximately double that measured from newly hatched, stage 1a larvae. However, quantitative measurements from stage 2 turbot at 7 days post-hatching (Table 3.2) revealed considerable regional differences in the thickness of the epidermis from one area of the body to the next; thus accounting for the large variability in measurements (indicated by the upper and lower ranges) and the high standard errors observed in table 3.1. A one way analysis of variance with Student-Newman-Keuls *post-hoc* analysis (Glantz, 1987) showed that the ventral epidermis overlying the coelom was significantly thinner ($P<0.001$) than the lateral and dorsal epidermis covering the head, mid-body and tail regions respectively of the stage 2 larva.

With absorption of the yolksac, thickening of the integument and with subsequent larval development, considerably fewer cutaneous chloride cells were detected in sections of larvae prepared for TEM. In fact by late developmental stage 2/early stage 3, of the remaining cutaneous chloride cells observed, the majority of cells typically displayed clear signs of degeneration, with partial breakdown of the membrane systems of the mitochondria and smooth-walled microtubules (Figs. 3.23 and 3.24). In contrast, however, the prebranchial chloride cells were seen to proliferate with increase in the age of larvae coincident with the development of the rudimentary gill tissue. The cells in stage 2c/3a larvae appeared to have a larger cross-sectional area than those observed in newly hatched individuals. The prebranchial cell mitochondria were also typically larger in cross section

Table 3.1. The mean thickness (\pm S.E) of the epidermis measured from turbot larvae during development (n=50; 5 larvae, 10 random measurements from each).

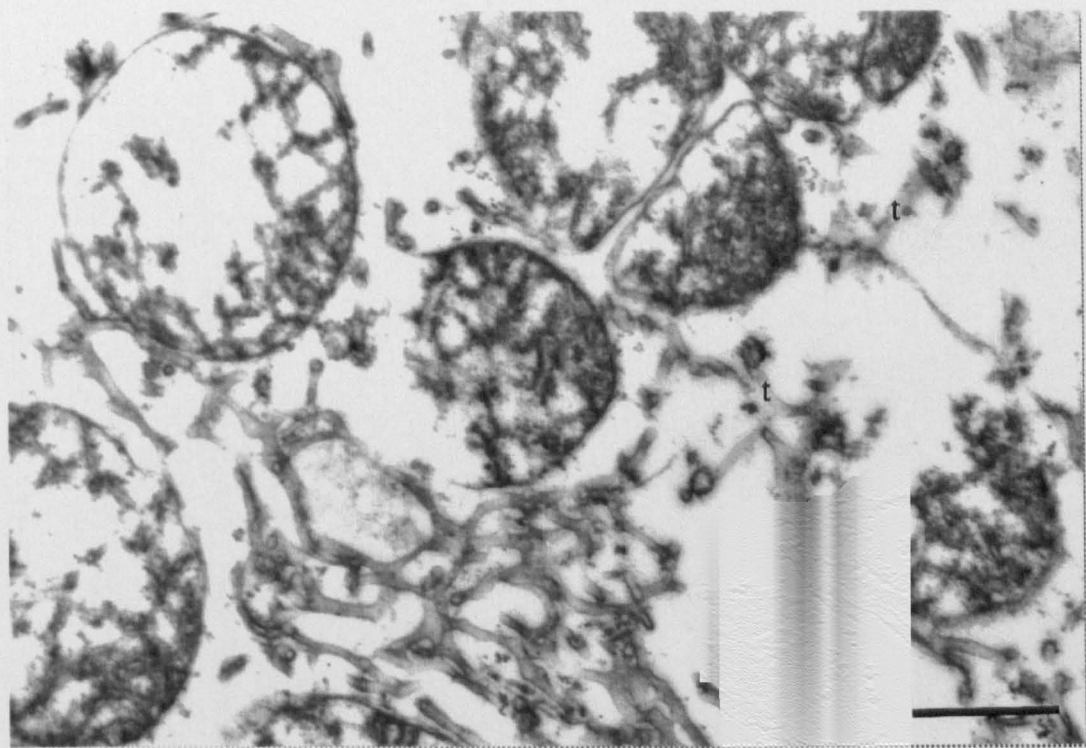
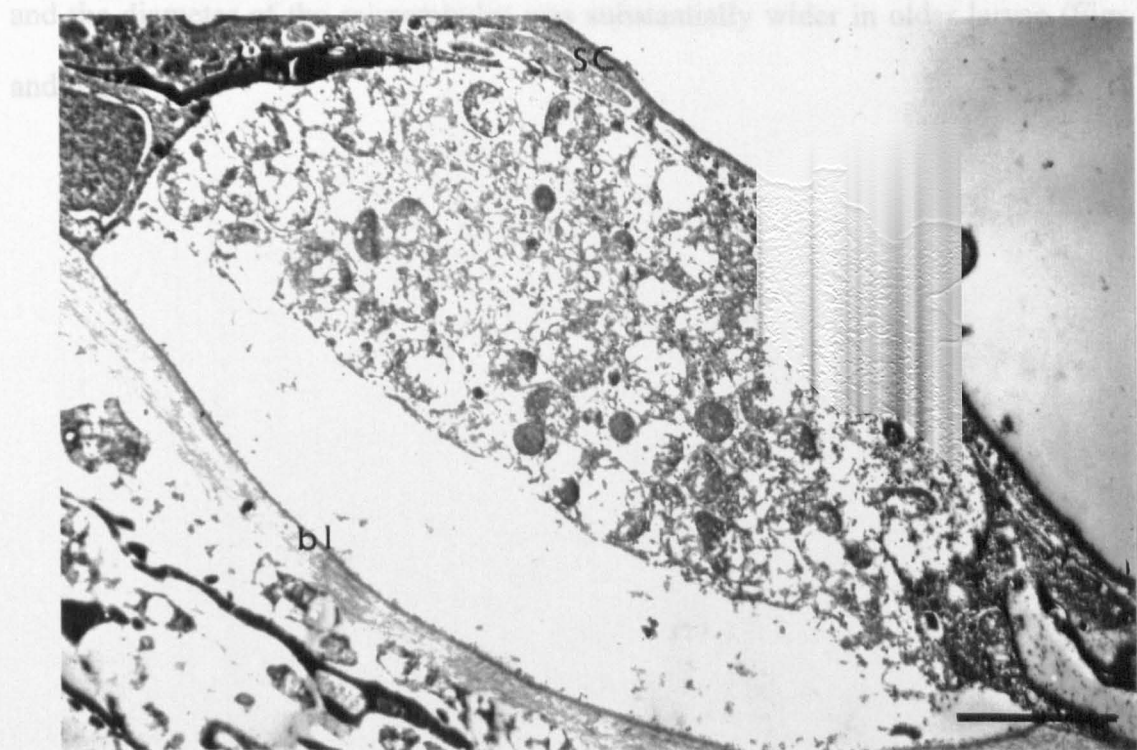
Larval Stage	Total epidermal thickness (μm)	Range of thickness (μm)	
		Lower	Upper
Substage 1a	2.52 \pm 0.38	1.8	4.8
Substage 1c-d	2.94 \pm 0.36	2.1	4.5
Substage 2b-c	4.08 \pm 0.16	1.7	5.7
Substage 3a-b	5.10 \pm 0.50	2.9	7.6

Table 3.2. Measurements of the dorsal, ventral and lateral epidermal thicknesses from three sites in the integument of stage 2 turbot larvae, at approximately 7 days post-hatching (n=52; 4 larvae, 13 measurements from each region).

		Mean Thickness ±S.E. (μm)		
		T.S. Head Region	T.S. Mid-body Region	T.S. Tail Region
Dorsal epidermis	Superficial Cell Layer	3.41 ±0.11	3.30 ±0.16	2.49 ±0.06
	Basal Cell Layer	1.35 ±0.04	1.37 ±0.06	1.21 ±0.03
	TOTAL	4.76 ±0.12	4.67 ±0.18	3.70 ±0.09**
Lateral epidermis	Superficial Cell Layer	3.10 ±0.09	3.04 ±0.13	2.77 ±0.06
	Basal Cell Layer	1.52 ±0.06	1.15 ±0.07	1.18 ±0.04
	TOTAL	4.62 ±0.11	4.19 ±0.16*	3.96 ±0.08**
Ventral epidermis	Superficial Cell Layer	2.32 ±0.06	1.65 ±0.06	1.82 ±0.04
	Basal Cell Layer	1.29 ±0.05	0.75 ±0.05	0.93 ±0.03
	TOTAL	3.62 ±0.10*	2.40 ±0.07*	2.75 ±0.06*

*Significantly different from other locations within the respective region: P<0.001; **P<0.05.

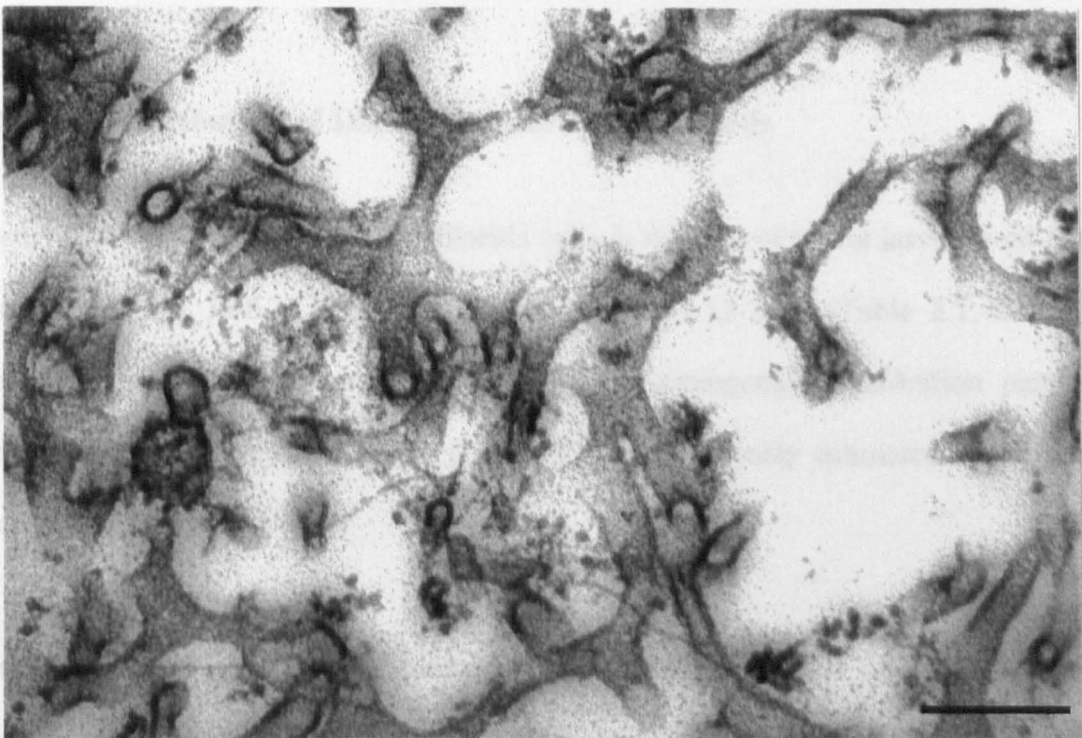
Figs. 3.23 and 3.24. Electron micrographs of a cutaneous chloride cell from a stage 3a turbot larva, 11 days post-hatching. Fig. 3.23. The complete cell ($\times 3,300$), clearly showing signs of severe degeneration/autolysis. Large intracellular spaces are evident, mitochondria are sparse and the tubular network is incomplete. bl: basal lamina; SC: superficial pavement cell layer. Fig. 3.24. Showing the apparent breakdown of the membrane systems and cristae of mitochondria and deterioration of the microtubular system (t) ($\times 20,000$). Scale bars are 3 and 0.5 μm respectively.



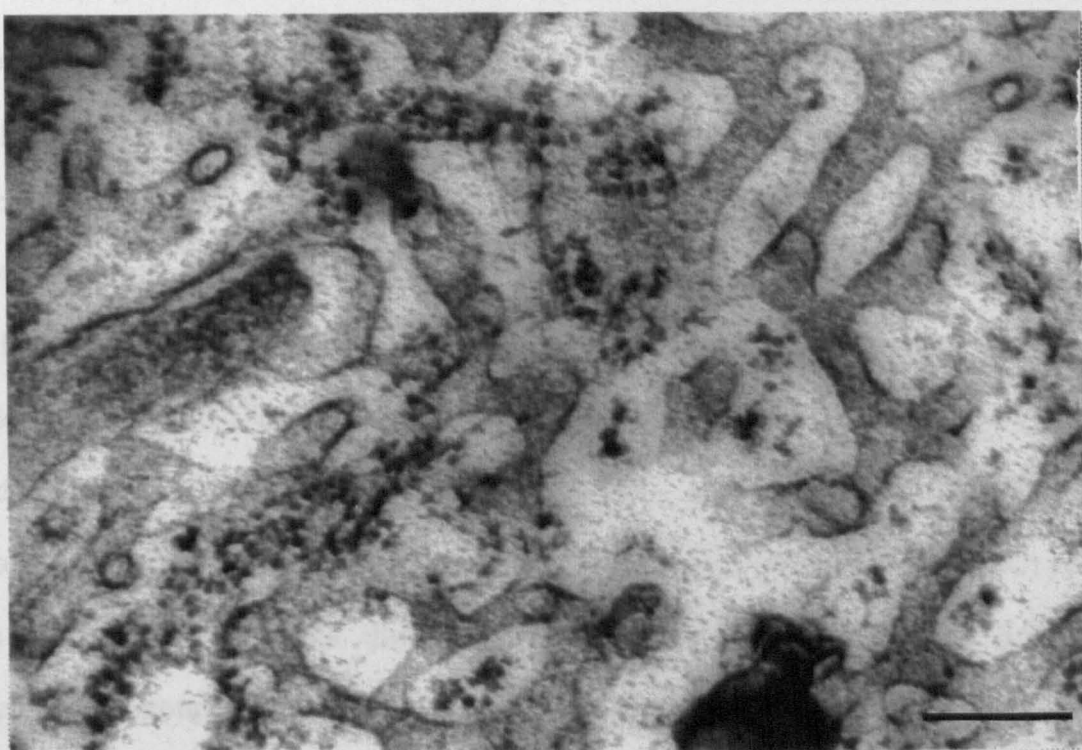
3. Results

and the diameter of the microtubules was substantially wider in older larvae (Figs. 3.25 and 3.26).

Figs. 3.25 and 3.26. High power electron micrographs of the microtubular system from prebranchial chloride cells ($\times 33,000$). Fig. 3.25 shows the microtubules in a cell from a stage 1a turbot and Fig. 3.26 from a 3a turbot. Note the expanded size of the tubules in the stage 3a larva. Scale bars are 0.3 μm .



most conspicuous were the large, pale-staining yolk sac cells, many of which contained very distinct chondrocyte-like nuclei (Fig. 3.2A) and heterochromatin bodies near the surface of the yolk sac (Fig. 3.2A). Other yolk sac cells contained more diffuse heterochromatin bodies.



3.2.

Vital Staining with Fluorescent Probes

3.2.1. The distribution of DASPMI-stained chloride cells

Observations of DASPMI-stained chloride cells in the skin of turbot larvae from hatching through to stage 3a-b, a period of approximately 11-13 days (Table 2.1, Materials & Methods), revealed considerable changes in the arrangement/distribution pattern and density of chloride cells with age (Fig. 3.27); as previously intimated in the electron microscopy study.

In newly hatched stage 1a larvae, mitochondria-rich chloride cells were found to occur in three anatomically distinct regions: the head region, yolksac and the trunk. The cells were most conspicuous in the yolksac region (Fig. 3.27) where numerous, widely dispersed chloride cells ($300\text{-}420 \text{ mm}^{-2}$) were observed evenly distributed over the surface of the yolksac (Fig. 3.28A). Chloride cells also typically occurred on the trunk, but the density of cells decreased dorsally (Fig. 3.28B) and few chloride cells were observed post-anally (Fig. 3.28A). Low densities of chloride cells were sometimes observed on the dorsal and occasionally ventral fin folds (Figs. 3.27 and 3.28B), but the cells were rarely, if ever, revealed on the posterior caudal fins. On the head, a small number of sparsely scattered cells were typically located posterior and adjacent to the eye, but the highest density of chloride cells ($920\text{-}1360 \text{ mm}^{-2}$) occurred bilaterally in the prebranchial region (Figs. 3.27 and 3.28A), anterior to the base of the primordial pectoral fin bud. Contrary to the extensive distribution of the more numerous, solitary chloride cells (Fig. 3.28C) covering the yolksac, head and trunk, the tightly aggregated prebranchial cells (Fig. 3.28D) were exclusively grouped in the epithelium encompassing the openings to the rudimentary branchial chambers.

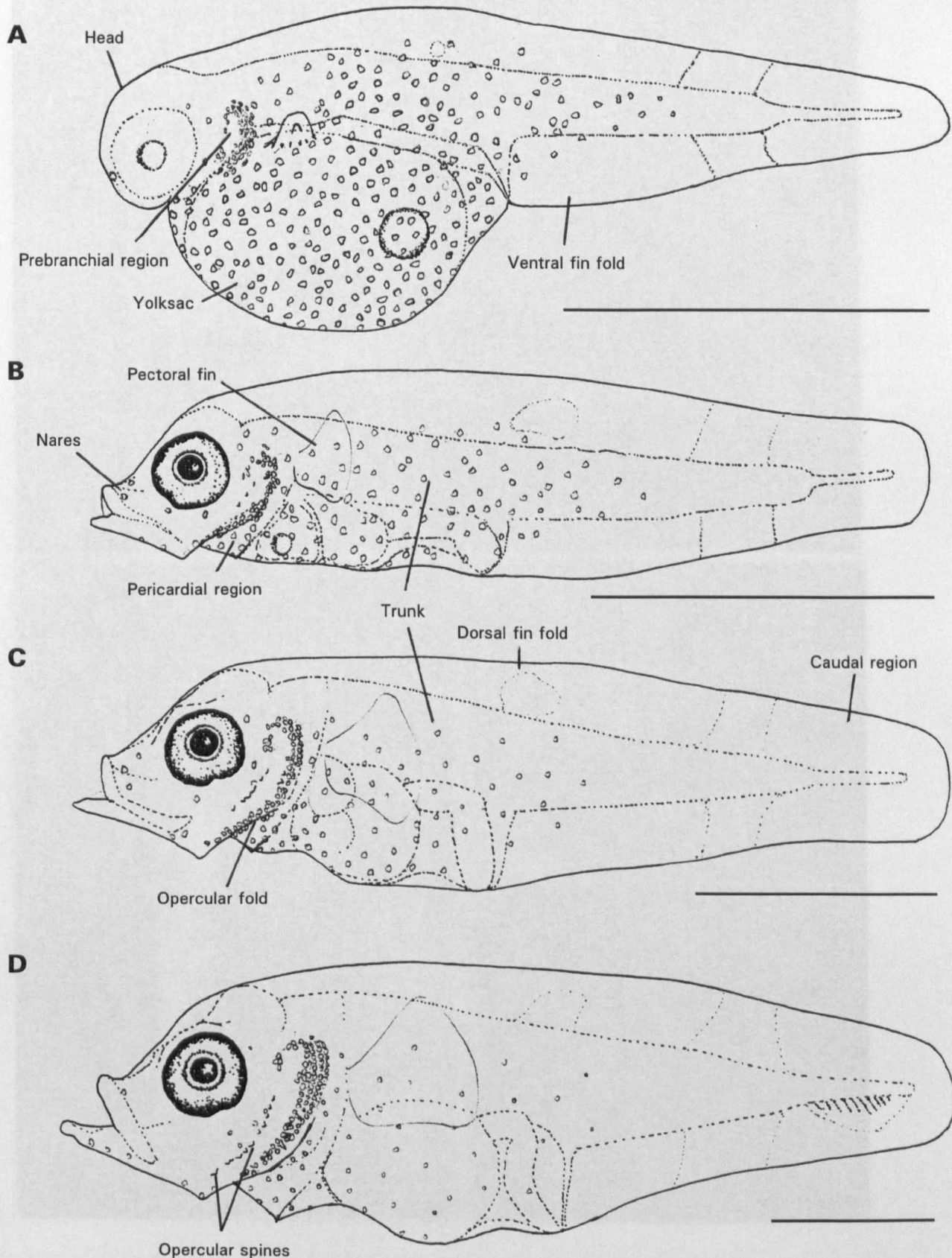


Fig. 3.27. Drawings showing the changes in the distribution of DASPMI-stained chloride cells in the skin of turbot larvae between 1 and 13 days post-hatching: **A**, Stage 1a, immediately after hatching; **B**, Stage 1d, 5–6 days post-hatching; **C**, Stage 2b, 8–9 days post-hatching; and **D**, Stage 3b, at 12–13 days post-hatching. Scale bar is 1 mm.

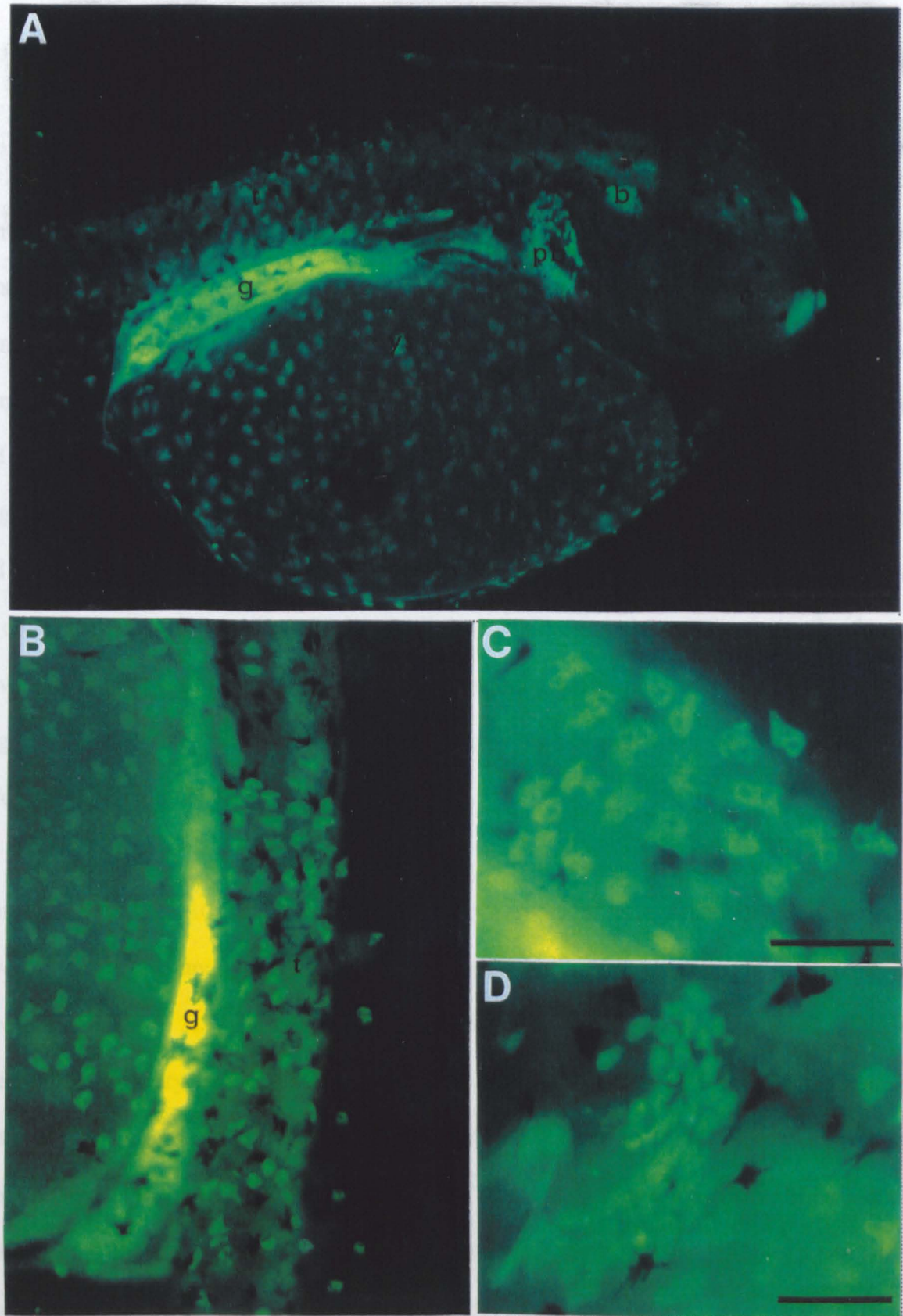


Fig. 3.28. Chloride cell distribution in the skin of the stage 1a yolk sac turbot larva as revealed by DASPMI-staining. A. Photomicrograph of a newly hatched larva showing the distribution of mitochondria-rich cells in the yolk sac (ys), mid-lateral trunk region (t) and the head. b: brain; e: eye; g: gut; pb: prebranchial chloride cells. B. Photomicrograph of the lateral trunk region overlying the gut (g). Note the antero-posterior (top to bottom) decrease in the number of fluorescing cells, with few cells occurring post-anally and low densities of cells on the dorsal fin fold (right). C and D. High powered photomicrographs of chloride cells from the yolk sac and prebranchial regions respectively. The prebranchial chloride cells are densely packed and closely juxtaposed which contrasts with the more numerous, but less densely distributed yolk sac chloride cells which are widely separated from one another. Scale bars: micrographs A and B are 0.2 and 0.1 mm respectively; micrographs C and D are 40 μm .

3. Results

By developmental stage 1c-d, 4-6 days post-hatching, with almost complete absorption of the yolk sac, the majority of chloride cells now primarily occurred on the lateral and ventral surfaces of the trunk posterior to the developing opercula (Fig. 3.27); although ventrally placed cells were often difficult to observe due to high gut fluorescence resulting from ingested fluorochrome (Fig. 3.29A). The ventral chloride cells, extending abundantly from the pericardial region to the anus, exhibited a gradient which decreased both dorsally and posteriorly, as in stage 1a larvae, but with fewer chloride cells occurring post-anally (Fig. 3.27 and 3.29A). On the head, scattered chloride cells persisted around the mouth and nares, lower jaw region and the border of the eye (Fig. 3.29A), but the highest density of cells still occurred prebranchially in the region where the gills eventually form. However, in contrast to the tightly packed prebranchial group observed in stage 1a larvae (Fig. 3.28D), the stage 1c-d prebranchial cells extended ventrally along the margins of the unfolding opercula (Figs. 3.27 and 3.29B).

From stage 2a-b, 8-10 days post-hatching, the number of integumental chloride cells covering the trunk and head region progressively declined with the subsequent larval development (Fig. 3.27). Indeed by developmental stage 3a, apart from a modest assembly of solitary cells in the pericardial region of the anterior trunk, just a sparse scattering of chloride cells remained on the lateral trunk wall. This disappearance of integumental chloride cells from the body wall was concurrent with the proliferation of prebranchial chloride cells in the evolving branchial tissue. In stage 2b-c larvae, the arrangement of the prebranchial cells (Fig. 3.27) suggested their location either on or adjacent to newly developing gill arches. Furthermore, by stage 3b, 3-4 rows of chloride cells were apparent (Fig. 3.27) which, by nature of their profile, were almost certainly established in the epithelium of the primordial gill filaments.

3.2.2. Chloride cell morphology

Fluorescence microscopy revealed several morphological differences between the chloride cells.

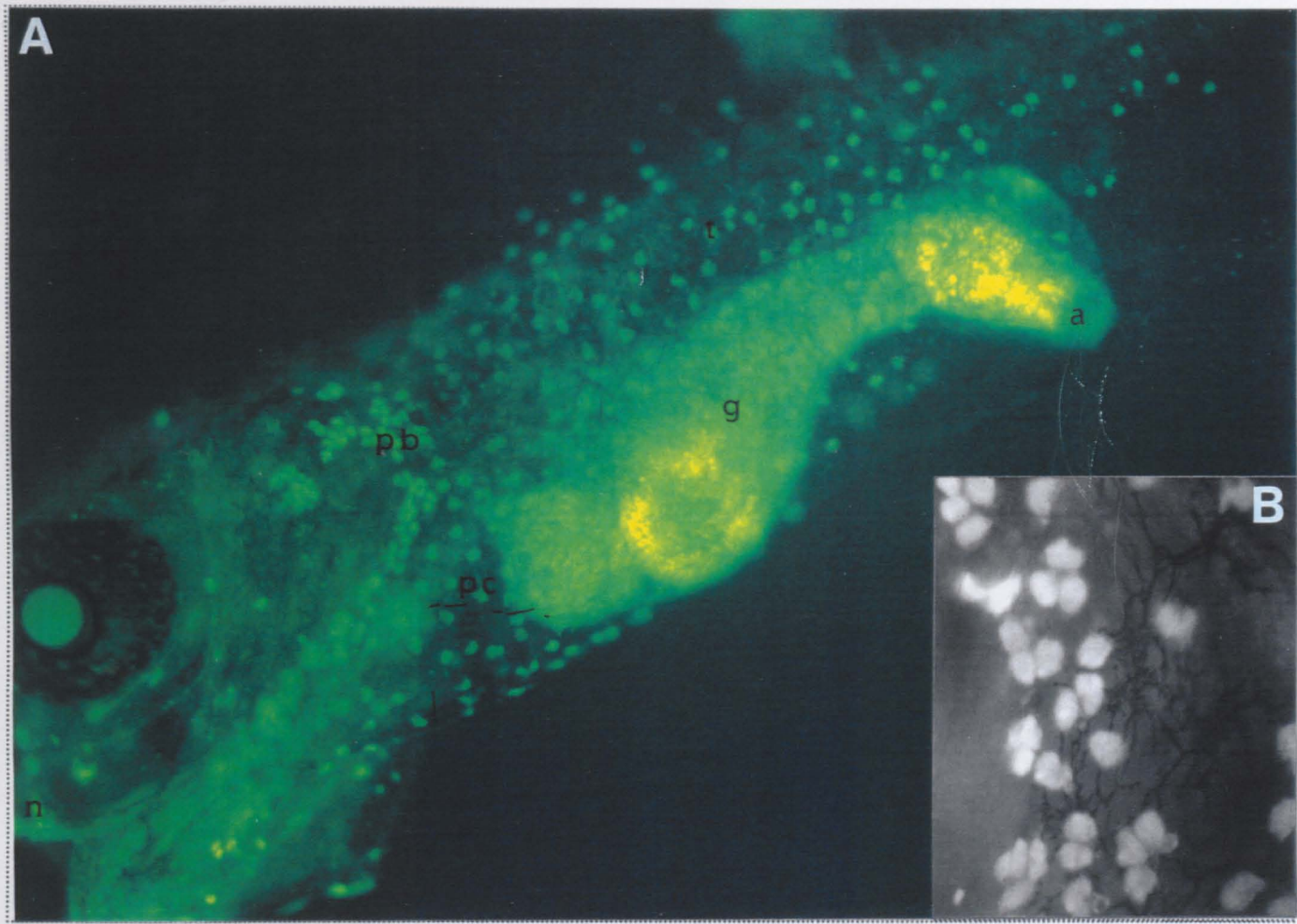


Fig. 3.29. The distribution of mitochondria-rich, DASPMI-stained chloride cells in the skin of the stage 1c-d turbot larva, 4-6 days post-hatching. A. Photomicrograph of the whole larva. Note the retention of yolk-sac chloride cells on the ventral trunk, occasionally masked by the highly fluorescing gut (g). a: anus; n: nares; pb: prebranchial cells; pc: pericardial region; t: trunk. B (inset). High power photomicrograph of the prebranchially sited chloride cells. Scale bars are 0.25 and 0.1 mm respectively.

3.2.2. Chloride cell morphology

Fluorescence microscopy revealed several morphological differences between the tightly grouped chloride cells in the prebranchial region and the quite separate, widely scattered, "cutaneous" chloride cells of the yolk sac/trunk and head. Fundamentally, the cutaneous chloride cells were flattened and quite irregular in shape, due to lateral cytoplasmic extrusions from the main cell body (Fig. 3.30A), whilst the prebranchial cells were typically much smaller and more spherically shaped (Fig. 3.30B). Indeed, measurements of the chloride cells from each location revealed that the mean cross sectional area of the cutaneous cells was significantly larger than that of the prebranchial cells in all the stages examined (Table 3.3). In spite of this, the cutaneous chloride cells showed a gradual and significant ($P<0.001$) decrease in size from hatching through to stage 3a-b, whilst, in contrast, the prebranchial cells showed a smaller but significant ($P<0.05$) increase in size with larval development.

3.2.3. Localisation and activity of Na^+,K^+ -ATPase

Injection of turbot larvae with 0.1 mM anthroylouabain resulted in the appearance of numerous, fluorescent, Na^+,K^+ -ATPase-rich cells (Fig. 3.31). Fluorescence was observed immediately after injection and lasted more than 10 minutes when viewed at low power magnification ($\times 6.3$ objective), although under high magnification ($\times 40$ objective) photobleaching occurred within 25-30 seconds. Anthroylouabain injection concentrations greater than 0.1 mM did not improve visibility, the higher concentrations only resulting in increased background fluorescence and loss of contrast.

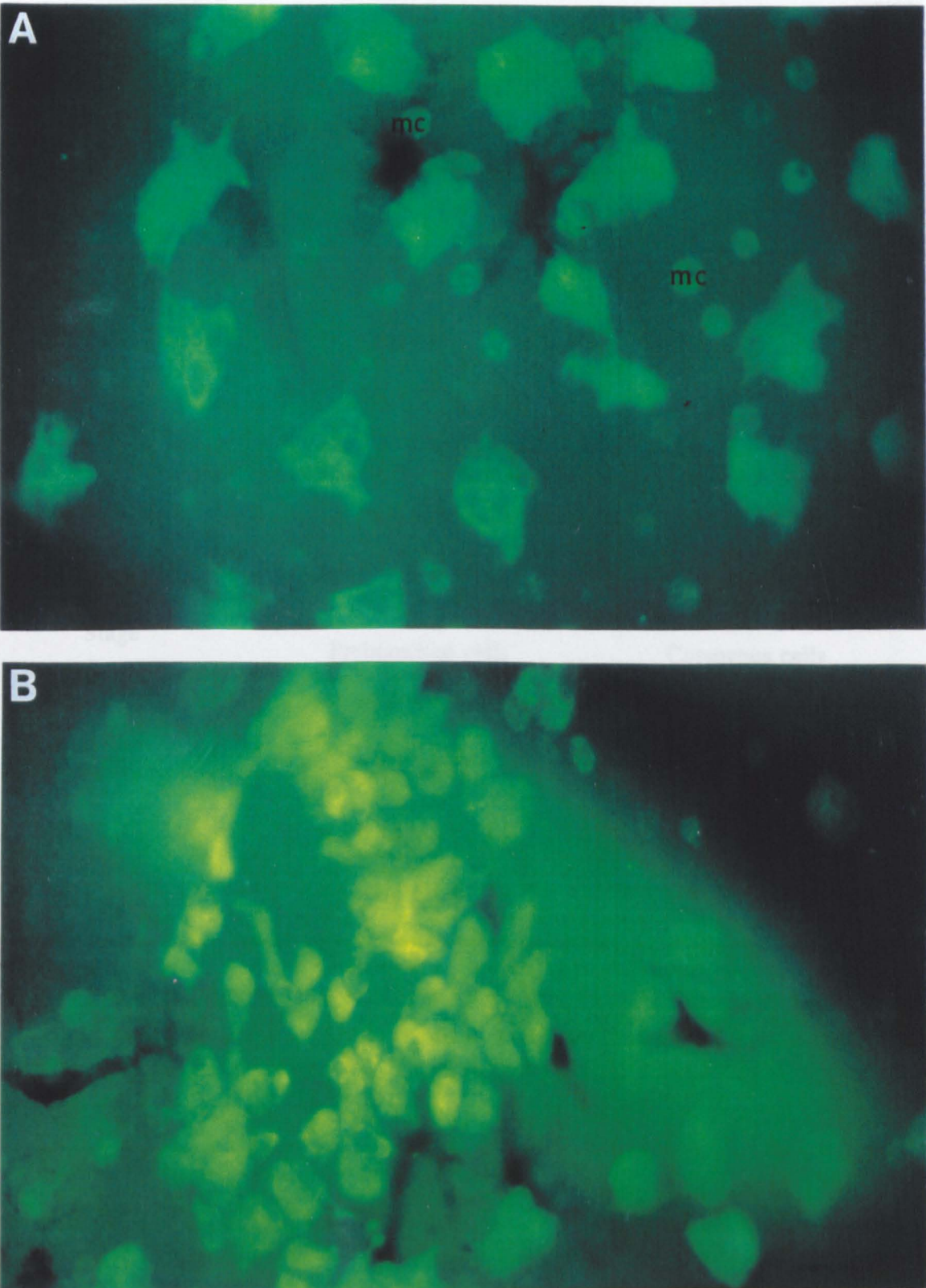


Fig. 3.30. Photomicrographs illustrating the morphological differences between cutaneous and prebranchially located chloride cells. A. Shows the large, flattened, cutaneous cells as revealed by DASPMI staining in the yolk sac epithelium. Note the irregularity in the shape of these cells due to lateral cytoplasmic extensions projecting from the cell body. Small, brightly fluorescing mucous cells (mc) are frequently observed between the chloride cells. B. Shows the tightly-aggregated and more spherically shaped prebranchial chloride cells. These cells are considerably smaller than the cutaneous chloride cells and appear to fluoresce more brightly. Note that areas without mitochondria, such as the cell nuclei seen in both micrographs, show low fluorescence. The scale bar is 30 μm in both micrographs.

Table 3.3. Measurements of the cross sectional area (\pm S.E., $n=20$) of DASPMI-stained chloride cells from the developmental stages of turbot larvae.

Stage	Mean cross sectional area (10^{-4} mm 2)	
	Prebranchial cells	Cutaneous cells
1a	1.58 \pm 0.10	6.30 \pm 0.39*
1c-d	1.87 \pm 0.08	4.89 \pm 0.23*
2b-c	2.11 \pm 0.07	4.02 \pm 0.24*
3a-b	2.37 \pm 0.08	2.95 \pm 0.17**

* $P<0.001$; ** $P<0.01$

On the basis of their size, morphology and location, the numerous anti- Na^+,K^+ -ATPase-rich cells during larval development were subdivided into three categories.

On the basis of their size, morphology and location, the numerous anti- Na^+,K^+ -ATPase-rich cells during larval development were subdivided into three categories.

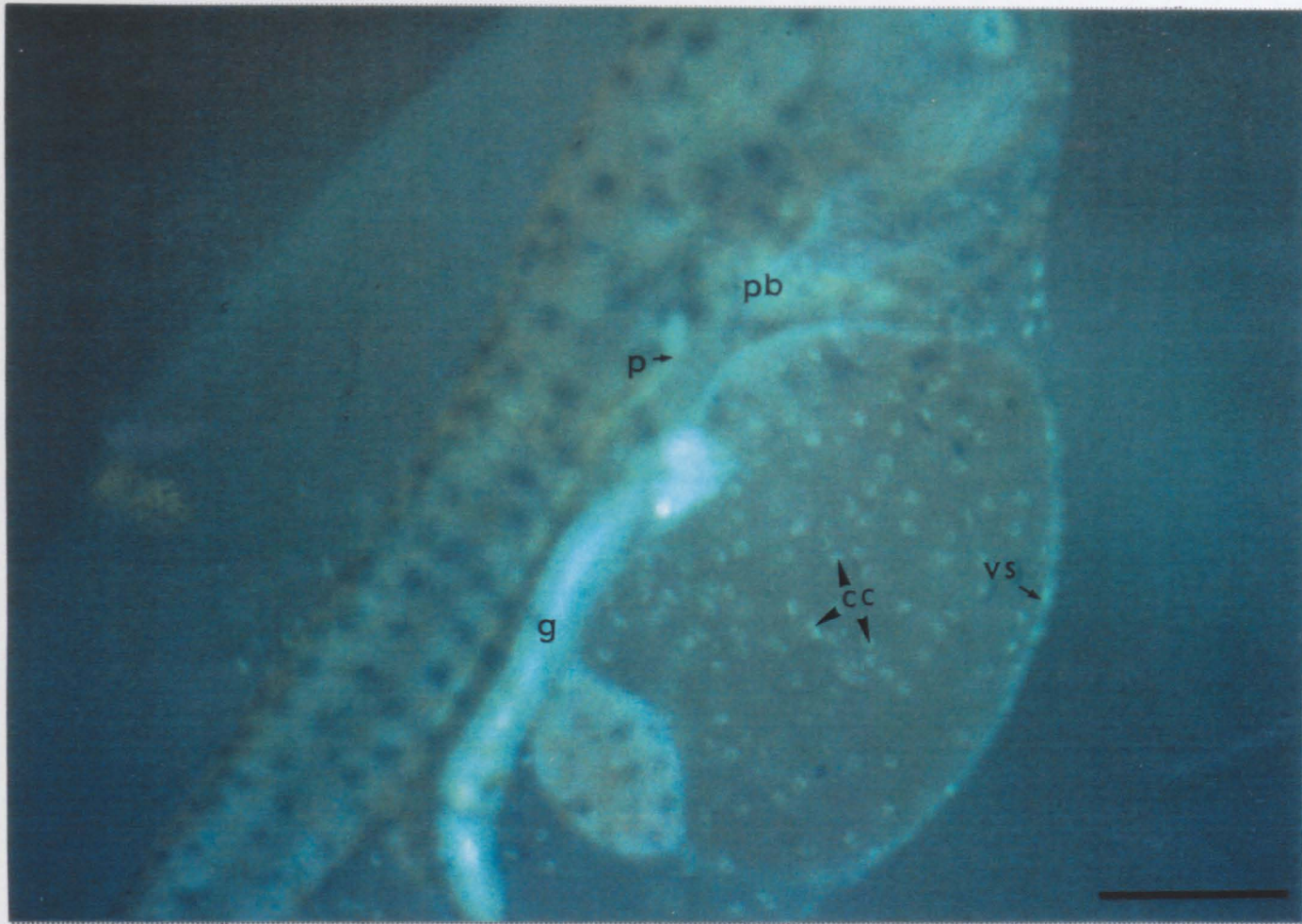


Fig. 3.31. Photomicrograph showing the distribution of Na^+,K^+ -ATPase-rich cells in the skin of a yolk-sac turbot larva as revealed by anthrotylouabain staining. The blue background fluorescence is observed in all preparations and is due to tissue autofluorescence, since it appears in the absence of anthrotylouabain. cc: cutaneous chloride cells; g: gut; ms: muscle tissue; p: pronephros; pb: prebranchial chloride cells; vs: vitelline sinus. The scale bar is 0.25 mm.

On the basis of their size, morphology and location, the numerous anthroylouabain-positive cells were positively identified as chloride cells by comparison with DASPMI-staining. Indeed, an area of reduced fluorescence caused by the cell nucleus could undoubtedly be observed in both staining procedures (Figs. 3.31 and 3.32). Simultaneous injection of control larvae with 0.1 mM anthroylouabain and 40 mM ouabain (to produce blood plasma concentrations of 2.5 µM and 1 mM respectively) completely abolished any cell fluorescence, demonstrating that the larval chloride cells contained functional ouabain-binding sites even at the earliest developmental stages post-hatching. However, observations of the anthroylouabain-stained cells in the skin of larvae from hatching to stage 2b revealed changes in the intensity and distribution of chloride cell Na^+,K^+ -ATPase with development.

In each of the larval stages examined, the anthroylouabain-stained prebranchial cells were always more highly fluorescing than the cutaneous chloride cells (Fig. 3.32). From hatching to developmental stage 1c-d, anthroylouabain fluorescence appeared to be uniformly distributed in the cytoplasm of all chloride cells, without exception (Figs. 3.32, 3.33A and B). However, by developmental stage 1d, some cutaneous chloride cells were noticeably less intensely stained than others (Fig. 3.33B), and signs of patchiness in the distribution of fluorochrome were sometimes detected. Beyond stage 2, the intensity of anthroylouabain fluorescence in the cutaneous cells rapidly declined (Fig. 3.33C), more so in some cells than in others, until, by late stage 2d/early stage 3, the cell fluorescence was barely visible at all (Fig. 3.33D).

On the basis of these observations, fluorescence imaging microscopy was employed to precisely quantify the anthroylouabain fluorescence and thus obtain direct measurements of the quantity of Na^+,K^+ -ATPase in labelled chloride cells. Indeed, the intensity of

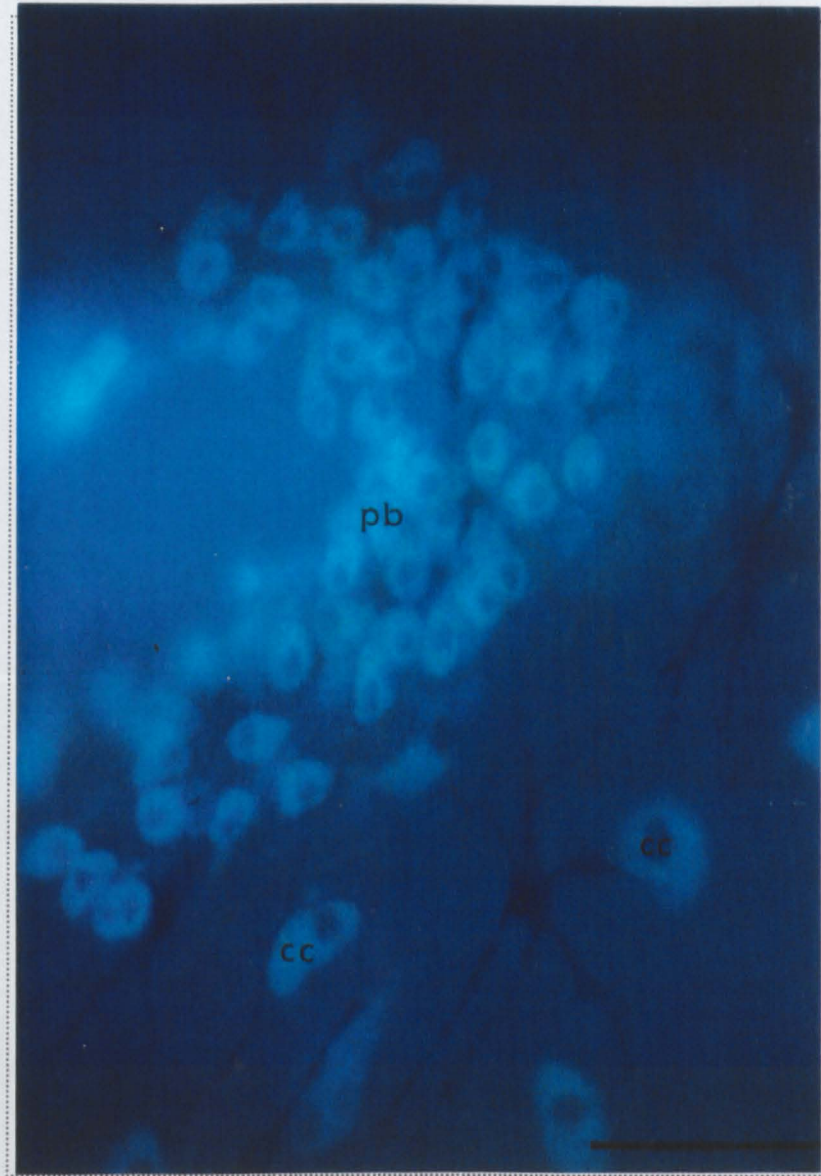


Fig. 3.32. Photomicrograph of anthrolyouabain-stained chloride cells in the prebranchial region of a stage 1a turbot larva. The closely aggregated prebranchial chloride cells (pb) fluoresce more brightly than the larger, flattened cutaneous cells (cc) observed below. Note the prominent cell nuclei appearing as darker, non-fluorescing areas. The scale bar is 25 μm .

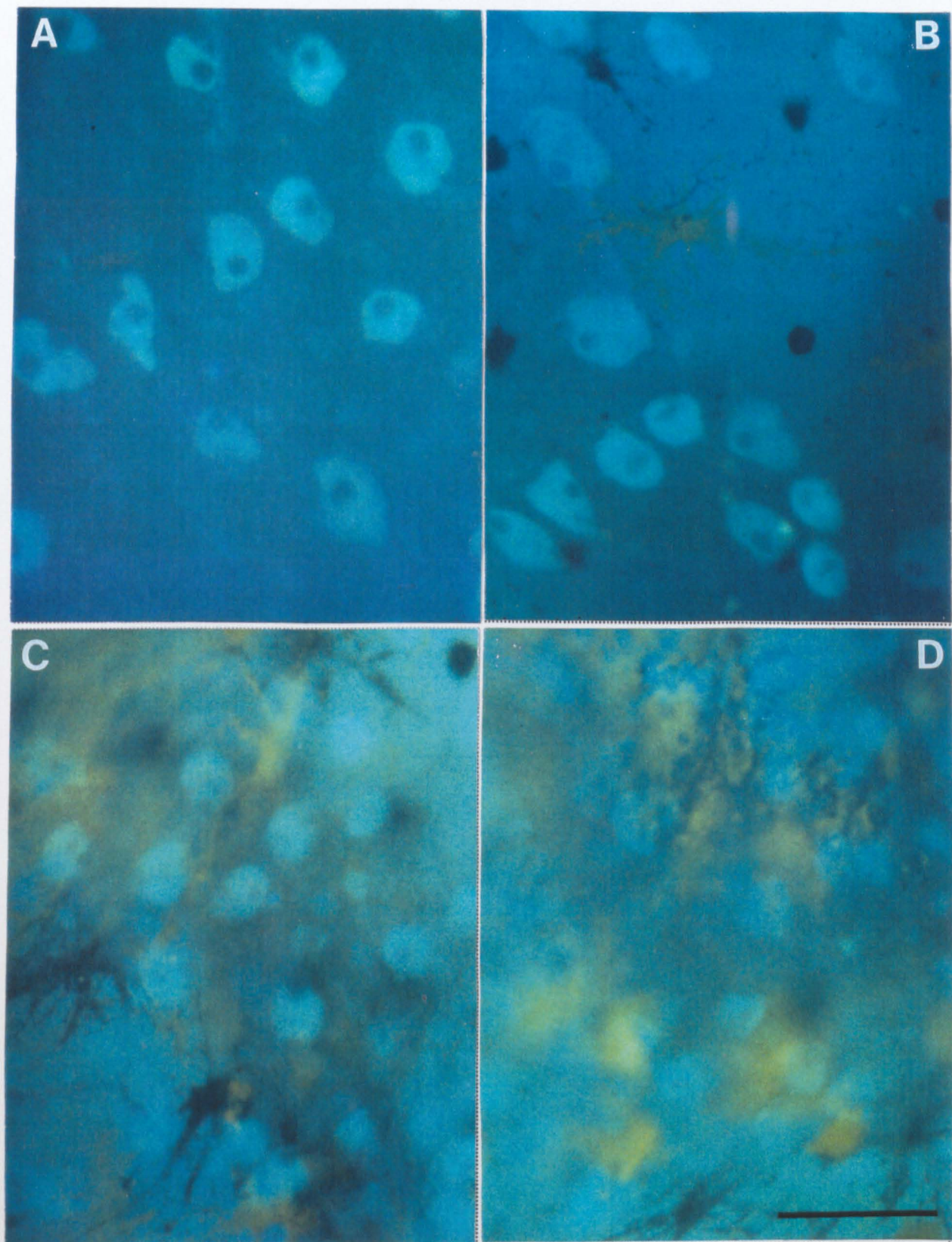


Fig. 3.33. Photomicrographs of anthrolyouabain-stained cutaneous chloride cells, showing changes in the localisation of Na^+,K^+ -ATPase with larval development: A, cells immediately after hatching, developmental stage 1a; B, at day 5 post-hatching, stage 1d; C, day 7-8 post-hatching, early stage 2; and D, at day 10 post-hatching, stage 2c. Scale bar is 50 μm .

fluorescence, measured as mean cell fluorescence, was significantly higher ($P>0.001$) in the prebranchial cells of all the developmental stages examined (Table 3.4), as previously intimated: photographs of captured video images from which the quantitative measurements were made are shown in figure 3.34. However, the total fluorescence, which takes the cross sectional area of each cell into account, was typically higher in the cutaneous chloride cells (Fig. 3.35).

The cutaneous cells exhibited a gradual decrease in fluorescence with increase in the age of larvae (Fig. 3.35), such that by day 7 after hatching (early stage 2), the total cutaneous cell fluorescence was just 25% of that measured from yolksac larvae on day 2 post-hatching. By contrast, the total prebranchial cell fluorescence increased significantly from days 2 to 3 ($P<0.001$) and 3 to 4 ($P<0.05$) post-hatching (Fig. 3.35) with absorption of the yolksac. A small but significant decrease in prebranchial cell fluorescence was observed between 4 and 5 days post-hatching, but measurements of the total fluorescence from larvae beyond 7 days post-hatch were consistently much lower. However, by day 7 the prebranchial cells were sited more deeply in the branchial chamber, which, in addition to the enriched pigmentation of the skin at this stage (seen in figures 3.33C and D), may have masked the true fluorescence exhibited by these cells.

Table 3.4. Measurements of the cross sectional area and mean cell fluorescence (\pm S.E., $n=50$) of anthroylouabain-positive chloride cells in turbot larvae aged between 2 and 7 days post-hatching.

Age (days post -hatching)	Prebranchial cells		Cutaneous cells	
	Area (10^{-4} mm 2)	Mean fluorescence (arbitrary units)	Area (10^{-4} mm 2)	Mean fluorescence (arbitrary units)
Day 2	1.45 \pm 0.06	117.88 \pm 4.30	5.60 \pm 0.25	80.58 \pm 3.72*
Day 3	1.76 \pm 0.07	142.48 \pm 4.69	4.82 \pm 0.26	90.08 \pm 4.27*
Day 4	1.89 \pm 0.06	148.22 \pm 4.18	4.56 \pm 0.17	73.69 \pm 3.16*
Day 5	1.81 \pm 0.06	129.79 \pm 4.42	4.24 \pm 0.15	57.52 \pm 5.19*
Day 6	1.84 \pm 0.07	122.53 \pm 4.70	3.95 \pm 0.20	63.14 \pm 4.47*
Day 7	1.48 \pm 0.05	73.65 \pm 3.52	3.46 \pm 0.10	30.55 \pm 2.02*

* $P<0.001$

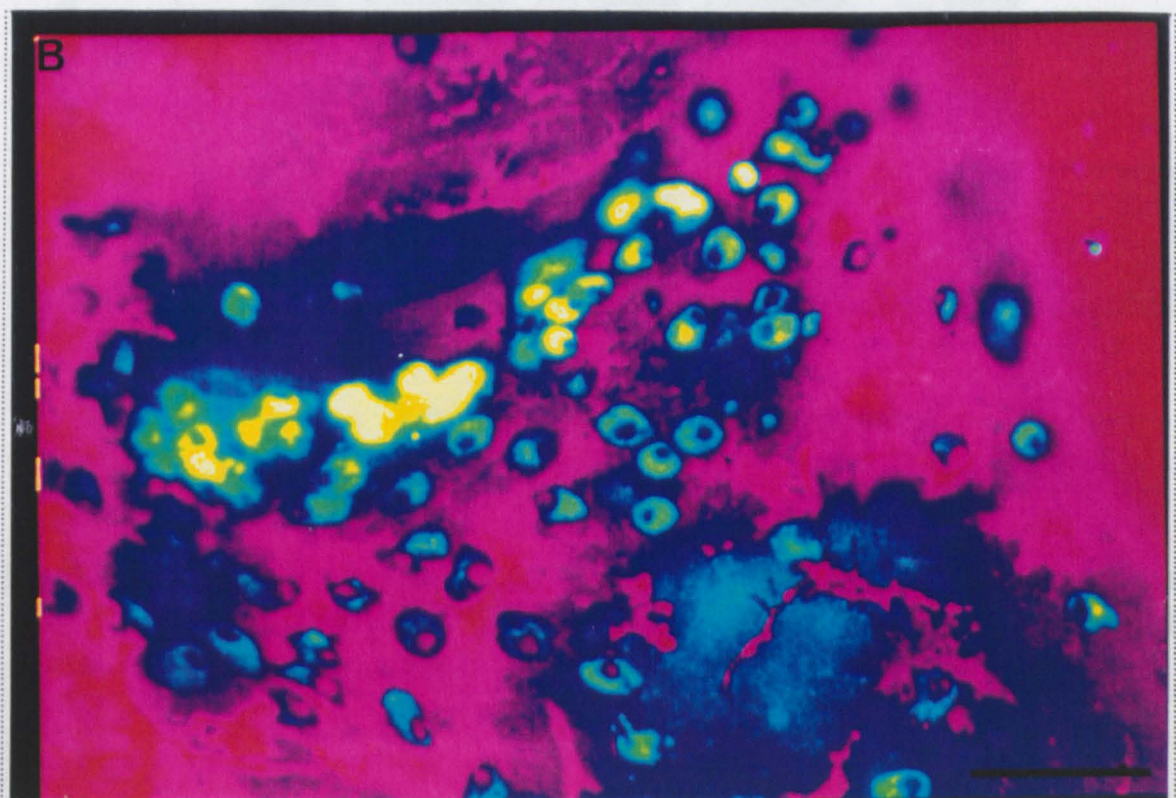
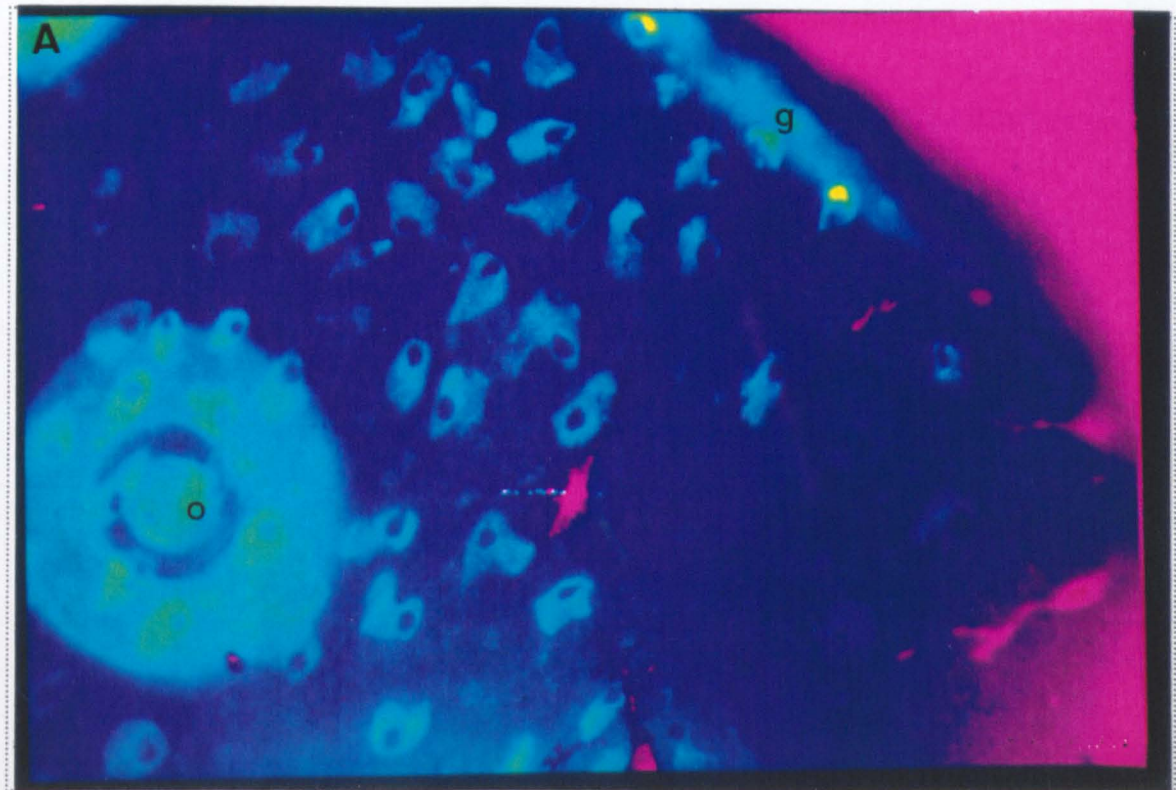


Fig. 3.34. Computer enhanced epifluorescence images of the skin of larval turbot showing anthrolyouabain fluorescence in the cutaneous and prebranchial chloride cells, A and B respectively. The images are colour coded, yellow signifying the highest fluorescence and red the lowest. o: yolk sac oil globule; g: gut. The scale bars are 30 μm in each case.

3.3. The Water Transport Rates and Diffusional Water Permeabilities of Early Post-hatch Turbot Larvae

The time courses of water uptake by the early post-hatched larvae of turbot (derived from equation 2-1, section 2.4) are shown in Table 3. In addition, the lines are drawn to the best fit second order polynomial regression equation to the data points.

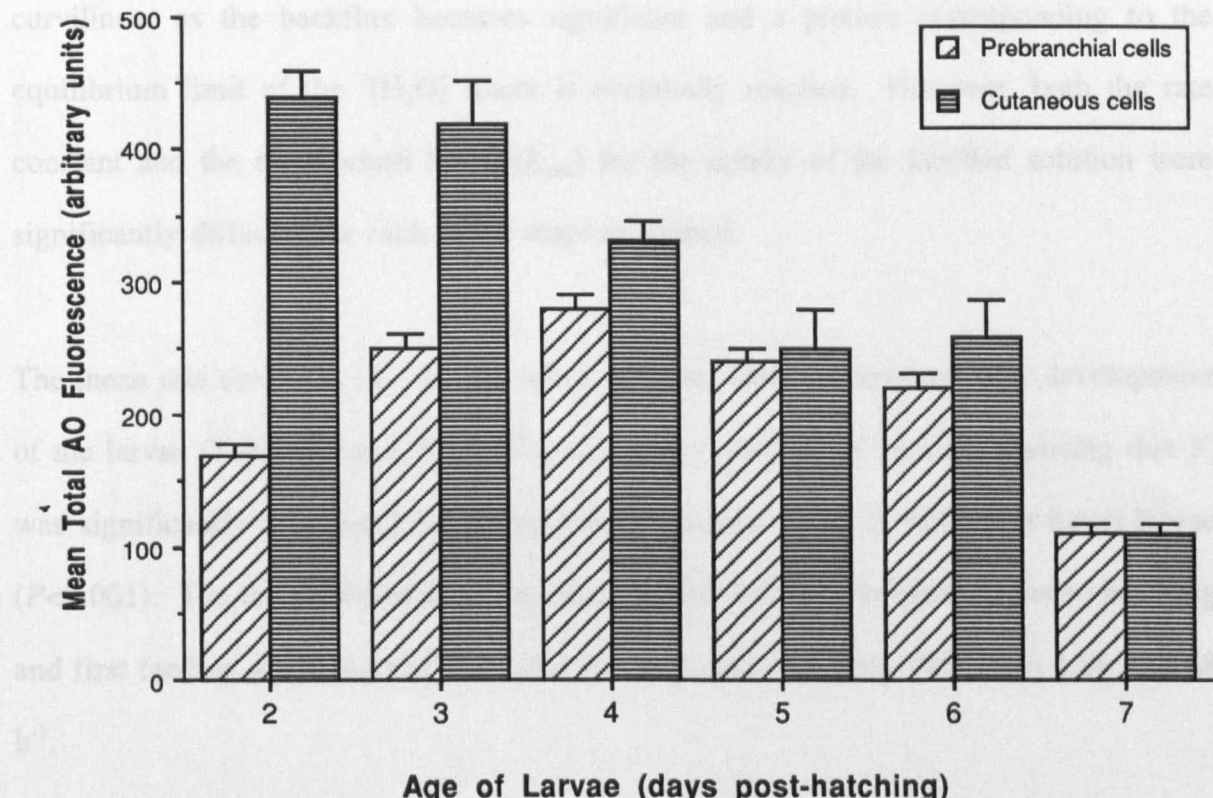


Fig. 3.35. Graph to show the mean total fluorescence (\pm S.E.) in anthroylouabain-stained prebranchial and cutaneous chloride cells of turbot aged from 2 to 7 days post-hatching.

3.3. The Water Turnover Rates and Diffusional Water Permeabilities of Early Post-hatch Turbot Larvae

The time courses of water uptake by the early developmental stages of turbot (derived from equation 2-1, section 2.4) are shown in figure 3.36. In each case, the lines are curvilinear as the backflux becomes significant and a plateau corresponding to the equilibrium limit of the ${}^3\text{H}_2\text{O}$ tracer is eventually reached. However, both the rate constant and the equilibrium limit (Q_{limit}) for the uptake of the labelled solution were significantly different for each larval stage examined.

The mean rate constants (K_i) for the influx of water clearly decreased with development of the larvae (Table 3.5 and Fig. 3.37); a one-way analysis of variance showing that K_i was significantly influenced by the age/developmental stage of early post-hatch larvae ($P<0.001$). The largest decrease in the rate of influx was seen to occur between hatching and first feeding stages 1a and 1c-d, the rate constants falling by 14% from 1.96 to 1.68 h^{-1} .

Between stages 1a and 2b-c, the equilibrium limits increased from 0.66 to 2.24 mg (or μl) larva^{-1} (Table 3.5). These values intimately corresponded with the mean water contents determined for each larval stage (Table 3.6). In addition, the larval surface area was seen to increase with development from $4.27 \pm 0.17 \text{ mm}^2$ at stage 1a to $4.37 \pm 0.18 \text{ mm}^2$ at stage 1c-d and to $7.87 \pm 0.20 \text{ mm}^2$ by stage 2b-c ($n=10$) (Appendix F).

Despite the decline in the rate of water turnover with development, the permeability of the turbot larva was seen to increase from hatching through to developmental stage 2b-c. The

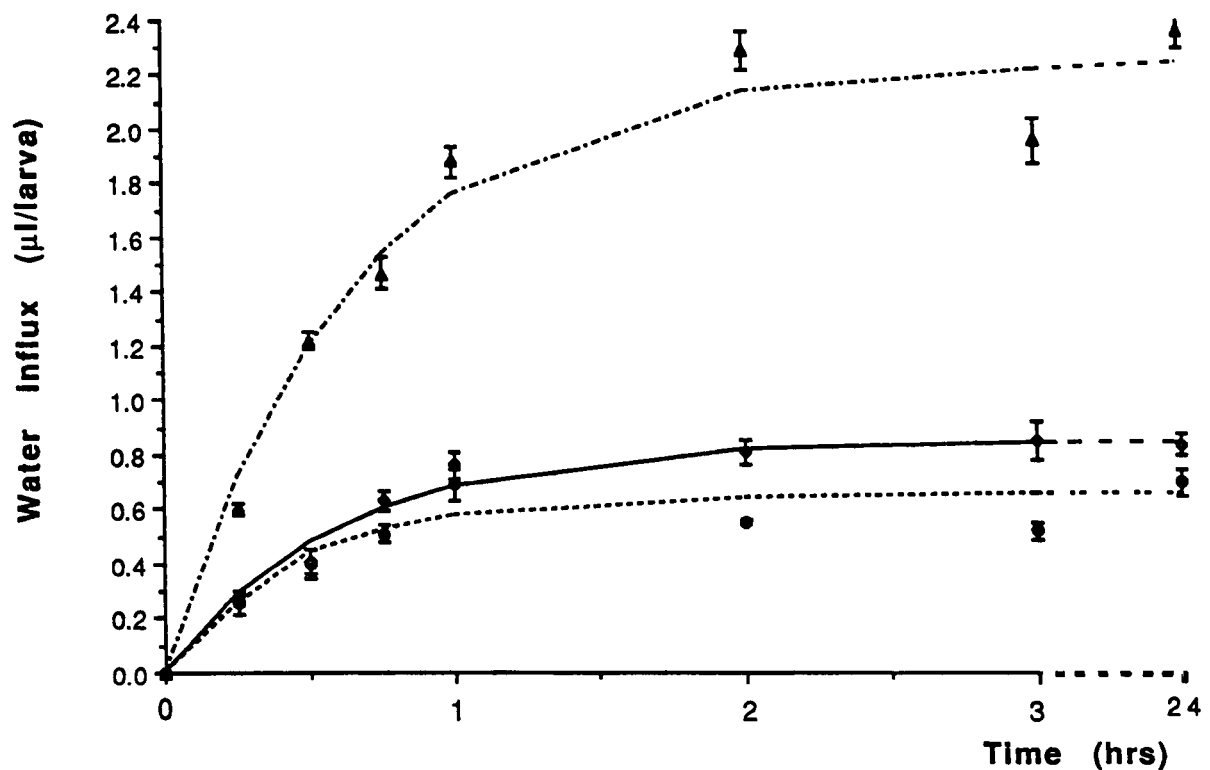


Fig. 3.36. Graph to show the time courses of water influx in the early developmental stages of the turbot larva. The points and bars are mean and standard error values respectively. •, stage 1a; ♦, stage 1c-d; and ▲, stage 2b-c.

Table 3.5. Parameters (\pm S.E.) of first order rate equations used for regression analysis of time courses of water uptake and for calculating the permeability of larvae at 15°C.

Stage	$Q_{\text{limit}}^{\dagger}$ (mg/larvae)	K_i (h^{-1})	P_{diff} ($\mu\text{m. s}^{-1}$) $\times 10^{-3}$
Substage 1a (day 1)	0.66 \pm 0.04	1.96 \pm 0.50	8.49
Substage 1c-d (day 4-6)	0.85 \pm 0.03	1.68 \pm 0.20	9.22
Substage 2b-c (day 8-10)	2.24 \pm 0.07	1.54 \pm 0.17	12.64

[†] The equilibrium limit (Q_{limit}) is taken at 24 h

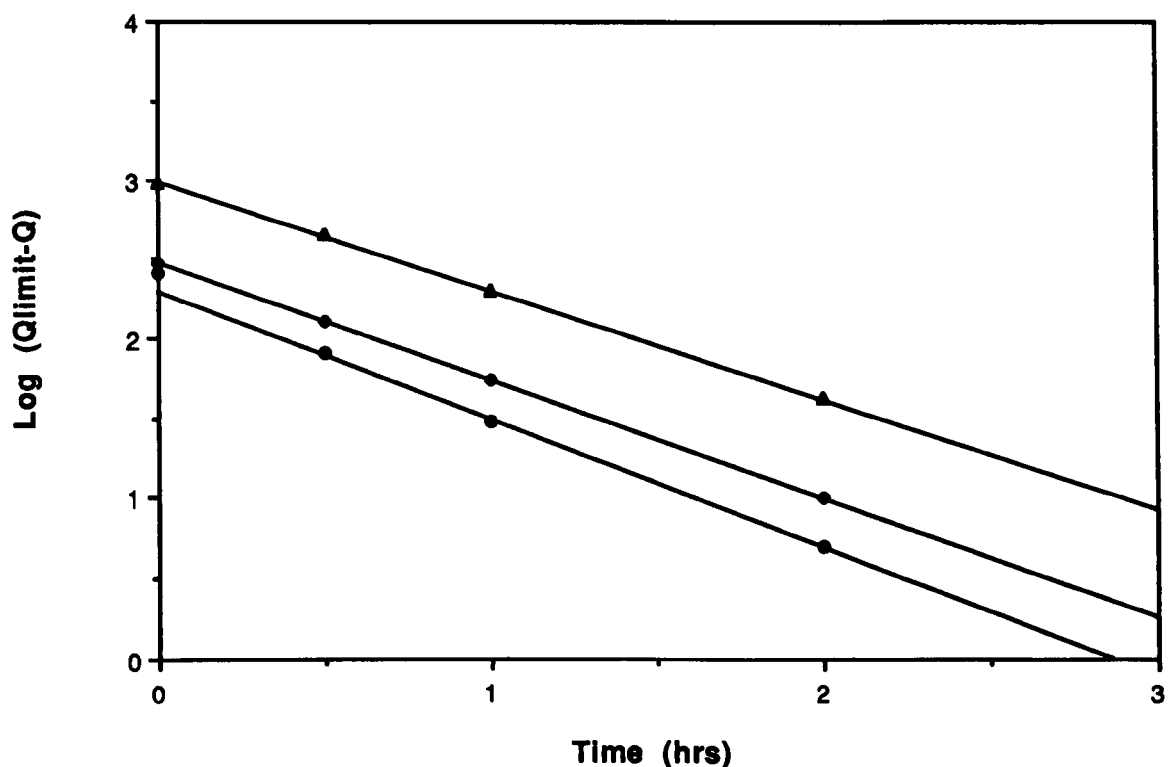


Fig. 3.37. Exponential transformations of the water influx data, based on Equation 2-1. The slopes of the lines give values for the hourly rate constants (K_i). •, stage 1a; ◆, stage 1c-d; and ▲, stage 2b-c.

Table 3.6. Measurements of the mean wet and dry weights of turbot larvae, from hatching to approximately 8-10 days post-hatching, used in the estimation of the water content of individuals.

Stage	Wet weight (mg)	Dry weight (mg)	Water Content (mg)	% Body Water
1a	0.62	0.01	0.61	98.4
1c-d	0.91	0.02	0.89	97.8
2b-c	2.43	0.09	2.34	96.3

3. Results

lowest permeability of $8.49 \times 10^{-3} \mu\text{m.s}^{-1}$ was observed in the newly-hatched turbot larva (Table 3.5). At stage 1c-d, the permeability was seen to increase by a small but not significant ($P>0.10$) margin. However, a significant increase ($P<0.001$) in the diffusional permeability was observed by developmental stage 2b-c, the P_{diff} increasing from 9.22 to $12.64 \times 10^{-3} \mu\text{m.s}^{-1}$ (Table 3.5).

3.4.

Microelectrode Studies

3.4.1. Measurement of the TEP

Transepithelial potentials were recorded at 15°C in developing turbot larvae from stage 1a (newly hatched) through to stage 3a (11-12 days post-hatching at 15°C). Stable serosal-positive TEP's were recorded from turbot larvae from hatching through to stage 2b-c (8-10 post-hatching), the stability of the potentials recorded indicating that microelectrode penetration caused no significant damage to the larval integument. Beyond stage 2c, however, successful penetration of the body cavity proved to be extremely difficult and hence stable, reproducible recordings of the TEP were rarely, if ever, obtained.

Initial measurements from several positions along the trunk of larvae revealed no significant differences in the recorded potential, although it was more difficult to achieve successful penetration at some sites. Consequently, all recordings were made from the anterior base of the dorsal fin fold which is located dorsal to the prebranchial chloride cells and the site of gill development. Microelectrodes, when placed at the base of the dorsal fin fold, were advanced into a fluid filled space which avoided errors resulting from tip placement in other tissues. If the tip of the microelectrode was advanced too far through the fin fold it would exit the larva and record a zero potential, thus recordings could be made from this region with greater confidence.

Microelectrodes used immediately or up to 3 hours after fabrication gave identical results. When the tip of a recording electrode was advanced through the larval integument, an abrupt positive shift in the voltage trace was observed (Fig. 3.38). However, the integument proved to be difficult to penetrate for most stages of larvae and where

III

IV

II

I

consecutive bursts
of negative capacitance

III

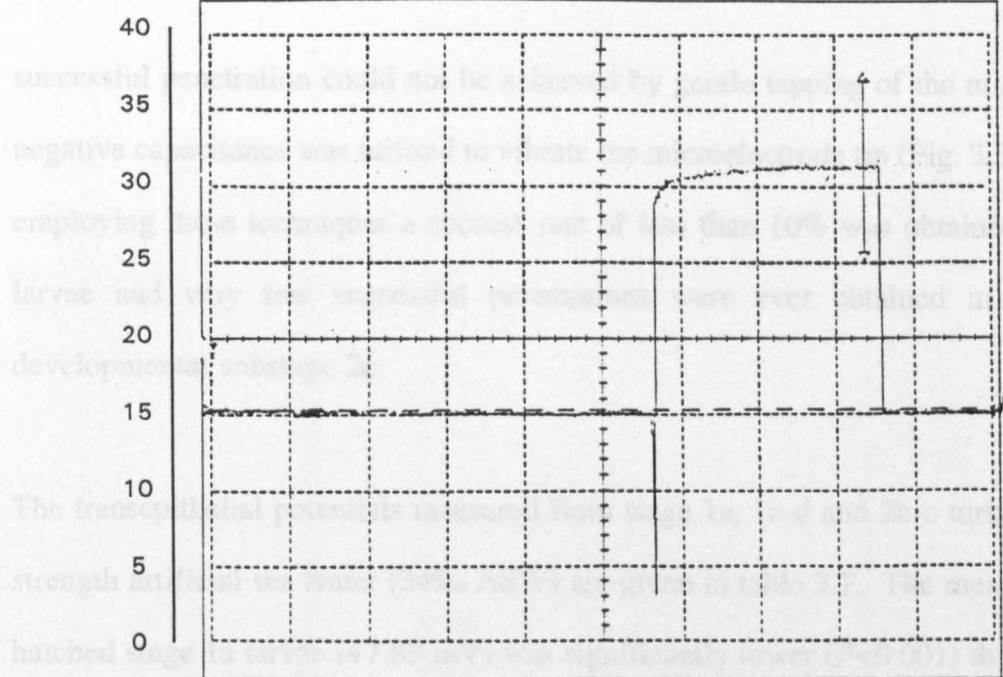
IV

II

I

mV

(a)



mV

(b)

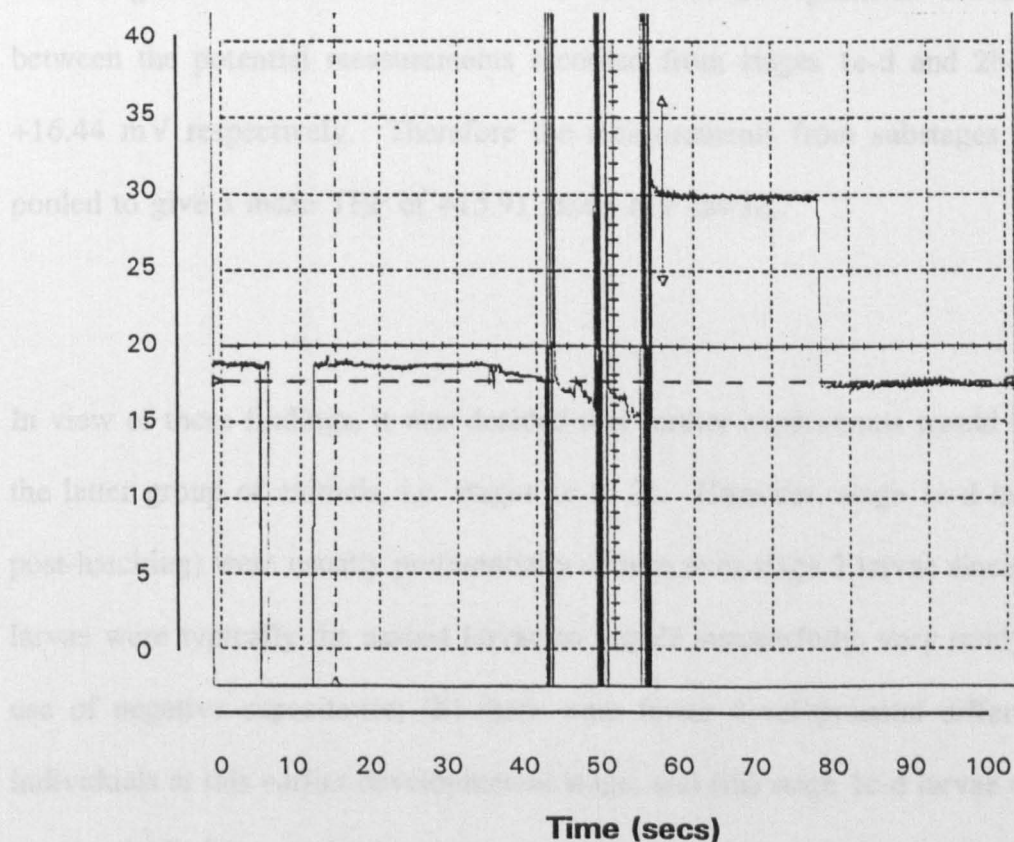
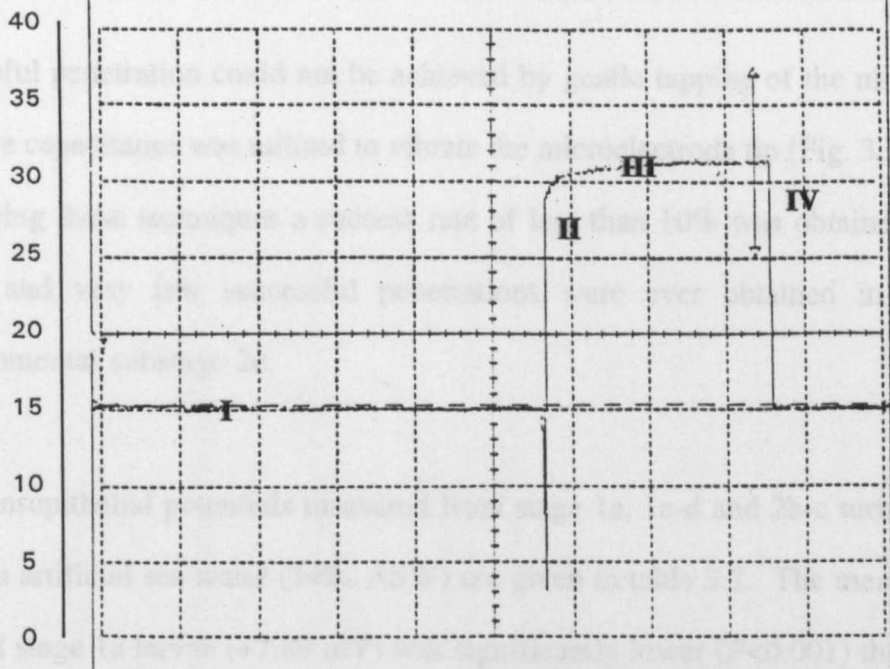


Fig. 3.38. Recordings of TEP's showing (a) the typical abrupt positive shift in voltage as the tip of a microelectrode is manually advanced into the fluid filled haemocoel of a turbot larva; and (b) the utilisation of negative capacitance to facilitate microelectrode impalement. At point I, the p.d. between the recording electrode and the reference electrode is arbitrarily zero. When the recording electrode successfully penetrates the body cavity, a voltage change is registered, point II. The potential is allowed to stabilise, point III, and at point IV the microelectrode is withdrawn.

mV

(a)



mV

(b)

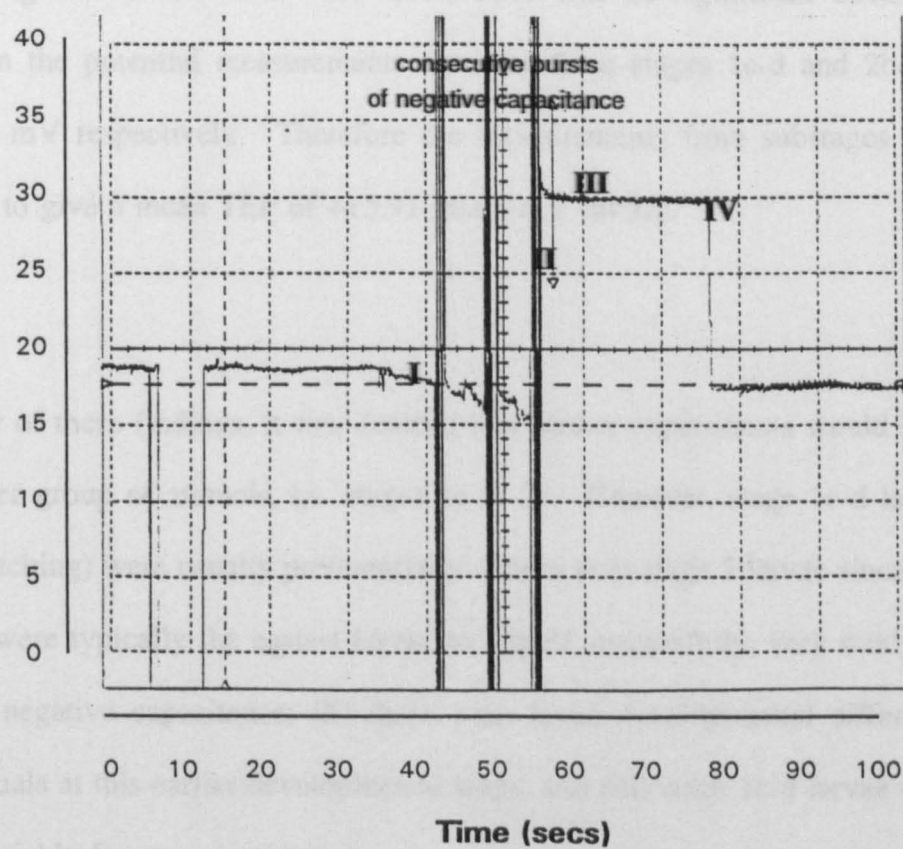


Fig. 3.38. Recordings of TEP's showing (a) the typical abrupt positive shift in voltage as the tip of a microelectrode is manually advanced into the fluid filled haemocoel of a turbot larva; and (b) the utilisation of negative capacitance to facilitate microelectrode impalement. At point I, the p.d. between the recording electrode and the reference electrode is arbitrarily zero. When the recording electrode successfully penetrates the body cavity, a voltage change is registered, point II. The potential is allowed to stabilise, point III, and at point IV the microelectrode is withdrawn.

successful penetration could not be achieved by gentle tapping of the micromanipulator, negative capacitance was utilised to vibrate the microelectrode tip (Fig. 3.38). Even when employing these techniques a success rate of less than 10% was obtained with stage 1a larvae and very few successful penetrations were ever obtained in larvae beyond developmental substage 2c.

The transepithelial potentials measured from stage 1a, 1c-d and 2b-c turbot larvae in full strength artificial sea water (34‰ ASW) are given in table 3.7. The mean TEP in newly hatched stage 1a larvae (+7.89 mV) was significantly lower ($P<0.001$) than that recorded from stages 1c-d and 2b-c. However, there was no significant difference ($P>0.40$) between the potential measurements recorded from stages 1c-d and 2b-c, +15.37 and +16.44 mV respectively. Therefore the measurements from substages 1c to 2c were pooled to give a mean TEP of $+15.91 \pm 0.63$ mV ($n=32$).

In view of these findings, it was decided that further experiments would be restricted to the latter group of animals, i.e. stages 1c to 2c. However, stage 1c-d larvae (4-6 days post-hatching) were usually preferentially chosen over stage 2 larvae since: (i) stage 1c-d larvae were typically the easiest larvae to impale successfully, very rarely requiring the use of negative capacitance; (ii) there were fewer developmental differences between individuals at this earlier developmental stage; and (iii) stage 1c-d larvae could be raised more quickly for experimentation.

Table 3.7. TEP measurements (\pm S.E.) recorded from different stages of turbot larvae bathed in ASW at 15°C.

Larval Stages	TEP (mV)	Range		<i>n</i>
		Lower	Upper	
Substage 1a (day 1)	+ 7.89 \pm 0.51	+5	+10	9
Substage 1c-d (day 4-6)	+15.38 \pm 0.95	+11	+23	16
Substage 2b-c (day 8-10)	+16.44 \pm 0.82	+11	+21	16

3.4.2. Nernst and Goldman kinetics

In general, the observed potentials were strongly positive with respect to the seawater bathing medium and were very much closer to the Nernst equilibrium potential for sodium (E_{Na}) than to that for chloride (E_{Cl}); both of which were calculated using estimations by Tytler & Bell (1989) of internal Na^+ and Cl^- concentrations for 9 day old cod larvae.¹ Viz, for sodium:

$$\text{and for chloride, } E_{Na} = \frac{8.314 \times 288.16}{96487} \ln \frac{[458.8]}{[189.0]} = +22.02 \text{ mV}$$

$$E_{Cl} = \frac{8.314 \times 288.16}{96487} \ln \frac{[148.0]}{[535.3]} = -31.92 \text{ mV}$$

the respective Nernst potentials suggesting that the conductance of sodium ions must be far greater than that of chloride ions. Hence, using these values in relation to the mean observed potential (+15.91 mV), the ratio of chloride to sodium conductance (i.e. P_{Cl}/P_{Na}) could be approximated (after Potts & Eddy, 1973b) as:

$$\frac{22.02 - 15.91}{15.91 + 31.92} = \frac{6.11}{47.83} = 0.126$$

and, accordingly, this approximation could then be substituted into the Goldman/Hodgkin-Katz relation (Equation 2-4) such that:

$$E = \frac{RT}{F} \ln \frac{[Na^+]_o + 0.126 [Cl^-]_i}{[Na^+]_i + 0.126 [Cl^-]_o}$$

¹ Although Divil (1994) has measured osmolarity and Cl^- concentrations in the blood of juvenile turbot, in the absence of measurements of internal Na^+ for this species in the literature, the data was incomplete and could not be used in calculations of the Nernst equilibrium potentials. However, the internal Cl^- concentration estimated for 9 day cod larvae (148 mM.l⁻¹) is similar to that measured by Divil in juvenile turbot (150.4 mM.l⁻¹). In view of this, and since the cod is also a stenohaline species and the composition of the larval body fluids is known to be similar to juveniles and adults (Guggino, 1980b; Alderice, 1988), the use of these measurements from larval cod are therefore justified.

Hence, at 15°C and in full strength salinity:

$$E = \frac{8.314 \times 288.16}{96487} \ln \frac{[458.8] + 0.126 [148.0]}{[189.0] + 0.126 [535.3]} = +15.7 \text{ mV}$$

In the following results, subsequent predictions of the TEP were thus obtained using this derivation of the Goldman relation incorporating the approximated permeability ratio as given.

3.4.3. The effect of incubation temperature on the TEP

The mean TEPs obtained from stage 1c-d turbot larvae incubated from hatching at 10, 15 and 20°C respectively are shown in figure 3.39. A one way analysis of variance showed that the TEP was significantly ($P<0.001$) influenced by the incubation temperature. Moreover, Dunnett's test (Zar, 1984) revealed that the mean potentials measured at 10 and 20°C (+9.7 and +20.6 mV respectively) (Table 3.8), were both significantly different from the potential measured at the control temperature, 15°C (Appendix G). The temperature coefficient (Q_{10}) for the mean potentials from 10 to 20°C was calculated as 2.12 and such a relationship could not be explained, in terms of passive ion movements, by the Nernst or Goldman equations (Table 3.9; Fig. 3.39).

3.4.4. The influence of ouabain

Injection of ouabain into the heart of stage 1c-d turbot larvae (0.5 mM ouabain.larva⁻¹) resulted in a highly significant ($P<0.001$, student t-test) and irreversible reduction in the measured potential. In control injections, however, where ouabain was absent from the

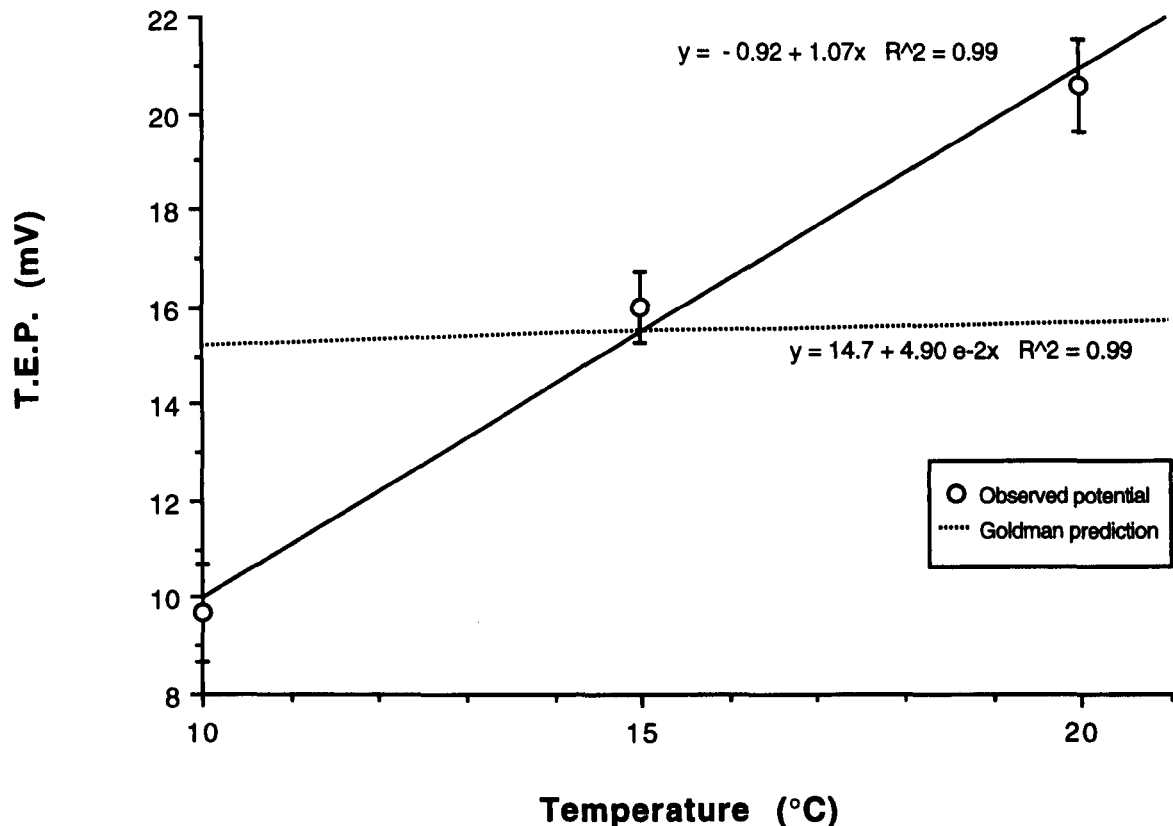


Fig. 3.39. Graph to show the effect of incubation temperature on the TEP recorded from stage 1c-d turbot larvae.

Table 3.8. TEP measurements (\pm S.E.) recorded from stage 1c-d larvae incubated at 10 and 20°C.

Temperature	TEP (mV)	Range		<i>n</i>	Q_{10}
		Lower	Upper		
Control (15°C)	+16.0 \pm 0.74	+10	+24	25	
10°C	+ 9.7 \pm 0.79	+6	+13	10	
20°C	+20.6 \pm 0.76	+17	+24	10	{ 2.12

Table 3.9. Nernst potentials for sodium and chloride[†], goldman predictions[†] and observed TEP measurements for stage 1c-d larvae incubated at 10, 15 and 20°C.

Incubation Temperature	Sodium Equilibrium Potential (mV)	Chloride Equilibrium Potential (mV)	Goldman Predicted TEP (mV)	Observed TEP (mV)
10°C	+21.64	-31.37	+15.18	+ 9.7
15°C	+22.02	-31.92	+15.45	+16.0
20°C	+22.41	-32.47	+15.72	+20.6

[†] For calculation purposes, the molarities of Na and Cl are given in Appendix H.

physiological saline, no significant change in the electrical potential was observed. Upon injection of the ouabain solution, a diphasic decline in the TEP was observed. Initially, the TEP rapidly declined to a lower, more steady-state potential, around 60-75% of the control level, within 5-6 mins. Thereafter, the potential showed a slower, more gradual decline which continued to fall in recordings made up to 30 mins. In view of this, the % inhibition by ouabain was measured 5 minutes after injection at which time the mean potential was determined as $+11.0 \pm 1.22$ mV ($n=5$); representing a 32% inhibition of the initial TEP measurement (Table 3.10).

3.4.5. The effect of environmental salinity on the TEP

The mean TEP's obtained from stage 1c-d turbot larvae incubated from hatching at 15°C in 24, 34 and 44‰ seawater respectively are given in table 3.11. A one way analysis of variance showed that the TEP was significantly ($P<0.001$) influenced by salinity. Moreover, a multiple comparison of the mean potentials using Dunnett's test showed that the measurements made in both 24 and 44‰ seawater were significantly different from the control measurements made in 34‰ seawater (Appendix G).

As figure 3.40 illustrates, the mean electrical potential showed a linear increase with increase in external salinity ($r^2=0.996$). Indeed, the mean TEP measured from larvae in 44‰ seawater was approximately double that made in 24‰ seawater. Moreover, the relationship between the TEP and the external salinity was found to closely approximate to Goldman predictions and Nernst relations for sodium (E_{Na}) (Table 3.12) suggesting that the measured potentials were largely diffusional in origin. Although this agreement was imperfect, the small discrepancies between the observed and predicted potentials could be

Table 3.10. The effect of serosally injected ouabain on the TEP measured from stage 1c-d turbot larvae (n=5).

	TEP (mV)	Range	
		Lower	Upper
Control potential (before injection)	+16.0 ±1.00	+13	+19
Ouabain (steady state)	+ 11.0 ±1.22*	+ 8	+15
% inhibition	31.65%	21.05%	47.06%

* $P<0.01$

Table 3.11. **TEP measurements (\pm S.E.) recorded from stage 1c-d larvae acclimatised in 24 and 44‰ seawater at 15°C.**

Salinity	TEP (mV)	Lower	Range	n
			Upper	
Control (34‰)	+16.0 \pm 0.74	+10	+24	25
24‰	+10.3 \pm 0.94	+7	+15	10
44‰	+23.1 \pm 1.25	+16	+29	10

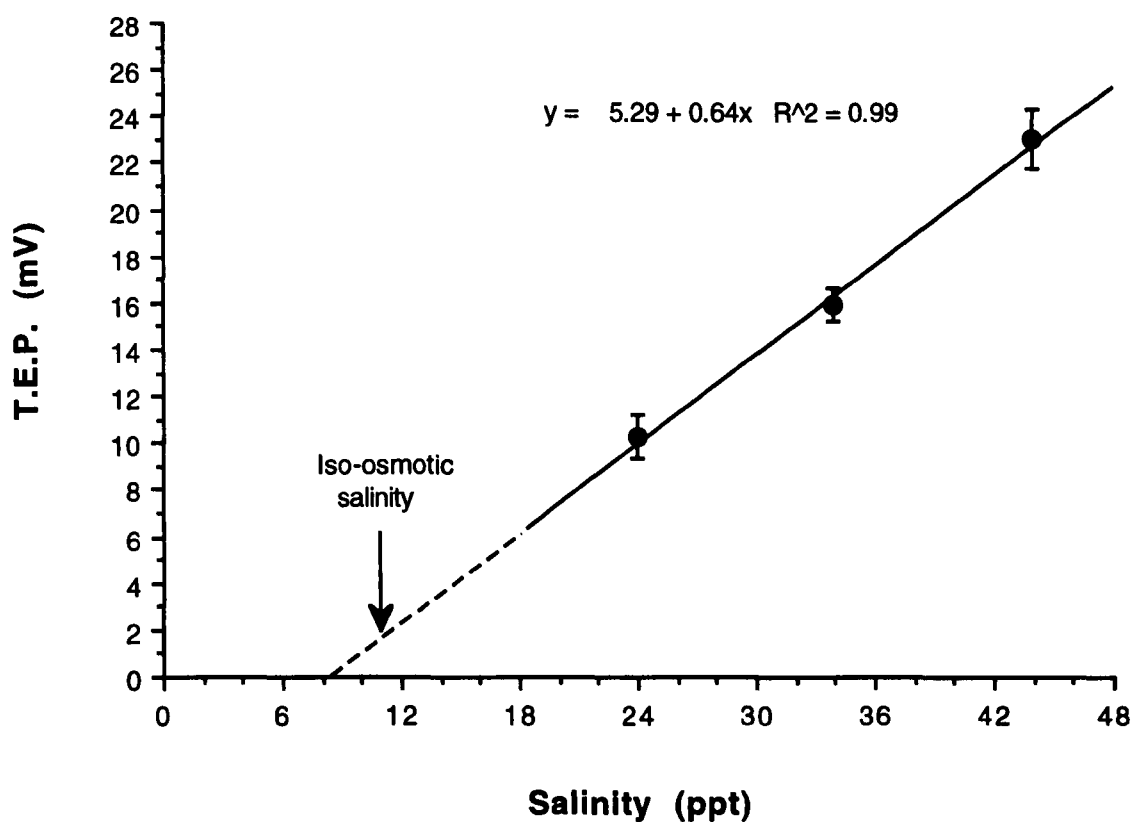


Fig. 3.40. Graph to show the effect of the external salinity on the TEP recorded from stage 1c-d turbot larvae.

Table 3.12. Nernst potentials for sodium and chloride[†], goldman predictions[†] and observed TEP measurements for stage 1c-d larvae incubated in 24, 34 and 44‰ seawater.

Incubation Salinity	Sodium Equilibrium Potential (mV)	Chloride Equilibrium Potential (mV)	Goldman Predicted TEP (mV)	Observed TEP (mV)
24‰	+14.64	-25.73	+ 9.87	+10.3
34‰	+22.02	-31.92	+15.45	+16.0
44‰	+27.71	-36.87	+19.53	+23.1

[†] For calculation purposes, the molarities of Na and Cl are given in Appendix H.

justified since all permeant ions in either the blood or the media will affect the potentials and the predictions were made only in relation to Na^+ and Cl^- .

3.4.6. The effects of alterations of external $[\text{Na}^+]$ and $[\text{Cl}^-]$ on the TEP

When 50% of the Cl^- ions in the external bathing medium were substituted with equimolar amounts of methylsulphate, a modest but significant ($P<0.05$, student t-test) reduction in the TEP was observed (Table 3.13). This potential was seen to decline further with the additional removal of further chloride ions (Fig. 3.41a), a one way analysis of variance showing that the TEP was significantly ($P<0.001$) influenced by the concentration of Cl^- in the external bathing medium. In 100% Cl^- -free ASW, the mean recorded potential was reduced to approximately 50% of the control potential measured in normal ASW.

Conversely, the substitution of Na^+ with choline had a much greater effect on the TEP, the replacement of Na^+ ions very significantly ($P<0.001$, student t-test) reducing the potential measurement and even reversing the polarity of the TEP at 75% substitution (Table 3.13). Thus, the TEP was significantly influenced by the external sodium concentration ($P<0.001$, ANOVA) and the reduction observed in the TEP with decrease in external Na^+ was linear (Fig. 3.41b).

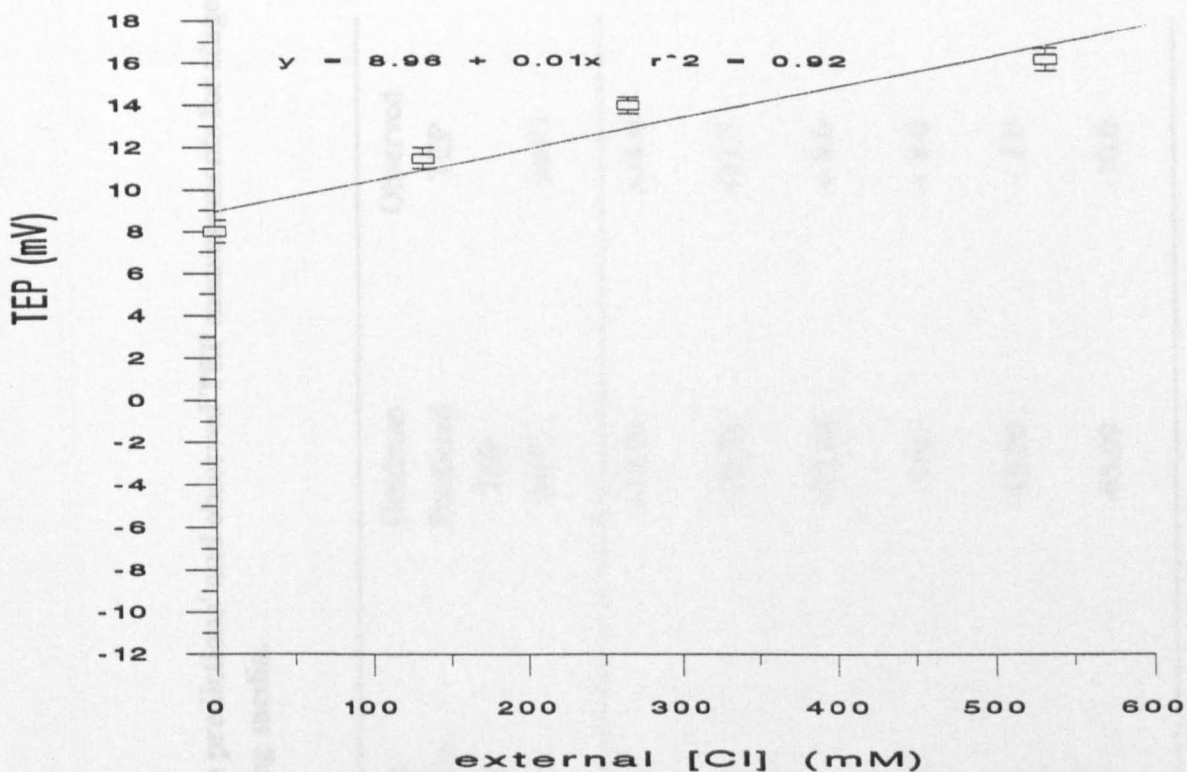
On both accounts, the observed potentials could not be explained by the calculated Nernst equilibrium and Goldman predictions (Table 3.14). Indeed, for Cl^- substitutions, the predictions, based on the passive movement of ions, suggested that the TEP should increase with the decrease in external Cl^- ions whilst in fact the opposite trend was

Table 3.13. TEP measurements made upon alteration of the Cl⁻ and Na⁺ ion concentrations in the external bathing solution (n=10).

Seawater Composition	TEP (mV)	Range	
		Lower	Upper
Control (1)	+16.2 ±0.53	+13	+19
50% Cl ⁻ free	+14.0 ±0.39**	+12	+16
75% Cl ⁻ free	+11.5 ±0.50*	+ 9	+14
100% Cl ⁻ free	+ 8.0 ±0.54*	+ 5	+10
Control (2)	+15.0 ±0.83	+10	+19
50% Na ⁺ free	+ 8.0 ±1.10*	+ 4	+14
75% Na ⁺ free	- 2.0 ±0.58*	- 5	+ 1
100% Na ⁺ free	-10.0 ±0.70*	-14	- 7

**P<0.05; *P<0.001

(a)



(b)

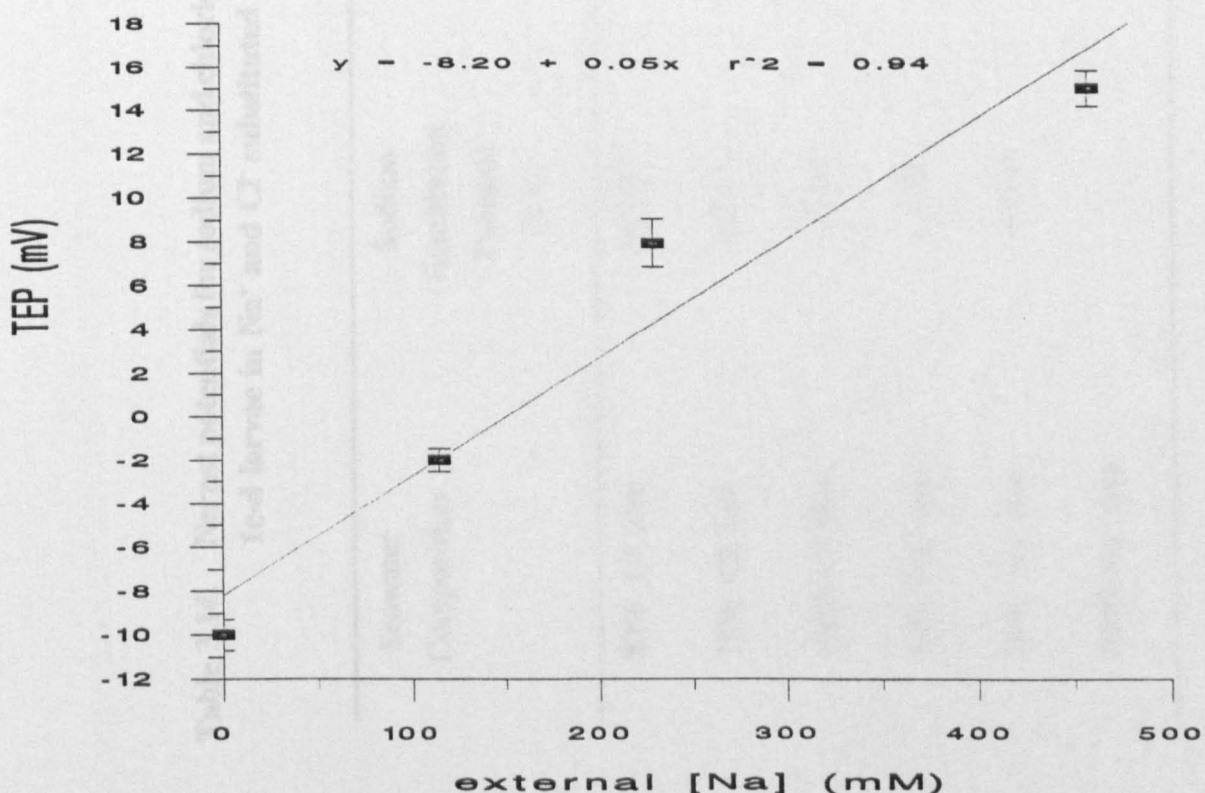


Fig. 3.41. Graphs to show the effect of external Cl^- and Na^+ concentrations on the TEP recorded from stage 1c-d turbot larvae.

Table 3.14. Nernst potentials for sodium and chloride[†], goldman predictions[†] and observed TEP measurements for stage 1c-d larvae in Na⁺ and Cl⁻ substituted ASW bathing media.

Seawater Composition	Sodium Equilibrium Potential (mV)	Chloride Equilibrium Potential (mV)	Goldman Predicted TEP (mV)	Observed TEP (mV)
50% Cl ⁻ free	+22.02	-14.72	+18.93	+14.0
75% Cl ⁻ free	+22.02	+ 2.50	+20.88	+11.5
100% Cl ⁻ free	+22.02	-	+23.00	+ 8.0
50% Na ⁺ free	+ 4.81	-31.92	- 0.82	+ 8.0
75% Na ⁺ free	-12.40	-31.92	-16.20	- 2.0
100% Na ⁺ free	-	-31.92	-65.09	-10.0

[†] The molarities of Na and Cl used in Nernst and Goldman predictions for the various substituted media, above, are given in Appendix H.

3. Results

observed. However, reintroduction of Na^+ and Cl^- to the bathing solutions quickly restored the potential to the control level.

4.1. The Skin as a Limiting Membrane to the Movement of Water and Ions

The skin of the nibot larva is very thin, averaging 42.5 μm in thickness in newly hatched larvae. For efficient gas/ox exchange, maximum function requires that the larval epithelium is relatively thin, but the very thickness of the skin might conceivably exacerbate the problems of salt influx and osmosis dominating the larva. However, electron microscopy revealed a number of microvilli-like protrusions to the skin of the

nibot larva which would presumably increase the surface area available for both diffusion and active transport, and reduce the concentration gradients tending to dominate and dominate the skin.

CHAPTER FOUR

Discussion

At the interface with the external environment, the skin of the nibot larva is composed of a single layer of epidermal cells (Fig. 1). The outer boundary of the epidermal layer is the basal membrane, which contains the basement membrane, the basal lamina, and the hemidesmosomes (Hawley & Eddy, 1991).

(Scott, 1989) of balance between ion movement and retention. However, whilst this may be advantageous for the adult fish, in the early stages of development (Hawley & Eddy, 1991), in particular, any increase in ion permeability may well in fact increase the ion concentration gradient across the epidermis. Because increasing the number of ions, nonetheless, can produce increased osmotic pressure, the diffusion of the glycoalyx increases following this increase in osmotic pressure (Hawley *et al.*, 1991). *In vivo*, Hawley *et al.* (1991) observed a reduction in the thickness of the glycoalyx in the epidermal cells from rainbow trout (*Oncorhynchus mykiss*) following exposure to increased concentrations of chloride. Furthermore, it was suggested that enhanced this

4.1. The Skin as a Limiting Membrane to the Movement of Water and Ions

The skin of the turbot larva is very thin, measuring <2.5 µm in thickness in newly hatched larvae. For efficient gaseous exchange, respiratory function requires that the larval epithelium is relatively thin, but the very thinness of the skin might conceivably exacerbate the problems of salt influx and water loss confronting the larva. However, electron microscopy revealed a number of specialised structural features in the skin of the turbot larva which would appear to provide some protection against the high osmotic and ionic gradients tending to dehydrate and salt-load the body fluids and tissues.

At the interface with the external environment, the external plasma membrane of the outer layer of epidermal cells was covered by a prominent glycocalyx coat. According to Powell *et al.* (1994), strong negative charges on the oligosaccharide moieties of glycocalyx components could be important in the electrostatic attraction and adsorption (Scott, 1989) of cations to the mucosal (exterior) surfaces of cells. However, whilst this may be advantageous for freshwater fish living in a hypotonic environment (Handy & Eddy, 1991), in seawater, cation adsorption to the extraepithelial covering would in fact increase the ion concentration gradient across the epithelium, thereby assisting the transfer of ions. Nonetheless, morphometric studies of the epidermis of adult guppy, *Poecilia reticulata* Peters, (Schwerdtfeger, 1979a,b) have shown that the thickness of the glycocalyx increases following adaption of the fish to seawater. Furthermore, Powell *et al.* (1995) observed a reduction in the height of the glycocalyx of branchial epithelial cells from rainbow trout (*Oncorhynchus mykiss* Walbaum) following exposure to sublethal concentrations of chloramine-T, a therapeutic agent used in aquaculture, and suggested this

reduction was coincident with a mechanism for the remedial uptake of ions with the possible influx of water. Thus, it is concluded that the transcellular movement of water and/or ions across the epithelial surface of the larval skin may be significantly impeded by the plasmalemma-associated glycocalyx, although the precise mechanisms for such processes remain unclear.

A thick external mucous covering might also retard transepithelial exchange through the surface epithelium to some extent (Guth & Engelhardt, 1989), and in the present study large numbers of mucous cells were a characteristic feature of the skin of the turbot larva suggesting that the overall production of mucous in this species is very high. Although the role of mucous in ionoregulation is still largely unclear, Pickford *et al.* (1966) have shown that removal of the mucous coat from the skin of various adult teleost species disturbs saltwater tolerance. In fact, young migrating elvers can adapt themselves to abrupt changes in salinity only when their mucous coat remains intact (Van Oosten, 1957). Yet, *in vitro*, mucous may not impede ion diffusion. For example, Marshall (1978) demonstrated that the diffusion coefficient of mucous isolated from the Pacific staghorn sculpin (*Leptocottus armatus* Girard) was similar to that of the control saline solution. However, *in vivo*, preparations of oesophageal epithelium from the New Zealand black flounder (*Rhombosolea retiaria* Hutton) have been shown to maintain a gradient of calcium, sodium and potassium activity in an "unstirred layer" (Kirsch, 1978), 50-1200 µm above the mucous coating (Shephard, 1982). Such a gradient could conceivably restrict osmotic water fluxes and ion movements by either increasing the resistance of the epidermis to diffusion (by increasing the thickness of the blood-water barrier), or by decreasing mixing and convection at the surface of the skin (Shephard, 1982; Ingersoll *et al.*, 1990). Hence, it can be concluded that, in the context of this study, the maintenance

of a thick mucous layer and indeed its interaction with the underlying glycocalyx matrix will be of considerable functional significance in the skin of the larval turbot.

With respect, the surface microridges observed in early post-hatch turbot may be important for anchorage of the "protective" mucous barrier to the superficial epidermal cell surfaces. Certainly amongst the cell surfaces so far examined with SEM, few cells in other animals are known to possess microridges, but the ones that do are found in places where maintaining a mucous layer is advantageous such as the polygonal cells of the toad bladder (Davis *et al.*, 1973) and the corneal epithelium of elasmobranchs (Harding, 1973). In addition, since microridges evidently increase the surface area of the superficial pavement cells, they may also be important for gaseous exchange and the excretion/absorption of small molecules (Jones *et al.*, 1966; Yamada, 1968; Hawkes, 1974). For example, the surface of the gills of the rainbow trout, *Salmo gairdneri* Richardson, have microridges which increase their absorptive capacity by 2.5 times (Olson & Fromm, 1973). Furthermore, Bereiter-Hahn (1971) has described the initiation of primary wound closure by microridges, demonstrating that the microridges could move by contraction of their basal microfilaments. Since an increased loss of water and diffusion of salts is known to occur through the damaged skin of injured marine teleost fish (Van Oosten, 1957), this phenomenon could also be functionally significant in early post-hatch larvae. However, any significance is likely to be secondary to the preceding functions reflecting exchange processes across the surface epithelium.

In the outer layer of the epidermis itself, forming the primary barrier to the diffusion of water and ions, the opposing membranes of adjacent cells (both pavement and chloride cells) were intimately fused at the cell apices by tight junctions or *zonulae occludens*, first

described by Farquhar & Palade (1963). Implicit in the morphological appearance of these junctions in the skin of the turbot is their apparent function as occluding barriers to the passage of small molecules, such as water and ions, through the narrow extracellular space between the cells (Karnaky, 1980). However, early physiological data provided by Froemter (1972) and Frizzel & Schultz (1972), accompanied by appropriate electron microscopic studies using extracellular tracers (Machen *et al.*, 1972; Whittembury & Rawlins, 1971), suggests that the junctions in some "transporting epithelia", such as the urinary bladder of the toad and the proximal tubules of the kidney, may permit significant paracellular ion permeation. In the present study, the tight junctions between both neighbouring pavement cells and pavement and chloride cells in the skin of the larva were all morphologically very similar, measuring 0.5 to 0.8 μm in depth, but, within the apical pits of prebranchial chloride cell complexes, the occluding junctions linking the prebranchial chloride cells with the interdigitating accessory cells were far less extensive, rarely exceeding 0.1 μm in depth. Similar, "shallow" junctions have also been described between chloride cells and accessory cells in the larvae of flounder *Kareius bicoloratus* (Hwang & Hirano, 1985) and in numerous ultrastructural studies of the gill and opercular epithelium of adult marine teleosts (Karnaky & Kinter, 1977; Ernst *et al.*, 1978; Sardet *et al.*, 1979; Sardet, 1980; Hootman & Philpott, 1980; Kawahara *et al.*, 1982). Current theories for the mechanism of salt secretion in seawater propose that Na^+ ion distributions across the epithelium are passive, and the shallow junctions between accessory cell interdigitations and the chloride cell apical membrane, which are lanthanum permeable (Sardet *et al.*, 1979; Nonnotte *et al.*, 1982), provide the paracellular pathway for sodium ion efflux (reviewed by Péqueux, 1988). Thus, in conclusion, in the heterogenous epithelium of the larval skin, only the shallow junctions between chloride cells and accessory cells are thought to be significantly "leaky" to water and ion permeation; the

"tight" *zonulae occludens* between adjacent pavement cells and pavement cells and neighbouring chloride cells effectively preventing or reducing the paracellular exchange of ions and water across the skin.

Significant to these findings is the observation that accessory cells, and thus leaky junctions, were only observed in association with the prebranchial chloride cells which, although densely packed, represented just a small area of the skin and a percentage of the total chloride cell population. Accordingly, since accessory cell associations are an important functional feature of chloride cells in saltwater adapted teleosts (reviewed by Pisam & Rambour, 1991), the apparent lack of accessory cells in the apical pits of the "extraprebranchial", cutaneous chloride cells raises a profound question; are the solitary cutaneous chloride cells covering the yolk sac and trunk functionally different from the prebranchial chloride cells?

4.2. The Chloride Cell as the Site of Active Transport

Evidence supporting an ionoregulatory role for chloride cells in the skin and gills of fish larvae has been provided by several authors (Lasker & Threadgold, 1968; Dépêche, 1973; Hwang & Hirano, 1985; Ayson *et al.*, 1994; Li *et al.*, 1995; Tytler & Ireland, 1995). The extensive ultrastructural similarities between the chloride cells observed in turbot larvae and those described in the gills and opercular epithelium of juvenile and adult teleost fish (Vickers, 1961; Philpott & Copeland, 1963; Threadgold and Houston, 1964; Karnaky *et al.*, 1976) clearly point to a common function, and it is generally accepted that the cells in adult marine teleosts are important in maintaining a constant internal osmotic pressure by the secretion of salt against the gradient of the external environment (Maetz, 1971; Motaïs & Garcia-Romeu, 1972; Maetz & Bornancin, 1975; Sardet *et al.*, 1979; Epstein *et al.*, 1980).

In the present study, chloride cells were the only cells in the skin of turbot larvae that showed a typical structure for active ion transport, *i.e.* numerous mitochondria, a well branched tubular system, and an apical opening exposed to the ambient medium (Hwang, 1989). According to Pisam & Rambour (1991), serosal-environmental contact is an important functional characteristic of seawater chloride cells and, in the present study, apical contact with the external medium was made via characteristic apical pits or crypts, whilst the basal membrane of the chloride cells was closely associated with the basal lamina and underlying haemocoel. It is logical that the cells involved in transfer of electrolytes between the blood and external environment should be exposed to both of these solutions. The chloride cell pits effectively increase the apical surface area available for release of transported ions from the cells membranous tubular system (Maetz and

Bornancin, 1975), and close association with the basal lamina and underlying haemocoel could conceivably provide the nutrient supply to support ion transport.

In scanning electron micrographs of yolksac turbot, the number of epidermal pits thought to belong to the cutaneous chloride cells was surprisingly small considering the large numbers of these cells observed in TEM. Roberts *et al.* (1973) considered that the chloride cells in the skin of larval plaice (*Pleuronectes platessa*) only open to the external environment to fulfil some special function, since, unlike similar cells in the adult gill, the larval cells are not eosinophilic. However, in the present study, the cutaneous cells were clearly open to the external environment via apical pits (Fig. 3.14), but, since the aperture to the pit space was typically very narrow, measuring <0.2 - 0.6 µm, in SEM the pit openings were presumably hidden by infoldings of the superficial pavement cells. Notwithstanding, the cutaneous chloride cell might well be of different function to the prebranchial chloride cell since, in contrast to the multicellular chloride cell complexes observed in the prebranchial epithelium of larvae, and the branchial tissue of juveniles (Pisam *et al.*, 1990), the cutaneous chloride cells were never seen in association with accessory cells. Surprisingly, this basic morphological observation seems to have been overlooked in earlier ultrastructural descriptions of the integumental chloride cells of marine larvae (Lasker & Threadgold, 1968; Dépêche, 1973; Guggino, 1980b, Somasundaram, 1985; Ayson *et al.*, 1994), in which no reference to the apparent absence of accessory cells has been made, yet the association of accessory cells with chloride cells is evidently an important functional feature of chloride cells in seawater-adapted teleosts (see review by Pisam & Rambourg, 1991).

To date, the most detailed description of the distribution and density of chloride cells in the skin of fish larvae was provided by Hwang (1989) using light and electron microscopy. In the present study, however, complementary non-invasive fluorochromes were also utilised to show the precise distribution patterns and activity of the chloride cells identified by electron microscopy. In newly hatched larvae, chloride cells were most conspicuous in the yolksac region but, with yolksac absorption and differentiation of the gut, concentrations of cells were subsequently observed in the ventral trunk, pericardial and prebranchial regions. However, beyond 5-6 days post-hatching, the number of cutaneous cells showed a progressive decline with further larval development concurrent with a proliferation of chloride cells in the prebranchial epithelium. Hwang and others have also shown that chloride cell number and location are both variable and specific from one species to the next, but the morphological significance of chloride cell distribution in larvae of different species and of different ages has not really been addressed. However, Guggino (1980b) and O'Connell (1981) both note the close association of larval chloride cells in the yolksac with vitelline blood vessels. Since this contact, and that with the external environment, is functionally important in chloride cells (Girard & Payan, 1980; Karnaky, 1986), the chloride cells in the skin of larvae will inevitably be restricted to thin and highly vascularised regions of the epithelium. Indeed, chloride cells were rarely observed in the epithelium covering the back of the head or dorsal trunk of turbot larvae, and measurements of the epidermal thickness from a stage 2 larva (Table 3.2; results) revealed that the dorsal epidermis in both regions was thicker than the lateral and ventral epidermis. Moreover, the cutaneous chloride cells were generally concentrated in the ventral trunk region overlying the coelom, and preliminary investigations of the blood circulatory system of the turbot larva (*pers. obser.*; Forteath, 1994) note that the hindgut is the most highly vascularised region of the peritoneum. Thus, the concentrations of cells in the yolksac/ventral trunk, pericardial and prebranchial regions could be explained in

terms of their association with well supplied blood vessels, the high movement of plasma fluid facilitating efficient ion exchange. Further work is currently in progress to determine the factors affecting chloride cell distribution in marine fish larvae in which this argument is further advanced for herring (Wales & Tytler, in press).

The cytoplasmic microtubular system of chloride cells contains binding sites for Na^+,K^+ -ATPase which were detected by fluorescence microscopy using anthroylouabain (AO). According to Fortes (1977), AO binds specifically to the catalytic peptide of Na^+,K^+ -ATPase on a one to one basis, and so the intensity of observed fluorescence can be used as a direct estimate of the number of binding sites and hence the number of enzyme molecules (McCormick, 1990). In the present study, the cutaneous chloride cells showed a gradual decrease in fluorescence with increase in the age of larvae. In contrast, however, the prebranchial cell fluorescence was seen to increase through yolksac absorption and first feeding stages. Since AO binds only to the phosphorylated form of Na^+,K^+ -ATPase (Moczydlowski & Fortes, 1980), these respective changes in fluorescence are reflective of the functional state of the larval chloride cells. Thus, during early larval development, the increase or decrease in the number of binding sites in the prebranchial and cutaneous chloride cells respectively, presumably indicates an increased or decreased capacity for ion pumping.

Indeed, electron micrographs of the prebranchial chloride cells showed that the microtubules housing the Na^+,K^+ -ATPase molecules were substantially expanded in stage 3 turbot suggesting *de-novo* synthesis of the enzyme (Karnaky *et al.*, 1976). Furthermore, this amplification of the basolateral tubular system resulted in significant prebranchial cell hypertrophy with early larval development. In contrast, clear signs of cutaneous chloride cell degeneration were observed shortly after yolksac absorption, the cells showing partial

4. Discussion

breakdown of the microtubular system and the membrane systems and cristae of mitochondria. The literature suggests that embryos and larvae develop chloride cells in the skin until their gills are "fully formed" or "functioning" (see review by Alderice, 1988; Ayson *et al.*, 1994). Indeed, in the present study, the degeneration of the cutaneous chloride cells during the post-yolksac stages was coincident with the proliferation of the prebranchial chloride cells with elaboration of the gills. However, the present findings suggest that the prebranchial chloride cells are equipped to participate in osmoregulation long before the gills are functional, even before the formation of lamellae. Although the exact timing is uncertain, in view of their early hypertrophy, the rapid increase in ouabain binding sites, and the subsequent autolysis of chloride cells in the skin, it is concluded that the chloride cells in the prebranchial epithelium of turbot larvae become the primary site for active ion extrusion shortly after yolksac absorption and differentiation of the gut.

4.3. Water Balance in the Early Post-hatch Stages of the Turbot

The average rate constants (K_i) for the turnover of water by early post-hatch turbot were similar to those reported for the larvae of several other species but were considerably higher than for adult fishes (Table 4.1). When comparisons are made with the turnover rates for adults at the same temperature, since the permeability of both the adult and larva have been shown to be highly sensitive to temperature change (Motais & Isaia, 1972; Tytler *et al.*, 1993), the rate constants in newly hatched turbot larvae were in the order of five to eight times higher than in adult fish, depending on the species. Low diffusional turnover rates are characteristic of teleosts in seawater as a way of reducing the amount of water loss. However, it is well established that the turnover rates are still sufficiently high that the adult fish loses enough water down its osmotic gradient to require some mechanism for water uptake (Evans, 1969; Motais *et al.*, 1969; Isaia, 1972). The same is evidently true for early post-hatch turbot. Even at the lowest turnover rate in stage 2b-c larvae, the results showed that all the body water was turned over at a rate of 37 times a day. At the highest rate in stage 1a larvae, however, the body water was turned over approximately 47 times per day.

Clearly the turnover of water is high in turbot larvae, but according to the calculated diffusional permeability coefficients (P_{diff}), which take surface area and body mass into account, the larva is relatively impermeable to water. When compared with adult marine fish, the P_{diff} was very much lower in larval turbot, but slightly higher than for most teleost eggs (Table 4.2). The lowest permeability was seen in newly-hatched turbot, but a significant increase in the P_{diff} (from $9.22 \times 10^{-3} \mu\text{m.s}^{-1}$ to $12.64 \times 10^{-3} \mu\text{m.s}^{-1}$) was observed shortly after developmental stage 1c-d. The barrier to water permeation in fish eggs has been identified as the vitelline membrane (Holliday, 1969; Potts & Rudy, 1969; Loeffler &

Table 4.1. Rate constants (K_i) for influx of tritiated water in adult, larval and embryonic teleosts.

Species	Temp (°C)	K_i (h^{-1})	Reference
Adults			
<i>Platichthys flesus</i>	16	0.20	Motaïs <i>et al.</i> (1969)
Larvae			
<i>Leptocottus armatus</i>	12	0.31	Rudy & Wagner (1970)
<i>Serranus scriba</i>	15	0.24	Isaia (1972)
<i>Anguilla anguilla</i>	15	0.35	Motaïs & Isaia (1972)
<i>Gadus callarius</i>	12	0.10	Fletcher (1978a)
<i>Fundulus heteroclitus</i> (hatchlings)	25	4.80	Guggino (1980a)
<i>Gadus morhua</i> (9 days post-hatching)	4.5	0.79	Tytler & Bell (1989)
<i>Clupea harengus</i> (4 days post-hatching)	10	1.70	Tytler <i>et al.</i> (1993)
<i>Scophthalmus maximus</i> (hatchlings)	15	1.96	Present study
Eggs			
<i>Fundulus heteroclitus</i> (4-10 days post-fertilisation)	25	0.06-0.37	Guggino (1980a)
<i>Scophthalmus maximus</i> (15.5-62°days post-fertilisation)	15	0.12-0.58	Tytler & Ireland (1993)

Table 4.2. The ${}^3\text{H}_2\text{O}$ permeability coefficients of diffusion for eggs, larvae and adults of teleost fish.

Species	Temp (°C)	P_{diff} (cm.s ⁻¹ × 10 ⁻⁶)	Reference
Eggs			
<i>Gadus morhua</i>	5	0.2-1.2	Mangor-Jensen (1986)
Larvae			
<i>Gadus morhua</i>	4.5	2.4	Tytler & Bell (1989)
<i>Clupea harengus</i>	7	1.0	Tytler & Blaxter (1988b)
<i>Scophthalmus maximus</i>	15	0.8-1.3	Present study
Adults			
<i>Serranus scriba</i>	16	17.0	Motaïs <i>et al.</i> (1969)
<i>Anguilla anguilla</i>	15	23.0	Motaïs & Isaia (1972)
<i>Platichthys flesus</i>	16	10.0	Motaïs <i>et al.</i> (1969)

Lovtrup, 1970), but this structure no longer forms the integument after hatching. Thus, Tytler & Bell (1989) reasoned that the low surface permeability of early post-hatch larvae must lie in the physical properties of the larval integument. For example, in the larvae of herring, *Clupea harengus*, Jones *et al.* (1966) have described conspicuous fibrous plates in the outer layer of epidermal cells which are reminiscent of scales and, according to Somasundaram (1985), may act as a barrier to the diffusional exchange of water. The epidermis of the turbot larva does not possess such structures, but the production of a thick mucous covering by the numerous mucous secreting cells described in the earlier ultrastructural report, might contribute to the low permeability of the turbot larva. The properties of an "unstirred layer" of surface mucous as a restricting barrier to the diffusion of water are discussed by Shephard (1981). However, since the uptake of water occurs across the gut, the interpretations of tritiated water measurements in whole animal permeability studies are compounded by the osmoregulatory ability of the developing gut itself, and this was previously overlooked by Tytler & Bell.

Indeed, the gut is seen to differentiate quickly after hatching (Dodds, 1994), and this may be reflected in the increased permeability of the turbot larvae observed shortly after yolksac absorption. However, since the relatively higher permeability in adult fish is the result of high diffusional exchange across the gills, the increase in permeability with larval development could be attributed to the formation and elaboration of the primordial gill structures instead. Perhaps the proliferation of prebranchial chloride cells and associated accessory cells would result in increased water loss via the additional "leaky" junctions. Also, formation of the gill structure presumably results in a large increase in the surface area of the larva which may in itself significantly affect the P_{diff} and water turnover rates. Indeed, Gray (1953) found that in seventeen species of teleost fish the gill surface area alone accounted for 1.3 to 18.3 times the surface area of the body surface. However, in

4. Discussion

the present study, the additional surface area resulting from gill formation was not taken into account in the determination of P_{diff} , therefore it is possible that the P_{diff} for stage 2b-c turbot could in fact be similar to that of stage 1 larvae. Notwithstanding, Mangor-Jensen & Adoff (1987) and Tytler & Blaxter (1988b) have shown not only that marine fish larvae actively drink the seawater medium from hatching, but that drinking rates increase in larvae with increase in age. Hence, the observation that the P_{diff} of early stage turbot larvae increases with development might substantiate earlier supposition by Tytler & Blaxter (1988a) and Tytler & Bell (1989) that the drinking rates of larvae are a direct function of the permeability of the larva to water. Whatever the case, the low permeability of early post-hatch turbot larvae is clearly an adaption to reduce osmotic water loss.

4.4. The Nature of the Transepithelial Potential and its Ionic Contributions

The nature of the recorded potential in turbot larvae was similar to that reported for many adult teleost species (Table 4.3). When electrodes are inserted into the peritoneal cavity, with a few exceptions (see Evans & Cooper, 1976; Evans, 1980*b*; Potts & Hedges, 1991), most adult teleosts are positive with respect to seawater. The orientation of the potential was also found to be positive with respect to the seawater bathing medium in the body cavities of all early post-hatch turbot, indicating either a net movement of cations into the larvae or of anions outwards.

Although electrical measurements only show the net movement of charges (Marshall, 1977), there are several indications which point to the outward pumping of chloride ions by turbot larvae. The estimated Nernst equilibrium potentials for Na^+ (E_{Na}) and Cl^- (E_{Cl}) were calculated as +22 and -32 mV respectively. Whereas the observed potential in larvae beyond developmental stage 1c-d (approximately +16 mV, but with an upper limit of +23 mV) approach the estimated E_{Na} , clearly the E_{Cl} indicates that all the larval stages examined maintain Cl^- far out of electrochemical equilibrium (Table 3.7, results), suggesting an active mechanism for chloride extrusion. Whether or not Na^+ is also actively excreted by turbot larvae is uncertain, but since the generated potential measured from stage 1a larvae immediately after hatching ($+7.89 \pm 0.51$ mV) is insufficient to maintain sodium balance simply by passive diffusion, it is likely that sodium as well as chloride ions are actively extruded.

In the literature on adult teleosts there is no argument regarding the active extrusion of Cl^- in seawater, but views on the presence of active Na^+ extrusion remain debatable (see reviews by Maetz, 1971; Maetz & Bornancin, 1975; Kirschner, 1977; Evans, 1980*a,b* and

**Table 4.3. Measured transepithelial potentials from adult teleost species
(in Potts & Hedges, 1991).**

Linnaean name	Common name	TEP (mV)
<i>Syngnathus acus</i>	great pipefish	- 3.0
<i>Syngnathus typhle</i>	deep-snouted pipefish	- 6.9
<i>Entelurus aequorius</i>	snake pipefish	+ 0.7
<i>Ciliata mustela</i>	five-bearded rockling	+24.3
<i>Gadus morhua</i>	cod	+21.0
<i>Merlangius merlangus</i>	whiting	+16.5
<i>Pollachius pollachius</i>	pollack	+17.4
<i>Trisopterus luscus</i>	pout	+ 9.3
<i>Chelon labrosus</i>	thick-lipped grey mullet	+ 6.2
<i>Dicentrarchus labrax</i>	bass	+20.0
<i>Trachurus trachurus</i>	horse mackerel	+11.7
<i>Agonus cataphractus</i>	pogge	+20.6
<i>Aspitrigla cuculus</i>	red gurnard	+22.5
<i>Limanda limanda</i>	dab	+21.5
<i>Microstomus kitt</i>	lemon sole	+14.8
<i>Pleuronectes platessa</i>	plaice	+24.3
<i>Platichthys flesus</i>	flounder	+27.8
<i>Solea solea</i>	sole	+19.2
<i>Lophius piscatorius</i>	anglerfish	+16.8

1982; Evans *et al.*, 1982). One must be reminded, however, that early post-hatch marine larvae are known to drink their seawater medium in response to osmotic water loss (Mangor-Jensen & Adoff, 1987; Tytler & Blaxter, 1988*a,b*; Tytler & Ireland, 1994). This net oral influx of both Na^+ and Cl^- ions, in addition to any net diffusional uptake which might take place, may be appreciable in larvae and must therefore represent a Na^+ load. Consequently, even if Na is maintained in passive equilibrium by developing turbot larvae, it would seem plausible that Na^+ , as well as Cl^- , is actively extruded against its electrochemical gradient, and this may be reflected in the difference between the E_{Na} and the observed TEP measurements obtained. Nevertheless, since the recorded potential is positive in seawater for larval turbot, this hypothesis still requires that the Cl^- pump must be more powerful.

It is possible that stress from handling, immobilisation in confined conditions and/or anaesthesia might have depressed the potentials measured from larval turbot in the present study. This is indicated by the large differences observed between the upper and lower ranges of the mean potentials measured from different larvae at the same stages of development (Table 3.7, results). The sensitivity and fragility of the microelectrodes made it essential to anaesthetise the larvae, but, as Potts & Hedges (1991) remark, anaesthesia alone is likely to have had little effect on the measured potential. However, if ion pumps are under hormonal control in fish larvae, which is evidently the case in the adult fish (Zadunaisky, 1984), shocked or stressed larvae, as a result of handling and/or restraint, are unlikely to exhibit their maximum potential. For example, Lee *et al.* (1991) point out that lower potentials could result from the release of catecholamines, such as noradrenaline, which have been shown to inhibit chloride secretion via alpha-adrenergic receptors (Zadunaisky, 1984; Foskett *et al.*, 1982). However, in newly hatched stage 1a turbot, all

recorded potentials were consistently low. According to Potts *et al.* (1991), when the potential is low in adult teleosts due to shock, some recovery usually occurs as the fish are left undisturbed. No such recovery was observed in the newly hatched turbot, the low potentials possibly reflecting the fragility of the larvae and, hence, the difficulties experienced in obtaining stable recordings. Indeed, as revealed by electron microscopy, when compared with the epidermis of developmental stages 1c-d and beyond, the rudimentary epidermis of the newly hatched stage 1a larva was very thin, <2.5 μm in thickness, and may have been torn during electrode impalements thereby preventing a proper seal. However, whilst it is possible that the low potentials recorded from stage 1a larvae were in fact an artifact resulting from damage to the integument during microelectrode penetration, alternatively, the subsequent elevation in the TEP by stage 1c-d is in good agreement with the development of hyperosmoregulatory ability by turbot larvae soon after hatching.

In order to confirm that the observed potentials were dependent upon an electrogenic component, the TEP was challenged by temperature, a simple and direct variable that would not introduce any further ionic gradients across the larval skin which might otherwise alter the potential. Recent work by Tytler *et al.* (1993) and Tytler & Ireland (1994) has shown that increase in temperature has a significant effect on the osmoregulatory process in fish larvae by increasing water permeability and drinking rates, thus requiring an increase in the excretion of excess ions. The TEP measured from stage 1c-d turbot showed a linear relationship with increasing temperature which could not be explained by the Nernst or Goldman equations of equilibrium potential in terms of passive diffusion of the major contributing ions along their electrochemical gradients (Fig. 3.39 and Table 3.9; results). Moreover, the Q_{10} (temperature coefficient of the TEP) between 10 and 20°C was 2.12, indicating the direct effect of temperature on the rates of enzyme

activity and therefore strongly suggesting the involvement of an electrogenic component in TEP generation. Recently, Tytler & Ireland (1995) demonstrated that the mitochondrial protein in the chloride cells of turbot larvae increases with increase in environmental temperature. Since ATP, required to drive the ion pump, is produced by the abundant mitochondria within chloride cells, this indicates an increased capacity for salt pumping by turbot larvae. Thus it is concluded that the higher the TEP in response to temperature, the greater the salt pumping activity of the larval chloride cells.

Furthermore, when ouabain, a specific inhibitor of Na, K activated ATPases, was injected into the heart of stage 1c-d turbot, a significant and irreversible decline in the TEP was observed indicating an effective (32%) inhibition of the basolaterally-located Na^+, K^+ -ATPase in the larval chloride cells. Specific inhibition of a Na pump alone, if it had any effect on the potential at all, might be expected to increase rather than decrease the potential across the skin, and it is highly unlikely that ouabain had any effect on a chloride activated ATPase, since DeRenzis & Bornancin (1977) have shown that anion-activated ATPases are insensitive to ouabain. It would appear, therefore, in order to produce the observed effect on what appeared to be largely a chloride pump, that the inhibition of Na^+, K^+ -ATPase must in some way affect the outward pumping of chloride ions by the larval chloride cells.

Indeed, the current model for chloride secretion by chloride cells, arising from simultaneous work by Klyce & Wong (1977) and Silva *et al.* (1977), describes a net sodium-dependent Cl^- flux which is linked to and indirectly energised by Na^+, K^+ -ATPase. The model (Fig. 4.1), sharing many characteristics with "secondary active Cl^- transport" in other salt-secreting epithelia (Frizzel *et al.*, 1979), suggests that the function of the basal Na^+, K^+ -activated ATPase is to maintain intracellular sodium concentrations at a low

level. The entry of Cl^- across the basolateral membrane of the cell is coupled to Na^+ , such that the electrochemical gradient favoring Na^+ entry (the inside of the cell is negative to the body fluids) accumulates Cl^- toward the interior in electrochemical equilibrium. The net inward movement of the cations across the basolateral membrane is equal to the outward movement of the anions across the apical membrane.

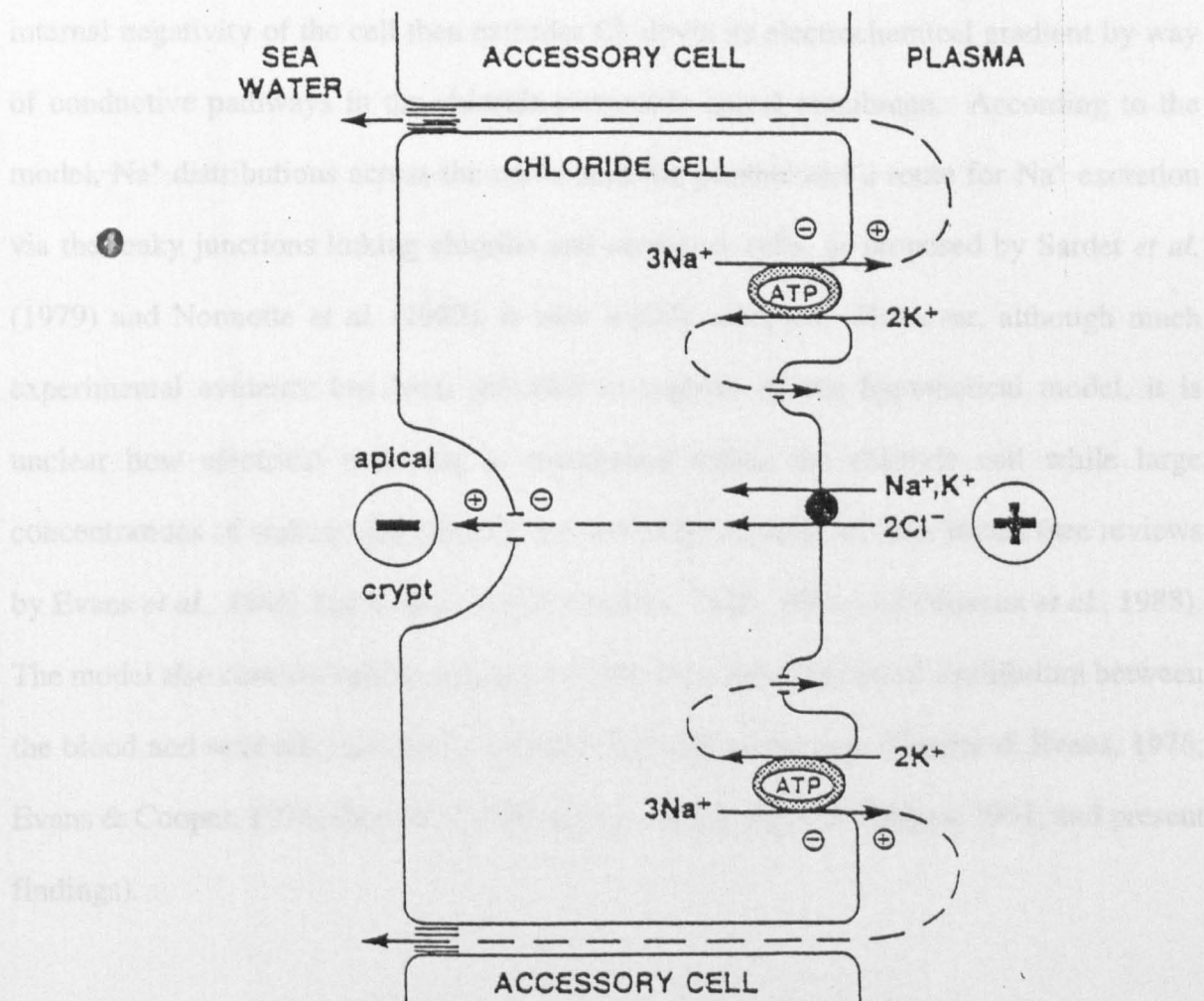


Figure 4.1. Hypothetical model for NaCl transport through the chloride cell. Uphill movements are indicated by solid lines; downhill movements by dashed lines. Adapted from the original proposal by Silva *et al.* (1977).

level. The entry of Cl^- across the basolateral membrane of the cell is coupled to Na^+ , such that the electrochemical gradient favouring Na^+ entry (the inside of the cell is negative to the body fluids) accumulates Cl^- intracellularly above its electrochemical equilibrium. The internal negativity of the cell then extrudes Cl^- down its electrochemical gradient by way of conductive pathways in the chloride-permeable apical membrane. According to the model, Na^+ distributions across the epithelium are passive and a route for Na^+ excretion via the leaky junctions linking chloride and accessory cells, as proposed by Sardet *et al.* (1979) and Nonnotte *et al.* (1982), is now widely accepted. However, although much experimental evidence has been provided in support of this hypothetical model, it is unclear how electrical neutrality is maintained within the chloride cell while large concentrations of sodium and chloride are moved by separate cellular routes (see reviews by Evans *et al.*, 1982; Zadunaisky, 1984; Karnaky, 1980, 1986; and Péqueux *et al.*, 1988). The model also controversially assumes that Na^+ is in electrochemical equilibrium between the blood and seawater, and this is certainly not always the case (Carrier & Evans, 1976; Evans & Cooper, 1976; Fletcher, 1978b; Evans, 1980b; Potts & Hedges, 1991; and present findings).

Evidence that the transepithelial potentials measured from early post-hatched turbot larvae are largely diffusional in origin was provided by salinity experiments. Over the salinity range $\frac{2}{3}$ to $1\frac{1}{3}$ seawater, the potentials measured from stage 1c-d larvae showed a linear dependence upon the external salinity, approximating to the Nernst potentials for Na and Goldman predictions with depolarisation of the TEP as the concentration of the external seawater was reduced. A similar pattern was shown by the flounder, *Platichthys flesus* L. (Potts & Eddy, 1973b) with acute salinity changes. In full-strength seawater, the transgill potential was measured as +19 mV in adult flounder, but in 75% seawater the

potential is lowered to +10 mV, even reversing in hypo-osmotic solutions. Indeed, extrapolation of the linear relationship observed in the present study (Fig. 3.40; results) also indicated that reversal of the transepithelial potential would occur in seawater concentrations less than 8‰ (approx 25% SW). In addition, according to this figure, the turbot larva hypothetically maintains an inside positive electrogenic potential under isosmotic conditions (~11‰ seawater) intimating that the major activity of the pump is the extrusion of chloride ions.

Since Na and Cl are the two major ions in seawater and in blood plasma, and are the major contributors both to the diffusion component and to the active component of the TEP, it is likely that the transport system in turbot larvae would be sensitive to the concentrations of Na^+ and/or Cl^- in the external bathing medium, as demonstrated for the adult gill and opercular epithelium of several other teleost species (Potts & Eddy, 1973b; Degnan *et al.*, 1977; Marshall, 1977). Indeed, in the present study, substitution experiments revealed that the TEP was highly influenced by the external concentration of both Na^+ and Cl^- ions respectively.

The turbot larva was found to be highly permeable to sodium. Substitution with the larger, less permeant choline ion depolarised and even reversed the orientation of the TEP (Fig. 3.41; results), demonstrating the acute sensitivity of the potential to the external sodium concentration. In addition, in agreement with the presence of a putative chloride pump, the replacement of Cl^- with methylsulphate ions lowered the TEP by approximately 7 mV, instead of increasing it as would be expected from a Cl^- conductance. Therefore, because this substitution should significantly reduce the Cl^- secretion without affecting the Na^+ diffusion potential, the observed depolarisation could only be explained by a reduction in the electrogenic transport of Cl^- by the larval chloride cells. Hence, both Na^+ and Cl^-

appear to be required for the normal operation of the active pump(s) in early stage turbot suggesting that the mechanisms for the extrusion of sodium and chloride ions is coupled in some manner. Moreover, since the TEP showed such dependency on the concentration of sodium in the bathing medium, it is concluded that external Na exerts a direct regulatory influence on the rate of Cl⁻ secretion by larval chloride cells, and may therefore be a vital component of the acute response of many larval species to changing salinities.

It is dangerous, however, to make definite conclusions concerning ionic interactions as a result of the existence of ion coupling since, as Potts (1984) points out, the interactions of a diffusion potential and an electrogenic pump are complicated and not fully predictable. For example, the decrease in potential observed in Cl⁻-free seawater might be smaller than expected because lowering the potential by turning off the pump would be offset by an increase in the potential caused by a chloride conductance. Furthermore, ion fluxes mediated by an electrically neutral mechanism, such as exchange diffusion (as described by Ussing, 1947) or the operation of a neutral ion pump, will not be detected by electrical measurements. Hence, the conclusions reached here apply only to ion movements with which is associated the movement of electric charge.

In addition, the ion substitution experiments provide valuable information on the role of Na⁺ and Cl⁻ ions in TEP generation and the permeability of the larval epithelium to these ions. If one assumes that Na flux is primarily responsible for producing the potential observed in turbot larvae, since the observed potential was close to E_{Na} , estimations of the internal Na concentration can be made from the regression line fitted for the relationship between the TEP and external [Na] (Fig. 3.41; results) when the electrical potential is 0 mV. However, the derived value of 162 mM does not represent the true internal concentration of Na since the electrogenic component is not considered and since Cl⁻ will

also affect the potential. Indeed, in view of the earlier salinity experiments which identified a positive TEP under isosmotic conditions, this predicted value is almost certainly underestimated. Nevertheless, the approximation is still comparable to estimates of the internal Na reported for the adults and larvae of several other species (Table 4.4).

The internal concentration of chloride can be predicted by the rearrangement of Fletchers thermodynamic model (Equation 2-8) such that:

$$t_{Cl}E_{Cl} = E - E_A - (t_{Na}E_{Na})$$

The potential (E) is known to be +15.91 mV when the external Na is 459 mM, the electrogenic component (E_A) derived from ouabain inhibition experiments is 32% of the measured potential, and the transport numbers for Na and Cl are calculated as 0.787 and 0.213 respectively, thus:

$$0.213 \times E_{Cl} = 15.91 - 5.04 - (0.787 \times 22.02)$$

and therefore,

$$E_{Cl} = \frac{-6.46}{0.213} = -30.3 \text{ mV}$$

The internal concentration of chloride that approximates to this figure is 158 mM, and this figure is very close to the internal Cl⁻ concentration measured from juvenile turbot and the adults of other teleost species, and indeed to the estimations made from other larvae (Table 4.4).

The permeability ratio (P_{Cl}/P_{Na}) calculated from the above transport numbers is 0.27. In contrast, the ratio used in Goldman predictions was considerably smaller (0.126 compared with 0.27), but, since the Goldman model ignores the contribution of any electrogenic

Table 4.4. The ionic composition of the body fluids of some adult and larval teleost fish species.

Species	Ion Content (mM.l ⁻¹)						Reference
	Na ⁺	K ⁺	Cl ⁻	Ca ²⁺	Mg ²⁺	SO ₄ ²⁻	
Adults							
Cod (<i>Gadus morhua</i>)	184.8	4.79	156.8	2.24	0.96	0.80	Fletcher (1978b)
SW eel (<i>Anguilla anguilla</i>)	175	3.2	154	-	-	-	Sharratt <i>et al.</i> (1964)
Juvenile turbot (<i>Scophthalmus maximus</i>)	-	6.23	150.4	5.69	1.51	-	Divil (1994)
Larvae							
Halibut (<i>Hippoglossus hippoglossus</i>)	-	-	156	-	-	-	Hahnenkamp <i>et al.</i> (1993)
9 day Cod (<i>Gadus morhua</i>)	189	-	148	-	-	-	Tyler & Bell (1989)

component to the potential, this difference is in fact justifiable. From Fletchers thermodynamically based model, under normal conditions the diffusional component (E_D) of the transepithelial potential (Equation 2-8) is determined, using the resolved transport numbers, as +10.88 mV. Since the observed potential of +15.91 mV is the sum of this diffusional component and an electrogenically maintained component (Equation 2-5), the derived electrogenic contribution of +5.03 mV (i.e. 15.91-10.88), which is in excellent agreement with the fall in potential observed upon inhibition with ouabain (i.e. 32% inhibition), confirms earlier supposition that the major activity of the pump must indeed be the extrusion of chloride ions.

4.5. Concluding Remarks

The ultrastructural evidence presented in the present study suggests that the skin of the turbot larva (the exchange surface) functions as a significant limiting barrier to the transepithelial movement of water and ions. In the heterogenous epidermis of the larva, consisting of both transporting and non-transporting cells, only the shallow junctions between chloride cells and accessory cells are believed to permit ion influx and/or water loss via the paracellular pathway; the extensive junctions between adjacent pavement cells and between pavement cells and neighbouring chloride cells effectively occluding the passage of ions and water through the extracellular space.

The conclusion that the skin of the turbot larva may effectively impede osmotic water loss is supported by the measurements of diffusional water permeability from early post-hatch turbot which intimate that, inspite of adverse surface area to mass ratios, the larvae are relatively impermeable to water compared with the gills of adults. Nevertheless, the rates of water turnover measured from early stage turbot are still sufficiently high that a net osmotic loss of water must be replaced if the animal is to maintain homeostasis.

Drinking activity is well established in early post-hatch turbot (Brown & Tytler, 1993; Tytler & Ireland, 1994) but the uptake of water through drinking will inevitably result in the companion uptake of ions which must be compensated for by equivalent rates of salt excretion. In the present study, primordial chloride cells in the skin and prebranchial epithelium of the turbot larva are proposed as the principal sites of ion excretion. In addition to ultrastructural methods, specific vital fluorochromes were used to reveal and quantify mitochondria and Na^+, K^+ -ATPase binding sites in the larval chloride cells during the early development of the turbot. The findings suggest that the prebranchial chloride

cells, which closely resemble the chloride cells described in the branchial epithelium of juveniles (Pisam *et al.*, 1990), are both numerous and well equipped to participate in active salt extrusion even at hatching. The potential importance of the cutaneous chloride cells in salt extrusion is also considered, but the apparent absence of accessory cell associations and the small number of apical pits observed in SEM and TEM sections raises questions as to the significance of these cells in ion excretion.

Manipulation of the transepithelial potentials, recorded in the electrophysiological approach to the study, clearly demonstrates the involvement of an electrogenic pump in the maintenance of ionic gradients across the skin of the turbot larva. The experimental evidence suggests that the TEP is largely the result of a Na^+ diffusion potential with an additive electrogenic potential due to Cl^- transport, which is somehow functionally connected to Na^+, K^+ -ATPase. Current theories for salt extrusion by chloride cells in adults describe a net sodium-dependent Cl^- flux that is linked to and indirectly energised by Na^+, K^+ -ATPase (Péqueux *et al.*, 1988). Since the concentration of Na^+ in the external bathing medium has a direct regulatory influence on the rate of Cl^- secretion, the mechanism of Cl^- flux across the skin of the turbot larva must also be coupled to Na^+ which implies a similar model for salt extrusion by the larval chloride cells. However, the passive distribution of Na^+ assumes a route for Na^+ efflux via the shallow junctions linking chloride cells and accessory cells, as proposed by Sardet *et al.* (1979) and Nonnotte *et al.* (1982), but the absence of accessory cells (and thus leaky junctions) in the cutaneous chloride cells implies significant functional differences between cutaneous and prebranchial chloride cells which could not be clarified within the limitations of this preliminary study of the larval skin.

With the application of specific ion flux studies, such as *de-novo* patch clamp analyses, in combination with further electrophysiological studies, such as the measurement of transepithelial ion activities using ion-selective microelectrodes, our understanding of transepithelial ion movements in marine fish larvae could be greatly enhanced. The suitability of transparent early stage larvae for the application of *in vivo* epifluorescence microscopy and image analysis techniques utilising specific vital fluorochromes is well established in the present study and provides interesting opportunities for further study. For example, it would be interesting to mark the appearance of Na^+,K^+ -ATPase in the primordial chloride cells as they develop in the embryonic skin. Thus, the present developments provide a broad foundation for future studies of the mechanisms of ion transport in developing fish larvae.

- Al-Maghazachi, S.J., Gibson, R. (1982). The development stages of larval turbot, *Scophthalmus maximus* (L.). *J. Exp. Mar. Biol. Ecol.* 62: 263-280.

Alderice, D.F. (1982). Osmotic and ion regulation in winter eggs and larvae. In: Fish Physiology XIAK. Edited by W. Sano & J. J. Randall. Academic Press, New York, pp.163-251.

Ayson, F.G., Kamada, T., Higashimura, S. (1984). The development of the heart of mitochondria-rich cells in the yolk sac, intestine and liver and gonads of Tilapia, *Oreochromis maculatus*, in freshwater and seawater. *J. Fish Biol.* 35: 129-135.

Bereiter-Hahn, J. (1971). The development of the heart and the formation of haemoflagellate in the zebrafish embryo. *Developmental Biology* 26: 111-125.

Bereiter-Hahn, J. (1976). Development of the heart in the zebrafish embryo as a functional model for studies of heart differentiation. *Developmental Biology* 51: 271-285.

References

Brander, G.C., King, P.A. (1977). The development of the heart in the zebrafish embryo. *Developmental Biology* 57: 271-285.

Brown, J.A., Evans, K. (1982). The development of the heart in the zebrafish embryo. *Developmental Biology* 93: 101-110.

Buchanan, J.H. (1976). The development of the heart in the zebrafish embryo. *Developmental Biology* 51: 271-285.

Carrier, J.C., Evans, K. (1982). The development of the heart in the zebrafish embryo. *Developmental Biology* 93: 101-110.

Cioni, C., De Meirlier, J. (1982). The development of the heart in the zebrafish embryo. *Developmental Biology* 93: 101-110.

Cousin, J.C.B., Gibson, R. (1982). The development of the heart in the zebrafish embryo. *Developmental Biology* 93: 101-110.

Creggian, P.C., Clegg, J.A. (1976). The development of the heart in the zebrafish embryo. *Developmental Biology* 51: 271-285.

References

- Al-Maghazachi, S.J., Gibson, R. (1984). The developmental stages of larval turbot, *Scophthalmus maximus* (L.). *J. Exp. Mar. Biol. Ecol.* **82**: 35-51.
- Alderice, D.F. (1988). Osmotic and ionic regulation in teleost eggs and larvae. In: Fish Physiology XI(A). Edited by W.S. Hoar & D.J. Randall. Academic Press. New York. pp.163-251.
- Ayson, F.G., Kaneko, T., Hasegawa, S., Hirano, T. (1994). Development of mitochondrion-rich cells in the yolk-sac membrane of embryos and larvae of Tilapia, *Oreochromis mossambicus*, in freshwater and seawater. *J. exp. Zool.* **270**: 129-135.
- Bereiter-Hahn, J. (1971). Light and electron microscopic studies on function of tonofilaments in teleost epidermis. *Cytobiologie* **4**: 73-102.
- Bereiter-Hahn, J. (1976). Dimethylaminostyrylmethylpyridiniumiodine (DASPMI) as a fluorescent probe for mitochondria in situ. *Biochim. Biophys. Acta* **423**: 1-14.
- Brander, G.C., Pugh, D.M., Bywater, R.J. (1982). *Veterinary Applied Pharmacology & Therapeutics* (4th ed.). Ballière Tindall. London.
- Brown, J.A., Tytler, P. (1993). Hypoosmoregulation of larvae of the turbot, *Scophthalmus maximus*: drinking and gut function in relation to environmental salinity. *Fish Physiol. Biochem.* **10**: 475-483.
- Carrier, J.C., Evans, D.H. (1976). The role of environmental calcium in freshwater survival of the marine teleost *Lagodon rhomboides*. *J. exp. Biol.* **65**: 529-538.
- Cioni, C., De Merich, D., Cataldi, E., Cataudella, S. (1991). Fine structure of chloride cells in freshwater- and seawater-adapted *Oreochromis niloticus* (Linnaeus) and *Oreochromis mossambicus* (Peters). *J. Fish biol.* **39**: 197-209.
- Cousin, J.C.B., Baudin Laurencin, F. (1987). Histological alterations observed in turbot, *Scophthalmus maximus* L., from days 15 to 40 after hatching. *Aquaculture* **67**: 218-220.
- Croghan, P.C., Curra, R.A., Lockwood, A.P.M. (1965). Electrical potential difference across the epithelium of isolated gills of the crayfish *Austropotamobius pallipes*. *J. exp. Biol.* **42**: 463-474.

- Davis, W.L., Goodman, D.B., Martin, J.H., Matthews, J.L., Rasmussen, H. (1973). Vasopressin (APV) induced changes in the toad urinary bladder epithelial surface - a scanning electron microscopical study. *J. Cell Biol.* **59**: 73a.
- Degnan, K.J., Karnaky, K.J. Jr., Zadunaisky, J.A. (1977). Active chloride transport in the *in vitro* opercular skin of a teleost (*Fundulus heteroclitus*), a gill-like epithelium rich in chloride cells. *J. Physiol.* **271**: 155-191.
- Dépêche, J. (1973). Ultrastructure of the yolk sac and pericardial sac surface in the embryo of the teleost *Poecilia reticulata*. *Z. Zellforsch.* **141**: 235-253.
- DeRenzi, G., Bornancin, M. (1977). A Cl⁻/HCO₃⁻ ATPase in the gills of *Carassius auratus*. Its inhibition by thiocyanate. *Biochim. Biophys. Acta* **467**: 192-207.
- DeSilva, C.D. (1973). The ontogeny of respiration in herring and plaice larvae. Ph.D. Thesis. University of Stirling. Scotland.
- Divil, E. (1994). The effects of temperature and salinity on growth, food intake, body and blood composition of juvenile turbot, *Scophthalmus maximus* L. M.Phil. Thesis. University of Liverpool. England.
- Dodds, L.A. (1994). A histological study of the ontogeny of the gut in relation to digestive processes in turbot (*Scophthalmus maximus*) larvae. Undergraduate dissertation. University of Stirling. Scotland.
- Eckert, R., Randall, D., Augustine, G. (1988). *Animal Physiology: Mechanism and Adaptations* (3rd ed.). W.H. Freeman and Company. New York. pp.683.
- Epstein, F.H.P., Silva, P., Kormnik, G. (1980). Role of Na-K-ATPase in chloride cell function. *Am. J. Physiol.* **238**: R246-R250.
- Ernst, S.A., Dodson, W.B., Karnaky, K.J. Jr. (1978). Structural diversity of occluding junctions in the low-resistance chloride-secreting opercular epithelium of seawater-adapted killifish (*Fundulus heteroclitus*). *J. Cell Biol.* **87**: 488-497.
- Evans, D.H. (1969). Studies on the permeability to water of selected marine, freshwater and euryhaline teleosts. *J. exp. Biol.* **50**: 689-703.
- Evans, D.H. (1979). Fish. In: *Osmotic and Ionic Regulation in Animals*, Volume 1. Edited by G.M.O. Maloiy. Academic Press. London. pp.305-390.

References

- Evans, D.H. (1980a). Osmotic and ionic regulation in freshwater and marine fishes. In: Environmental Physiology of Fishes. Edited by M.A. Ali. Plenum Press. New York. pp.93-122.
- Evans, D.H. (1980b). Kinetic studies of ion transport by fish gill epithelium. *Am. J. Physiol.* **238:** R224-R230.
- Evans, D.H. (1982). Salt and water exchange across vertebrate gills. In: Gills. Edited by D.F. Houlihan, J.C. Rankin & T.J. Shuttleworth. Cambridge University Press. Cambridge. pp.228.
- Evans, D.H., Claiborne, J.B., Farmer, L., Mallory, C., Krasny, E.J. Jr. (1982). Fish gill ionic transport: methods and models. *Biol. Bull.* **163:** 108-130.
- Evans, D.H., Cooper, K. (1976). The presence of Na^+-Na^+ and Na^+-K^+ exchange in sodium extrusion by three species of fish. *Nature* **259:** 241-242.
- Farquhar, M.G., Palade, G.E. (1963). Junctional complexes in various epithelia. *J. Cell Biol.* **17:** 375-412.
- Fletcher, C.R. (1978a). Osmotic and ionic regulation in the cod (*Gadus callarius* L.). I. Water balance. *J. comp. Physiol.* **124:** 149-156.
- Fletcher, C.R. (1978b). Osmotic and ionic regulation in the cod (*Gadus callarius* L.). II. Salt balance. *J. comp. Physiol.* **124:** 157-168.
- Forteath, D. (1994). The ontogeny of the blood circulatory system in turbot (*Scophthalmus maximus*) larvae. Undergraduate dissertation. University of Stirling. Scotland.
- Fortes, P.A.G. (1977). Anthroylouabain: a specific fluorescent probe for the cardiac glycoside receptor. *Biochemistry* **16:** 531-540.
- Foskett, J.K., Machen T.E., Bern, H.A. (1982). Chloride secretion and conductance of teleost opercular membrane: effects of prolactin. *Am. J. Physiol.* **242:** R380-389.
- Foskett, J.K., Scheffey, C. (1982). The chloride cell: definitive identification as the salt-secretory cell in teleosts. *Science* **215:** 164-166.
- Frizzell, R.A., Field, M., Schütz, S.G. (1979). Sodium coupled chloride transport by epithelial tissues. *Am. J. Physiol.* **236:** F1-F8.

References

- Frizzell, R.A., Schütz, S.G. (1972). Ionic conductances of extracellular shunt pathway in rabbit ileum. Influence of shunt on transmural sodium transport and electrical potential differences. *J. Gen. Physiol.* **59**: 318-346.
- Froemter, E. (1972). The route of passive ion movement through the epithelium of *Necturus* gallbladder. *J. mem. biol.* **8**: 259-301.
- Girard, J.P., Payan, P. (1980). Ion exchanges through respiratory and chloride cells in freshwater- and seawater-adapted teleosteans. *Am. J. Physiol.* **238**: R260-R268.
- Glantz, S.A. (1987). *Primer of Biostatistics* (2nd ed.). McGraw Hill. New York. pp.379.
- Goldman, D.E. (1943). Potential, impedance and rectification in membranes. *J. Gen. Physiol.* **27**: 37-60.
- Gray, I.F. (1953). The relation of body weight to body surface area in marine fishes. *Biol. Bull.* **105**: 285-288.
- Guggino, W.B. (1980a). Water balance in the embryos of *Fundulus heteroclitus* and *F. bermudae* in seawater. *Am. J. Physiol.* **238**: R36-R41.
- Guggino, W.B. (1980b). Salt balance in the embryos of *Fundulus heteroclitus* and *F. bermudae* adapted to seawater. *Am. J. Physiol.* **238**: R42-R49.
- Guth, D., von Engelhardt, W. (1989). Is gastrointestinal mucus an ion-selective barrier? In: Mucus and Related Topics. Edited by E. Chantler & N.A. Ratcliffe. The Company of Biologists. Cambridge. pp.117-121.
- Hahnenkamp, L., Senstad, K., Fyhn, H.J. (1993). Osmotic and ionic regulation of yolksac larvae of Atlantic halibut (*Hippoglossus hippoglossus*). In: Physiological and Biochemical Aspects of Fish Development. Edited by B.T. Walther & H.J. Fyhn. University of Bergen. Bergen. Norway. pp.259-262.
- Handy, R.D., Eddy, F.B. (1991). Effects of ioorganic cations on Na⁺ adsorption to the gill and body surface of rainbow trout, *Oncorhynchus mykiss*, in dilute solutions. *Can. J. Fish. Aquat. Sci.* **48**: 1829-1837.
- Harding, C.V. (1973). Corneal epithelial surfaces in elasmobranchs and teleosts as seen with the scanning electron microscope. *Biol. Bull.* **145**: 438.
- Hawkes, J.W. (1974). Structure of fish skin: I. General organization. *Cell Tissue Res.* **149**: 147-158.

- Heron, A.C. (1969). A dark-field condenser for viewing transparent plankton animals under a low-power stereomicroscope. *Int. J. Life Ocean. Coast. Waters* **2**: 321-324.
- Hodgkin, A.L. (1951). The ionic basis of electrical activity in nerve and muscle. *Biol. Rev. Cambridge Philos. Soc.* **26**: 339-409.
- Hodgkin, A.L., Katz, B. (1949). The effect of sodium ions on the electrical activity of the giant axon of the squid. *J. Physiol.* **108**: 37-77.
- Hølleland, T. (1990). The distribution of chloride cells in embryonic and larval stages of herring, *Clupea harengus*. In: Program "Development and Aquaculture of Marine Fish Larvae", Bergen, Norway, August 12-15, 1990. Abstr. No. P45.
- Hølleland, T., Fyhn, H.J. (1986). Osmotic properties of eggs of the herring *Clupea harengus*. *Marine Biology* **91**: 377-383.
- Holliday, F.G.T. (1962). Osmoregulation in marine teleost eggs and larvae. *Californian Coop. Ocean. Fish. Invest. Rep.* **10**: 89-95.
- Holliday, F.G.T. (1969). The effects of salinity on the eggs and larvae of teleosts. In: Fish Physiology I. Edited by W.S. Hoar & D.J. Randall. Academic Press. New York. pp.293-311.
- Holliday, F.G.T., Blaxter, J.H.S. (1960). The effects of salinity on the developing eggs and larvae of the herring. *J. mar. biol. Ass. U.K.* **39**: 591-603.
- Holliday, F.G.T., Jones, M.P. (1965). Osmotic regulation in the herring (*Clupea harengus*). *J. mar. biol. Ass. U.K.* **45**: 305-311.
- Holliday, F.G.T., Jones, M.P. (1967). Some effects of salinity on the developing eggs and larvae of the plaice (*Pleuronectes platessa*). *J. mar. biol. Ass. U.K.* **47**: 39-48.
- Hootman, S.R., Philpott, C.W. (1978). Rapid isolation of chloride cells from pinfish gills. *Anat. Rec.* **190**: 687-720.
- Hootman, S.R., Philpott, C.W. (1979). Ultracytochemical localization of Na^+,K^+ -Activated ATPase in chloride cells from gills of a euryhaline teleost. *Anat. Rec.* **193**: 99-130.
- Hootman, S.R., Philpott, C.W. (1980). Accessory cells in teleost branchial epithelium. *Am. J. Physiol.* **238**: R199-R206.

References

- House, C.R. (1963). Osmotic regulation in the brackish water teleost *Blennius pholis*. *J. exp. Biol.* **40**: 87-104.
- Hwang, P.P. (1989). Distribution of chloride cells in teleost larvae. *J. Morphol.* **200**: 1-8.
- Hwang, P.P. (1990). Salinity effects on development of chloride cells in the larvae of ayu (*Plecoglossus altivelis*). *Marine Biology* **107**: 1-7.
- Hwang, P.P., Hirano, R. (1985). Effects of environmental salinity on intercellular organization and junctional structure of chloride cells in early stages of teleost development. *J. exp. Zool.* **236**: 115-126.
- Ingersoll, C.G., Sanchez, D.A., Meyer, J.S., Gulley, D.D., Tietge, J.E. (1990). Epidermal response to pH, aluminum, and calcium exposure in brook trout (*Salvelinus fontinalis*) fry. *Can. J. Fish. Aquat. Sci.* **47**: 1616-1622.
- Isaia, J. (1972). Comparative effects of temperature on the sodium and water permeabilities of the gills of a stenohaline freshwater fish (*Carassius auratus*) and stenohaline marine fish (*Serranus scriba*, *Serranus cabrilla*). *J. exp. Biol.* **57**: 359-366.
- Iwai, T. (1969). On the "chloride cells" in the skin of larval puffer, *Fugii niphobles* (Jordan & Snyder). *La Mer* **7**: 26-31.
- Jones, A. (1972). Studies of egg development and larval rearing of turbot *Scophthalmus maximus* L., and brill *Scophthalmus rhombus* L., in the laboratory. *J. mar. biol. Ass. U.K.* **52**: 965-986.
- Jones, M.P., Holliday, F.G.T. and Dunn, A.E.G. (1966). The ultrastructure of the epidermis of the herring (*Clupea harengus*) in relation to the rearing salinity. *J. mar. biol. Ass. U.K.* **46**: 235-239.
- Karnaky, K.J. Jr. (1980). Ion-secreting epithelia: chloride cells in the head region of *Fundulus heteroclitus*. *Am. J. Physiol.* **238**: R185-R198.
- Karnaky, K.J. Jr. (1986). Structure and function of the chloride cell of *Fundulus heteroclitus* and other teleosts. *Am. Zool.* **26**: 209-224.
- Karnaky, K.J. Jr., Kinter, L.B., Kinter, W.B., Stirling, C.E. (1976). Autoradiographic localization of Na,K-ATPase in killifish (*Fundulus heteroclitus*) adapted to low and high salinity environments. *J. Cell Biol.* **70**: 157-177.

- Karnaky, K.J. Jr., Kinter, W.B. (1977). Killifish opercular skin: a flat epithelium with a high density of chloride cells. *J. exp. Zool.* **199**: 355-364.
- Karnaky, K.J. Jr., Philpott, C.W. (1969). The cytochemical demonstration of surface-associated polyanions in a cell specialized for electrolyte transport. *J. Cell Biol.* **43**: 64.
- Karnovsky, M.J. (1965). A formaldehyde-glutaraldehyde fixative of high osmolality for use in electron microscopy. *J. Cell Biol.* **27**: 137A.
- Karnovsky, M.J. (1971). Use of ferrocyanide-reduced osmium tetroxide in electron microscopy. In: Abstracts of the 11th Ann. Mtg. Amer. Soc. Cell Biol. New Orleans: Amer. Soc. Cell Biol. p.146.
- Katsura, K., Hamada, K. (1986). Appearance and disappearance of chloride cells throughout the embryonic and postembryonic development of the goby, *Chaenogobius urotaenia*. *Bull. Fac. Fish. Hokkaido Univ.* **37**: 95-100.
- Kawahara, T., Sasaki, T., Higashi, S. (1982). Intercellular junctions in chloride and pavement cells of *Oplegnathus fasciatus*. *J. Electron Microsc.* **31**: 162-170.
- Keys, A.B. (1931). The heart-gill preparation of the eel and its perfusion for the study of a natural membrane in situ. *Z. verlg. Physiol.* **15**: 352-362.
- Keys, A.B., Willmer, E.N. (1932). Chloride secreting cells in the gills of fishes with special reference to the common eel. *J. Physiol.* **76**: 368-378.
- King, J.A.C., Abel, D.C., DiBona, D.R. (1989). Effects of salinity on chloride cells in the euryhaline cyprinodontid fish *Rivulus marmoratus*. *Cell Tiss. Res.* **240**: 675-692.
- Kirsch, R. (1978). Role of the esophagus in osmoregulation in teleost fishes. In: Osmotic and Volume Regulation. Alfred Benzon Symposium XI, Munksgaard. Academic Press. New York.
- Kirschner, L.B. (1977). The sodium chloride excreting cells in marine vertebrates. In: Transport of Ions and Water in Animals. Edited by B.L. Gupta, R.B. Moreton, J.L. Oschman & B.W. Wall. Academic Press. London. New York. San Francisco. pp.427-452.
- Kirschner, L.B. (1979). Control mechanisms in crustaceans and fishes. In: Osmoregulation in Animals. Edited by R. Gilles. Wiley Interscience. New York. pp.157-222.
- Kjørsvik, E., Davenport, J., Lönnning, S. (1984). Osmotic changes during the development of eggs and larvae of the lump sucker, *Cyclopterus lumpus* L. *J. Fish Biol.* **24**: 311-322.

- Klyce, S.D., Wong, R.K.S. (1977). Site and mode of adrenaline action on chloride transport across the rabbit corneal epithelium. *J. Physiol.* **266**: 777-799.
- Krogh, A. (1939). *Osmotic Regulation in Aquatic Animals*. Cambridge University Press. London. New York.
- Lasker, R., Threadgold, L.T. (1968). "Chloride cells" in the skin of the larval sardine. *Exp. Cell Res.* **52**: 582-590.
- Lee, C.G.L., Low, W.P., Lam, T.J., Munro, A.D., Ip, Y.K. (1991). Osmoregulation in the mudskipper, *Boleophthalmus boddarti*. II. Transepithelial potential and hormonal control. *Fish Physiol. Biochem.* **9**: 69-75.
- Li, J., Eygensteyn, J., Lock, R.A.C., Verbost, P.M., Van Der Heijen, A.J.H., Wendelaar Bonga, S.E., Flik, G. (1995). Branchial chloride cells in larvae and juveniles of freshwater tilapia *Oreochromis mossambicus*. *J. exp. Biol.* **198**: 2177-2184.
- Lockwood, A.P.M. (1963). *Animal Body Fluids and Their Regulation*. Heinemann. London pp.177.
- Loeffler, C.A., Lovtrup, S.L. (1970). Water balance in the salmon egg. *J. exp. Biol.* **52**: 291-298.
- Machen, T.E., Erlij, D., Wooding, F.B.P. (1972). Permeable junctional complexes. The movement of lanthanum across rabbit gallbladder and intestine. *J. Cell Biol.* **54**: 302-312.
- Maetz, J. (1971). Fish gills: Mechanisms of salt transfer in freshwater and seawater. *Phil. Trans. R. Soc. Lond.* **B262**: 209-249.
- Maetz, J. (1974). Aspects of adaptation to hypo-osmotic and hyperosmotic environments. In: *Biochemical and Biophysical Perspectives in Marine Biology*, Volume 1. Edited by D.C. Malins & J.R. Sargent. Academic Press. New York. pp.1-152.
- Maetz, J., Bornancin, M. (1975). Biochemical and biophysical aspects of salt secretion by chloride cells in teleosts. *Fortschr. Zool.* **23**: 322-362.
- Maetz, J., Skadhauge, E. (1968). Drinking rates and gill ionic turnover in relation to external salinities in the eel. *Nature* **217**: 371-373.
- Mangor-Jensen, A. (1986). Osmoregulation in eggs and larvae of the cod (*Gadus morhua* L.): basic studies and the effects of oil exposure. In: *Fish Larval Physiology and Anatomy*. Edited by H.J. Fyhn. University of Bergen. Bergen. Norway. pp.117-164.

- Mangor-Jensen, A., Adoff, G.R. (1987). Drinking activity of the newly hatched larvae of cod (*Gadus morhua* L.). *Fish Physiol. Biochem.* **3**: 99-103.
- Marshall, W.S. (1977). Transepithelial potential and short-circuit current across the isolated skin of *Gillichthys mirabilis* (Teleostei: Gobiidae), acclimated to 5‰ and 100‰ seawater. *J. comp. Physiol.* **114**: 157-165.
- Marshall, W.S. (1978). On the involvement of mucous secretion in teleost osmoregulation. *Can. J. Zool.* **56**: 1088-1091.
- Marshall, W.S., Nishioka, R.S. (1980). Relation of mitochondria-rich cells to active chloride transport in the skin of a marine teleost. *J. exp. Zool.* **214**: 147-188.
- Mattey, D.L., Morgan, M., Wright, D.E. (1980). A scanning electron microscope study of the pseudobranchs of two marine teleosts. *J. Fish Biol.* **18**: 331-343.
- McCormick, S.D. (1990). Fluorescent labelling of Na^+,K^+ -ATPase in intact cells using a fluorescent derivative of ouabain: salinity and teleost chloride cells. *Cell Tissue Res.* **260**: 529-533.
- Moczydlowski, E.G., Fortes, P.A.G. (1980). Kinetics of cardiac glycoside binding to sodium, potassium adenosine triphosphatase studied with a fluorescent derivative of ouabain. *Biochemistry* **19**: 969-977.
- Motaïs, R., Garcia-Romeu, F. (1972). Transport mechanisms in the teleostean gill and amphibian skin. *Ann. Rev. Physiol.* **34**: 141-176.
- Motaïs, R., Isaia, J. (1972). Temperature-dependence of permeability to water and sodium of the gill epithelium of the eel, *Anguilla anguilla*. *J. exp. Biol.* **56**: 587-600.
- Motaïs, R., Isaia, J., Rankin, J.C., Maetz, J. (1969). Adaptive changes of the water permeability of the teleostean gill epithelium in relation to external salinity. *J. exp. Biol.* **51**: 529-546.
- Nagel, W. (1976). The intracellular electrical potential profile of the frog skin epithelium. *Pflügers Arch.* **365**: 135-143.
- Nagel, W., Essig, A. (1982). Relationship of transepithelial electrical potential to membrane potentials and conductance ratios in frog skin. *J. Membr. Biol.* **69**: 125-136.
- Nonnotte, G., Colin, D.A., Nonnotte, L. (1982). Na^+ and Cl^- transport and intercellular junctions in the isolated skin of a marine teleost (*Blennius pholis* L.). *J. exp. Zool.* **224**: 39-44.

References

- O'Connell, C.P. (1981). Development of organ systems in the northern anchovy *Engraulis mordax* and other teleosts. *Am. Zool.* **21**: 429-446.
- Olson, K.R., Fromm, P.O. (1973). A scanning electron microscopic study of secondary lamellae and chloride cells of rainbow trout (*Salmo gairdneri*). *Z. Zellforsch.* **143**: 439-449.
- Pease, D.C. (1964). *Histological Techniques for Electron Microscopy* (2nd ed). Academic Press. New York.
- Péqueux, A., Gilles, R., Marshall, W.S. (1988). NaCl transport in gills and related structures. In: Advances in Comparative and Environmental Physiology, Volume 1. Edited by R. Greger. Springer-Verlag. Heidelberg. pp.1-73.
- Philpott, C.W. (1980). Tubular system membranes of teleost chloride cells: osmotic response and transport sites. *Am. J. Physiol.* **238**: R171-R184.
- Philpott, C.W., Copeland, D.E. (1963). Fine structure of chloride cells of three species of *Fundulus*. *J. Cell Biol.* **18**: 389-404.
- Pickford, G.E., Pang, P.K.T., Sawyer, W.H. (1966). Prolactin and serum osmolality of hypophysectomized killifish, *Fundulus heteroclitus*, in fresh-water. *Nature* **209**: 1040-1041.
- Pisam, M., Boeuf, G., Prunet, P., Rambourg, A. (1990). Ultrastructural features of mitochondria-rich cells in stenohaline freshwater and seawater fishes. *Am. J. Anat.* **187**: 21-31.
- Pisam, M., Rambourg, A. (1991). Mitochondria-rich cells in the gill epithelium of the teleost fishes: an ultrastructural approach. *Int. Rev. Cytol.* **130**: 191-232.
- Potts, W.T.W. (1984). Transepithelial potentials in fish gills. In: Fish Physiology X(B). Edited by W.S. Hoar & D.J. Randall. Academic Press. New York. pp.105-128.
- Potts, W.T.W., Eddy, F.B. (1973a). The permeability to water of the eggs of certain marine teleosts. *J. comp. Physiol.* **82**: 305-315.
- Potts, W.T.W., Eddy, F.B. (1973b). Gill potentials and sodium fluxes in the flounder *Platichthys flesus*. *J. comp. Physiol.* **87**: 29-48.
- Potts, W.T.W., Fletcher, C.R., Hedges, A.J. (1991). The in vivo transepithelial potential in a marine teleost. *J. Comp. Physiol. B* **161**: 393-400.

- Potts, W.T.W., Foster, M.A., Rudy, P.P., Parry-Howells, G. (1967). Sodium and water balance in the cichlid teleost, *Tilapia mossambicus*. *J. exp. Biol.* **47**: 461-470.
- Potts, W.T.W., Hedges, A.J. (1991). Gill potentials in marine teleosts. *J. Comp. Physiol. B* **161**: 401-405.
- Potts, W.T.W., Parry, G. (1964). *Osmotic and Ionic Regulation in Animals*. Pergamon Press. New York. pp.423.
- Potts, W.T.W., Rudy, P.P. Jr. (1969). Water balance in the eggs of the Atlantic salmon (*Salmo salar*). *J. exp. Biol.* **50**: 239-246.
- Powell, M.D., Speare, D.J., Wright, G.M. (1994). Comparative ultrastructural morphology of lamellar epithelial, chloride and mucous cell glycocalyx of the rainbow trout (*Oncorhynchus mykiss*) gill. *J. Fish Biol.* **44**: 725-730.
- Powell, M.D., Wright, G.M., Speare, D.J. (1995). Morphological changes in rainbow trout (*Oncorhynchus mykiss*) gill epithelia following repeated exposure to chloramine-T. *Can. J. Zool. Rev. Can. Zool.* **73**: 154-165.
- Purves, R.D. (1981). *Microelectrode Methods for Intracellular Recording and Ionophoresis*. Academic Press. London. pp.146.
- Reynolds, E.S. (1963). The use of lead citrate at high pH as an electron-opaque stain in electron microscopy. *J. Cell Biol.* **17**: 208-212.
- Riis-Vestergaard, J. (1982). Water and salt balance of halibut eggs and larvae (*Hippoglossus hippoglossus*). *Marine Biology* **70**: 135-139.
- Riis-Vestergaard, J. (1984). Water balance in cod eggs. In: *The Propagation of Cod Gadus morhua L.*, Volume 1. Edited by E. Dahl, D.S. Danielsen, E. Moksnes & P. Solemdal. Flødevigen Rapportser 1. pp.87-103.
- Roberts, R.J., Bell, M., Young, H. (1973). Studies on the skin of Plaice (*Pleuronectes platessa* L.): II. the development of larval plaice skin. *J. Fish Biol.* **5**: 103-108.
- Robertson, J.D. (1954). The chemical composition of the blood of some aquatic chordates, including members of the Tunicata, Cyclostomata and Osteichthys. *J. exp. Biol.* **31**: 424-442.

- Rombout, J.H.W.M., Lamers, C.H.J., Hanstede, J.G. (1978). Enteroendocrine APUD cells in the digestive tract of larval *Barbus conchonius* (Teleostei, Cyprinidae). *J. Embryo. Exp. Morph.* **47**: 121-135.
- Rudy, P.P. Jr., Wagner, R.C. (1970). Water permeability in the Pacific hagfish *Polistrema stouti* and the staghorn sculpin *Leptocottus armatus*. *Comp. Biochem. Physiol.* **34**: 399-403.
- Sardet, C. (1980). Freeze fracture of the gill epithelium of euryhaline teleost fish. *Am. J. Physiol.* **238**: R207-R212.
- Sardet, C., Pisam, M., Maetz, J. (1979). The surface epithelium of teleostean fish gills: cellular and junctional adaptations of the chloride cell in relation to salt adaptation. *J. Cell Biol.* **80**: 96-117.
- Sargent, J.R., Bell, M.V., Kelly, K.F. (1980). In: *Epithelial Transport in the Lower Vertebrates*. Edited by B. Lahlou. Cambridge University Press. Cambridge. pp.251-267.
- Schöen, H.F., Erlj, D. (1985). Current-voltage relations of the apical membranes of the frog skin. *J. Gen. Physiol.* **86**: 257-287.
- Schwerdtfeger, W.K. (1979a). Morphometrical studies of the ultrastructure of the epidermis of the guppy (*Poecilia reticulata* Peters) following adaption to seawater and treatment with prolactin. *Gen. Comp. Endocrinol.* **38**: 476-483.
- Schwerdtfeger, W.K. (1979b). Qualitative and quantitative data on the fine structure of the guppy (*Poecilia reticulata* Peters) epidermis following treatment with thyroxine and testosterone. *Gen. Comp. Endocrinol.* **38**: 484-490.
- Scott, J.E. (1989). Ion binding: patterns of 'affinity' depending on types of acid groups. In: *Mucous and Related Topics*. Edited by E. Chantler & N.A. Ratcliffe. The Company of Biologists. Cambridge. pp.111-115.
- Sharratt, B.M., Chester Jones, I., Bellamy, D. (1964). Water and electrolyte composition of the body and renal function of the eel (*Anguilla anguilla*). *Comp. Biochem. Physiol.* **11**: 9-18.
- Shelbourne, J.E. (1957). Site of chloride regulation in marine fish larvae. *Nature* **180**: 920-922.
- Shephard, K.L. (1981). The influence of mucous on the diffusion of water across fish epidermis. *Physiol. Zool.* **54**: 224-229.
- Shephard, K.L. (1982). The influence of mucous on the diffusion of ions across the oesophagus of fish. *Physiol. Zool.* **55**: 23-34.

- Silva, P., Solomon, R., Spokes, K., Epstein, F.H. (1977). Ouabain inhibition of gill Na,K-ATPase relationship to active chloride transport. *J. exp. Zool.* **199**: 419-426.
- Smith, H.W. (1929). The composition of the body fluids of the goosefish (*Lophius piscatorius*). *J. biol. Chem.* **82**: 71-75.
- Smith, H.W. (1930). The absorption and excretion of water and salts by marine teleosts. *Am. J. Physiol.* **93**: 485-505.
- Smith, P.G. (1969a). The ionic relations of *Artemia salina* (L.). I. Measurements of electrical potential difference and resistance. *J. exp. Biol.* **51**: 727-738.
- Smith, P.G. (1969b). The ionic relations of *Artemia salina* (L.). II. Fluxes of sodium, chloride and water. *J. exp. Biol.* **51**: 739-757.
- Somasundaram, B. (1985). Effects of zinc on epidermal ultrastructure in the larva of *Clupea harengus*. *Marine Biology* **85**: 199-207.
- Sverdrup, H.H., Johnson, M.W., Flemming, R.H. (1955). *The Oceans*. Prentice-Hall Inc. New Jersey. pp.186.
- Tanaka, M. (1973). Studies on the structure and function of the digestive system of teleost larvae. D.Agr. Thesis. Kyoto University. Japan.
- Taylor, P.M. (1985). Electrical-potential difference and sodium ion fluxes across the integument of *Corophium volutator* (Crustacea; Amphipoda), a euryhaline hyperosmotic regulator. *J. exp. Biol.* **114**: 477-491.
- Thomas, R.C. (1978). *Ion Sensitive Microelectrodes: How to Make and Use Them*. Academic Press. London. New York. pp.110.
- Threadgold, L.T., Houston, A.H. (1964). An electron microscope study of the "chloride cell" of *Salmo salar* L. *Exp. Cell Res.* **34**: 1-23.
- Todd, K.D. (1996). The effects of cadmium on the early developmental stages of the turbot *Scophthalmus maximus*. Ph.D. Thesis. University of Stirling. Scotland.
- Tytler, P., Bell, M.V. (1989). A study of diffusional permeability of water, sodium and chloride in yolk-sac larvae of cod (*Gadus morhua* L.). *J. exp. Biol.* **147**: 125-132.
- Tytler, P., Bell, M.V., Robinson, J. (1993). The ontogeny of osmoregulation in marine fish: effects of changes in salinity and temperature. In: *Physiological and Biochemical Aspects*

- of Fish Development. Edited by B.T. Walther & H.J. Fyhn. University of Bergen. Bergen. Norway. pp.249-258.
- Tytler, P., Blaxter, J.H.S. (1988a). The effects of external salinity on the drinking rates of the larvae of herring, plaice and cod. *J. exp. Biol.* **138**: 1-15.
- Tytler, P., Blaxter, J.H.S. (1988b). Drinking in yolk-sac stage larvae of the halibut, *Hippoglossus hippoglossus* (L.). *J. Fish Biol.* **32**: 493-494.
- Tytler, P., Ireland, J. (1993). The influence of temperature, salinity and external calcium on diffusional permeability of the eggs of turbot (*Scophthalmus maximus*). *Aquaculture* **115**: 335-345.
- Tytler, P., Ireland, J. (1994). Drinking and water absorption by the larvae of herring (*Clupea harengus*) and turbot (*Scophthalmus maximus*). *J. Fish Biol.* **44**: 103-116.
- Tytler, P., Ireland, J. (1995). The influence of temperature and salinity on the structure and function of mitochondria in chloride cells in the skin of the larvae of the turbot (*Scophthalmus maximus*). *J. therm. Biol.* **20**: 1-14.
- Ussing, H.H. (1947). Interpretation of the exchange of radiosodium in isolated muscle. *Nature* **160**: 262-263.
- Van Oosten, J. (1957). Skin and scales. In: Physiology of Fishes, Volume I. Edited by M.E. Brown. Academic Press. New York. pp.207-244.
- Vickers, J. (1961). A study of the so-called "chloride secretory" cells of the gills of teleosts. *Q. J. microsc. Sci.* **104**: 507-518.
- Wales, W., Tytler, P. (in press). Changes in chloride cell distribution during early larval stages of *Clupea harengus*. *J. Fish Biol.*
- Weisbart, M. (1968). Osmotic and ionic regulation in embryos, alevin and fry of the five species of the five species of Pacific salmon. *Can. J. Zool.* **163**: 237-264.
- Wellings, S.R., Brown, G.A. (1969). Larval skin of the flathead sole, *Hippoglossoides elassodon*. *Z. Zellforsch.* **100**: 167-179.
- Whittembury, B., Rawlins, F.A. (1971). Evidence of a paracellular pathway for ion flow in the kidney proximal tubule: electron microscopic demonstration of lanthanum precipitate in the tight junction. *Pflügers Arch.* **330**: 302-309.

References

- Yamashita, K. (1978). Chloride cells in the skin of the larvae of red seabream *Pagrus major*. *Japan. J. Ichthyol.* **25**: 211-215.
- Zadunaisky, J.A. (1984). The chloride cell: the active transport of chloride and the paracellular pathways. In: Fish Physiology X(B). Edited by W.S. Hoar & D.J. Randall. Academic Press. New York. pp.129-176.
- Zar, J.H. (1984). *Biostatistical Analysis* (2nd ed.). Prentice Hall. New Jersey. pp.718.
- Zeuthen, T. (1978). Mechanisms of epithelial fluid transport: 1. intracellular gradients in electrical potential and ion activity in absorptive epithelia. In: Comparative Physiology: Water, Ions and Fluid Mechanics. Edited by K. Schmidt-Nielson, L. Bolis & S.H.P. Maddrell. Cambridge University Press. Cambridge. London. N.Y. Melbourne. pp.3-19.

Appendices

Appendix A: Fixatives & Buffers

Modified Karnovsky's Fixative

Dissolve 2.0 g paraformaldehyde in 50 ml of distilled H₂O by heating at 60°C and stirring. Add 1-5 drops of 1 M sodium borohydride and continue stirring until the solution. Add 50 ml 0.2 M sodium cacodylate buffer (pH 7.2). Add 10 ml 25% glutaraldehyde stock solution. Add 37 mg anhydrous calcium chloride. Make up to 100 ml with distilled water. Use within 4 hrs.

This fixative has an osmolarity similar to serum (~1050 mOsm/L) and is therefore half the concentration of Karnovsky's original fixative. The CsCl prevent the tissue from swelling.

1% Osmium Tetroxide

Clean 1 g osmium vials with ethanol. Bring each vial to 50 ml of distilled H₂O to produce a 2% stock

Appendix B: Preparation of Serial Sections for Electron Microscopy

Transmission Electron Microscopy

Appendices

Stage 1: Rinse in distilled water for 10 minutes to remove fixative.

Stage 2: Wash in PBS for 10 minutes.

Stage 3: Wash in PBS.

Stage 4: Wash in PBS.

Stage 5: Place in PBS.

Stage 6: Place in PBS.

Stage 7: Place in PBS.

Stage 8: Place in PBS.

Stage 9: Place in PBS.

Stage 10: Place in PBS.

Stage 11: Place in PBS.

Stage 12: Polyacrylate.

Scanning Electron Microscopy

Stage 1: Place in PBS.

Stage 2: Wash in PBS.

Stage 3: Place in PBS.

Stage 4: Place in PBS.

Stage 5: Place in PBS.

Stage 6: Place in PBS.

Stage 7: Place in PBS.

Stage 8: Glutaraldehyde.

Stage 9: Mosaic of pictures.

Stage 10: Spatter coat with gold.

Appendices

Appendix A: Fixatives & Buffers

Modified Karnovsky's Fixative

Dissolve 2.0 g paraformaldehyde in 20 ml of distilled H₂O by heating at 60°C and stirring. Add 1-5 drops of 1 M sodium hydroxide until solution clears. Cool the solution. Add 50 ml 0.2 M sodium cacodylate buffer (pH 7.2). Add 10 ml 25% gluteraldehyde stock solution. Add 37 mg anhydrous calcium chloride. Make up to 100 ml with distilled water. Use when fresh.

This fixative has an osmolarity similar to seawater (1005 mOsm.l⁻¹) and is therefore half the concentration of Karnovsky's original fixative. The CaCl₂ prevents the tissue from swelling.

1% Osmium Tetroxide

Clean 1 g osmium vials with ethanol. Break vials into 50 ml of distilled H₂O to produce a 2% stock solution and leave overnight. Add 50 ml of 50 mM sodium cacodylate (pH 7.2).

Appendix B: Preparation of Material for Electron Microscopy

Transmission Electron Microscopy

- Stage 1: Place in modified Karnovsky's fixative for 3-4 hr at room temperature
- Stage 2: Wash in cold cacodylate buffer for 2 hr
- Stage 3: Post-fix in 1% osmium tetroxide in cacodylate buffer for 4 hr
- Stage 4: Wash overnight in cacodylate buffer
- Stage 5: Place in 70% ethanol for 1½ hr
- Stage 6: Place in 95% ethanol for 1½ hr
- Stage 7: Place in 100% ethanol for 1½ hr
- Stage 8: Place in 100% ethanol for 1½ hr
- Stage 9: Place overnight in 1:1 ethanol/LR White resin
- Stage 10: Place in 100% LR White for 24 hr
- Stage 11: Embed in LR White in polypropylene bean capsules
- Stage 12: Polymerise in an oven at 60°C for 22 hr

Scanning Electron Microscopy

- Stage 1: Place in modified Karnovsky's fixative for at least 1 week at 4°C
- Stage 2: Wash in 0.1 M cacodylate buffer for 2 hr
- Stage 3: Place in 70% ethanol/acetone for 1½ hr
- Stage 4: Place in 95% ethanol/acetone for 1½ hr
- Stage 5: Place in 100% ethanol/acetone for 1½ hr
- Stage 6: Place in 100% ethanol/100% acetone overnight
- Stage 7: Place in 100% acetone for 2 hr
- Stage 8: Change acetone and dry with critical point dryer for 2 hr
- Stage 9: Mount on aluminium stubs
- Stage 10: Sputter coat with gold/palladium

Keep stubs in exsiccators until observation with the SEM.

Appendix C: Anthroylouabain injection

Since ouabain does not enter cells in its distribution phase (Brander *et al.*, 1982), the intercellular water available, estimated from measurements of the mean wet and dry weights of post-hatch turbot larvae, was assumed to be one third of the total body water content. Once this value was known, the volume of 0.1 mM anthroylouabain (AO) required to produce a final plasma concentration of $2.5 \mu\text{m.larva}^{-1}$ could thus be determined.

Age of larvae (days post-hatching)	Wet [†] weight (mg)	Dry [†] weight (mg)	Total water content (μl)	Intercellular water available (μl)	Volume of 0.1 mM AO injected (nl)	Number of micrometer units*
1	0.48	0.01	0.47	0.157	3.93	10.6
2	0.46	0.01	0.45	0.150	3.75	10.1
3	0.55	0.01	0.54	0.180	4.50	12.2
4	0.78	0.02	0.76	0.253	6.33	17.1
5	0.90	0.02	0.88	0.293	7.33	19.8
6	1.18	0.02	1.16	0.387	9.68	26.1
7	1.32	0.03	1.29	0.333	8.33	22.5
8	1.68	0.05	1.63	0.543	13.58	36.7
9	2.21	0.08	2.13	0.710	17.75	48.0
10	2.11	0.07	2.04	0.680	17.00	45.9
11	2.60	0.11	2.49	0.830	20.75	56.1

[†] Measurements of wet and dry weights were made as in section 2.4

* 1 micrometer unit = 0.37 nl

Appendix D: The ionic constituents and measurements of the osmolarity of full strength artificial seawater (ASW), choline/sodium and methylsulphate/chloride substitution media used in TEP ion replacement experiments

Constituents (g.l ⁻¹) [*]	MW	34%o ASW [†]	50% Ch/Na	75% Ch/Na	100% Ch/Na	50% SO ₄ /Cl	75% SO ₄ /Cl	100% SO ₄ /Cl
NaCl	58.5	23.477	10.052	3.350	-	7.820	-	-
KCl	74.5	0.664	0.664	0.664	0.664	0.664	0.664	-
CaCl ₂	111	1.102	1.102	1.102	1.102	1.102	1.102	-
MgCl ₂	95	4.981	4.981	4.981	4.981	4.981	4.981	-
Na ₂ SO ₄	142	3.917	3.917	3.917	-	22.920	32.410	32.410
NaHCO ₃	84	0.192	0.192	0.192	-	0.192	0.192	0.192
SrCl ₂	159	0.024	0.024	0.024	0.024	0.024	0.013	-
H ₃ BO ₃	62	0.026	0.026	0.026	2.030	8.320	12.480	16.362
NaF	42	0.003	0.003	0.003	-	0.003	0.003	0.003
KBr	119	0.096	0.096	0.096	0.096	0.096	0.096	0.096
ChCl	139.5	-	32.010	47.990	55.980	-	-	-
Ch ₂ SO ₄	304	-	-	-	8.380	-	-	-
CaSO ₄	136	-	-	-	-	-	-	1.350
MgSO ₄	120	-	-	-	-	-	-	6.291
K ₂ SO ₄	174	-	-	-	-	-	-	1.551

[†] Using the formula of Lyman & Flemming (1940) (in Sverdrup *et al.*, 1955).

Bathing Medium	Constituents (g.l ⁻¹) [*]							Osmolarity (mM)
	Na ⁺	K ⁺	Cl ⁻	Ca ²⁺	Mg ²⁺	SO ₄ ²⁻	Ch ⁺	
34%o ASW	10.55	0.38	19.00	0.40	1.26	2.65	-	1109
50% Ch ⁺ /Na ⁺	5.28	0.38	19.00	0.40	1.26	2.65	23.86	1086
75% Ch ⁺ /Na ⁺	2.64	0.38	19.00	0.40	1.26	2.65	35.78	1098
100% Ch ⁺ /Na ⁺	-	0.38	19.00	0.40	1.26	2.65	44.61	1094
50% SO ₄ ²⁻ /Cl ⁻	10.55	0.38	9.50	0.40	1.26	15.50	-	1091
75% SO ₄ ²⁻ /Cl ⁻	10.55	0.35	4.75	0.40	1.26	21.91	-	1100
100% SO ₄ ²⁻ /Cl ⁻	10.55	0.38	-	0.40	1.26	28.75	-	1101

* To convert g.l⁻¹ into mM.l⁻¹ divide by the molecular weight (MW) and multiply by 1000.

Appendix E: Derivation of the Nernst equation (from Eckert *et al.*, 1988)

The Nernst equation is based on the concept of a thermodynamic equilibrium between the osmotic work required to move a given number of ions across a membrane in one direction and the electrical work required to move an equivalent number of charges back across the membrane in the opposite direction. The osmotic work required to transfer 1 mol.equiv of an ion X from a concentration $[X]_I$ to a concentration 10 times higher, $[X]_{II}$, can be derived from the gas laws as:

$$W = RT \ln \frac{[X]_I}{[X]_{II}} \quad (1)$$

where W is the mechanical (or osmotic) work (force times distance).

Osmotic work can be related to electrical work through the equality:

$$W = EFz \quad (2)$$

in which the potential difference, E , is multiplied by the Faraday constant (F), namely, the charge per mole of univalent ion. The valency of the ion, z , corrects for multivalent species.

Thus, by substituting Equation 2 into Equation 1, we obtain:

$$EFz = RT \ln \frac{[X]_I}{[X]_{II}} \quad (3)$$

and hence,

$$E = \frac{RT}{Fz} \ln \frac{[X]_I}{[X]_{II}} \quad (4)$$

which is the general form of the Nernst equation.

Appendix F: Determination of the Surface Area of Larval Stages

(i) Stage 1a

Larva	Total Length (mm)	Sphere				Cone			Total SA of Larva (mm ²)
		Diameter 1	Diameter 2	Radius (r)	SA ($4\pi r^2$)	Length (l)	Radius (r)	SA (πrl)	
1	2.34	1.13	0.90	0.51	3.25	1.21	0.24	0.90	4.14
2	2.02	0.98	1.02	0.50	3.14	1.04	0.27	0.88	4.01
3	2.21	1.07	1.14	0.55	3.84	1.14	0.30	1.07	4.91
4	2.30	1.11	1.21	0.58	4.24	1.19	0.32	1.18	5.42
5	2.16	1.05	0.96	0.50	3.16	1.11	0.25	0.88	4.04
6	2.08	1.01	1.06	0.52	3.36	1.07	0.28	0.94	4.29
7	2.29	1.11	0.78	0.47	2.80	1.18	0.20	0.76	3.56
8	2.49	1.21	0.82	0.51	3.22	1.28	0.22	0.87	4.09
9	2.10	1.02	1.07	0.52	3.42	1.08	0.28	0.96	4.38
10	2.08	1.01	0.95	0.49	3.01	1.07	0.25	0.84	3.85
Mean	2.21	1.07	0.99	0.51	3.34	1.14	0.26	0.93	4.27

(ii) Stage 1c-d

Larva	Larval Length (l)	Depth (in mm) at positions:					Mean Depth (d)	SA (πdl) in mm ²
		(i)	(ii)	(iii)	(iv)	(v)		
1	2.81	0.48	0.58	0.60	0.52	0.32	0.50	4.41
2	3.02	0.52	0.63	0.65	0.56	0.34	0.54	5.14
3	3.00	0.45	0.54	0.56	0.48	0.30	0.47	4.40
4	2.90	0.47	0.56	0.58	0.50	0.31	0.48	4.40
5	2.74	0.39	0.48	0.49	0.42	0.26	0.41	3.51
6	2.68	0.57	0.69	0.71	0.61	0.37	0.59	4.98
7	2.98	0.52	0.62	0.64	0.55	0.34	0.53	4.99
8	2.80	0.40	0.49	0.50	0.43	0.26	0.42	3.67
9	3.06	0.44	0.53	0.55	0.47	0.29	0.46	4.41
10	2.92	0.40	0.49	0.50	0.43	0.26	0.42	3.82
Mean	2.89	0.47	0.56	0.58	0.50	0.31	0.48	4.37

(iii) Stage 2b-c

Larva	Larval Length (l)	Depth (in mm) at positions:					Mean Depth (d)	SA (πdl) in mm^2
		(i)	(ii)	(iii)	(iv)	(v)		
1	3.48	0.64	0.92	0.90	0.67	0.44	0.71	7.80
2	3.45	0.69	0.98	0.96	0.71	0.47	0.76	8.23
3	3.82	0.59	0.84	0.82	0.61	0.40	0.65	7.81
4	3.72	0.70	1.00	0.85	0.73	0.48	0.75	8.77
5	3.30	0.67	0.96	0.94	0.70	0.46	0.74	7.71
6	3.63	0.56	0.80	0.78	0.58	0.38	0.62	7.07
7	3.50	0.55	0.79	0.77	0.57	0.38	0.61	6.73
8	3.45	0.70	1.00	0.98	0.73	0.48	0.78	8.40
9	3.60	0.71	1.02	0.82	0.74	0.48	0.76	8.55
10	3.56	0.62	0.88	0.86	0.64	0.42	0.68	7.63
Mean	3.55	0.64	0.92	0.87	0.67	0.44	0.71	7.87

Appendix G: Statistical Analyses

Temperature effect on the TEP: A One Way Analysis of Variance with Dunnett's test.

MTB > Oneway 'TEP' 'Temp';
 SUBC> Dunnett 0.01 2.

ANALYSIS OF VARIANCE ON TEP

SOURCE	DF	SS	MS	F	p
Temp	2	602.1	301.0	29.23	0.000
ERROR	42	432.5	10.3		
TOTAL	44	1034.6			

INDIVIDUAL 95% CI'S FOR MEAN BASED ON POOLED STDEV

LEVEL	N	MEAN	STDEV	(---*---	(---*---	(---*---
1	10	9.700	2.497	(---*---		
2	25	16.000	3.674		(---*---	
3	10	20.600	2.413			(---*---
POOLED STDEV =		3.209		10.0	15.0	20.0
						25.0

Dunnett's intervals for treatment mean minus control mean

Family error rate = 0.0100
 Individual error rate = 0.00508

Critical value = 2.96
 Control = level 2 of Temp

Level	Lower	Center	Upper
1	-9.854	-6.300	-2.746 (-----*-----)
3	1.046	4.600	8.154 (-----*-----)
		-5.0	0.0
10.0			5.0

Regression Analysis.

MTB > Regress 'Mean TEP' 1 'Temp'.

The regression equation is Mean TEP = - 0.70 + 1.07 Temp

Predictor	Coef	Stdev	t-ratio	p
Constant	-0.699	1.670	-0.42	0.748
Temp	1.0719	0.1074	9.98	0.064

s = 0.7597 R-sq = 99.0% R-sq(adj) = 98.0%

Salinity effect on the TEP: A One Way Analysis of Variance with Dunnett's test.

MTB > Oneway 'TEP' 'Salinity';
 SUBC> Dunnett 0.01 2.

ANALYSIS OF VARIANCE ON TEP

SOURCE	DF	SS	MS	F	p
Salinity	2	824.6	412.3	31.78	0.000
ERROR	42	545.0	13.0		
TOTAL	44	1369.6			

INDIVIDUAL 95% CI'S FOR MEAN
BASED ON POOLED STDEV

LEVEL	N	MEAN	STDEV	
1	10	10.300	2.983	(----*---)
2	25	16.000	3.674	(--*--)
3	10	23.100	3.957	(---*---)
POOLED STDEV = 3.602				10.0 15.0 20.0 25.0

Dunnett's intervals for treatment mean minus control mean

Family error rate = 0.0100
Individual error rate = 0.00508

Critical value = 2.96

Control = level 2 of Salinity

Level	Lower	Center	Upper
1	-9.690	-5.700	-1.710 (-----*-----)
3	3.110	7.100	11.090
	(-----*-----)		
		-5.0	0.0
			5.0
10.0			

Regression Analysis.

MTB > Regress 'Mean TEP' 1 'Salinity'.

The regression equation is Mean TEP = - 5.29 + 0.640 Salinity

Predictor	Coef	Stdev	t-ratio	p
Constant	-5.293	1.413	-3.75	0.166
Salinity	0.64000	0.04041	15.84	0.040

s = 0.5715 R-sq = 99.6% R-sq(adj) = 99.2%

Appendix H: The concentrations of Na^+ and Cl^- in the various external bathing media used in the determination of Nernst relations and Goldman kinetics.

Bathing Medium	Ion Content (mM.l^{-1})	
	Na^+	Cl^-
Full strength ASW	458.84	535.26
24ppt ASW	340.81	417.22
44ppt ASW	576.88	653.29
50% Ch^+/Na^+ substitution	229.36	535.22
75% Ch^+/Na^+ substitution	114.79	535.22
100% Ch^+/Na^+ substitution	-	535.23
50% $\text{SO}_4^{2-}/\text{Cl}^-$ substitution	458.84	267.61
75% $\text{SO}_4^{2-}/\text{Cl}^-$ substitution	458.84	133.80
100% $\text{SO}_4^{2-}/\text{Cl}^-$ substitution	458.84	-

In all calculations, the gas constant, R , was taken as 8.314; the absolute temperature, T , was given as degrees Kelvin (K), where 0°C is 273.16 K; and the Faraday constant, F , i.e. the charge per mole of univalent ion, was taken as 96487.

**Appendix I: Scientific and common names of plant and animal species
to which reference is made in the present study**

Chlorophyta

Nannochloropsis sp. unicellular green alga

Crustacea

Brachionus plicatilis Müller rotifer
Artemia salina (Linnaeus) brine shrimp

Fish

<i>Agonus cataphractus</i> (Linnaeus)	pogge, armed bullhead, hook-nose
<i>Anguilla anguilla</i> (Linnaeus)	eel
<i>Anguilla rostrata</i> (Lesueur)	American eel
<i>Aspitrigla cuculus</i> (Linnaeus)	red gurnard
<i>Chaenogobius urotaenia</i> (Bleeker)	goby
<i>Chelon labrosus</i> (Risso)	thick-lipped grey mullet
<i>Ciliata mustela</i> (Linnaeus)	five-bearded rockling
<i>Clupea harengus</i> Linnaeus	herring
<i>Dicentrarchus labrax</i> (Linnaeus)	bass
<i>Engraulis modax</i> (Linnaeus)	northern anchovy
<i>Entelurus aequorius</i> (Linnaeus)	snake pipefish
<i>Fugu niphobles</i> (Jordan & Snyder)	puffer
<i>Fundulus heteroclitus</i> Linnaeus	common killifish
<i>Gadus morhua</i> Linnaeus	cod
<i>Hippoglossoides elassodon</i> Jordan & Gilbert	flathead sole
<i>Hippoglossus hippoglossus</i> (Linnaeus)	halibut
<i>Kareius bicoloratus</i> Basilew-Sky	flounder
<i>Lebistes (Poecilia) reticulatus</i> Peters	guppy
<i>Leptocottus armatus</i> Girard	pacific staghorn sculpin
<i>Limanda limanda</i> (Linnaeus)	dab
<i>Lophius piscatorius</i> Linnaeus	angler or monkfish
<i>Merlangius merlangus</i> (Linnaeus)	whiting
<i>Microstomus kitt</i> (Walbaum)	lemon sole
<i>Oncorhynchus mykiss</i> (Walbaum)	rainbow trout ¹
<i>Pagrus major</i> (Temminck & Schlegel)	red seabream

¹ Two unambiguous discoveries involving rainbow trout (reviewed by Smith & Stearley, 1989) resulted in a name change for *Salmo gairdneri*. Firstly, osteological and biochemical findings revealed that rainbow trout were more closely related to Pacific salmon (*Oncorhynchus*) than to brown trout and Atlantic salmon. Secondly, the rainbow trout was demonstrated to be the same species as the Kamchatka trout (*Salmo mykiss*), hence the present classification *Oncorhynchus mykiss*.

<i>Platichthys flesus</i> Linneaus	flounder ²
<i>Pleuronectes platessa</i> Linnaeus	plaice
<i>Poecilia reticulata</i> Peters	guppy
<i>Pollachius pollachius</i> (Linnaeus)	pollack
<i>Rhombosolea retiaria</i> Hutton	New Zealand black flounder
<i>Salmo gairdneri</i> (Richardson)	rainbow trout
<i>Scophthalmus maximus</i> (Linnaeus)	turbot
<i>Serranus scriba</i> (Linnaeus)	sea perch
<i>Solea solea</i> (Linnaeus)	sole
<i>Syngnathus acus</i> Linnaeus	greater pipefish
<i>Syngnathus typhle</i> Linnaeus	deep-snouted pipefish
<i>Trachurus trachurus</i> (Linnaeus)	horse mackerel or scad
<i>Trisopterus luscus</i> (Linnaeus)	pouting or bib

Bibliography:

- Hart, J.L. (1973). *Pacific Fishes of Canada*. Bulletin 180. Fisheries Research Board of Canada. Ottawa. pp.740.
- Lythgoe, G.J. (1991). *Fishes of the Seas - The North Atlantic and Mediterranean*. MIT Press. Cambridge. Massachusetts pp.256.
- Paulin, C., Stewart, A., Roberts, C., McMillan, P. (1989). *New Zealand Fish: A Complete Guide*. GP Books. National museum of New Zealand. Wellington. pp.279.
- Robins, C.R., Bailey, R.M., Bond, C.E., Brooker, J.R., Lachner, E.A., Lea, R.N., Scott, W.B. (1991). *Common and Scientific Names of Fishes from the United States and Canada* (5th ed.). American Fisheries Society Special Publication No.20. American Fisheries Society. Maryland. pp.183.
- Robins, C.R., Bailey, R.M., Bond, C.E., Brooker, J.R., Lachner, E.A., Lea, R.N., Scott, W.B. (1991). *World Fishes Important to North Americans*. American Fisheries Society Special Publication No.21. American Fisheries Society. Maryland. pp.243.
- Smith, G.R., Stearley, R.F. (1989). The classification and scientific names of rianbow and cutthroat trouts. *Fisheries* **14**: 4-10.
- Wheeler, A. (1992). A list of the common and scientific names of fishes of the British Isles. *J. Fish Biol.* **41**: Supplement A. pp.37.

² Although the flounder and plaice were earlier appointed to separate genera (*Platichthys* and *Pleuronectes* respectively), the differences between them seem minor, and since the two species occasionally produce naturally occurring hybrids, the flounder is now generally classified as *Pleuronectes flesus*.